The Role of the FAT Domain in Controlling Localization and Activation of the Focal Adhesion Kinase (FAK)

Dissertation by

Rayan Mohammad Naser

In Partial Fulfillment of the Requirements

For the Degree of

Doctor of Philosophy

King Abdullah University of Science and Technology

Thuwal, Kingdom of Saudi Arabia

November, 2019

EXAMINATION COMMITTEE PAGE

The dissertation of Rayan Mohammad Naser is approved by the examination committee.

Committee Chairperson: Professor Stefan Arold
Committee Members: Professor Manuel Aranda, Professor Lukasz Jaremko, Professor Anthony Watts

ABSTRACT

The Role of the FAT Domain in Controlling Localization and Activation of the Focal Adhesion Kinase (FAK)
Rayan Mohammad Naser

Focal adhesion kinase (FAK) controls the assembly of focal adhesion sites and transduces signals from several membrane receptors. Controlled activation and localization of FAK functionally links cell adhesion, migration and survival. FAK is overexpressed in many cancer types, promoting tumor invasiveness and metastasis. The molecular mechanisms allowing FAK to fulfil numerous different functions and act as versatile 'nanomachines' are poorly understood. We have previously revealed that ligand-induced dimerization along with intramolecular interactions control FAK activation and localization where the C-terminal focal adhesion targeting (FAT) domain is strictly involved. In this study, we combine NMR with X-ray crystallography, as well as biophysical and computational methods to understand the molecular mechanisms that link the large-scale dynamics and intramolecular and intermolecular interactions of FAT into FAK's capacity to integrate various stimuli into a site-specific function. Our results reveal FAT-mediated dynamical interplays between binding of known and newly discovered FAT ligands, and multimerization and autoactivation of FAK. Additionally, we investigate the impact of neuronal alternative splicing on FAT dynamics and interactions. Collectively, our results elucidate FAT's role in allosterically controlling various FAK functions, and might inspire allosteric protein-protein interaction inhibitors against FAK-dependent cancer cell proliferation.

ACKNOWLEDGEMNTS

First and above all, greatest praise goes to Allah, the almighty, for planning for me KAUST journey and providing me the strength and capability to proceed and achieve my aims successfully. I thank Allah for all the blessings He granted, most of which I still cannot count. I thank Allah for granting me the suitable environment and extraordinary people that both contributed greatly in this project.

Many thanks go to the BESE division and CBRC center, professors, students and stuff and core-lab team. I was glad to be in such a cooperative environment where and every person is ready to share knowledge and offer help whenever needed. Thank you all for giving me everything I needed to complete my degree, starting from the knowledgeable courses, passing through offering valuable advices and insuring a good research environment. I would like to specially thank Dr. Abdelhamid Emwas for the NMR core lab who saved me many times specially on weekends when I stood puzzled in front of the magnet. Even though it was not his job, he was so kind to explain me NMR principles and techniques. Also, special thanks to Dr. Christian Canlas, from the NMR core lab as well, who was so patient with me and helped running and analyzing NMR experiments.

Of course, life cannot be bright all the time, yet, I'm grateful for the hardships that challenged the naïve aspect of my character. Obstacles and annoyances were

needed to teach me to say no when I don't feel comfortable, object when it's against my roles and not to be shy to stand for myself!

I would like to express my deepest appreciation to my mentor and supervisor Professor Stefan Arold for providing me the opportunity to be part of StruBE lab. Despite coming from a completely different field, he offered me a smooth start in the field of structural biology which is a challenging field for any biologist. He provided his direct guidance and supervision and, in addition, he ensured a well-equipped laboratory gathering knowledgeable and cooperative researchers. He guided us to move out of the state of being students and becoming a researchers and scientists. I want also to thank him for his exceptional guidance during the writing process which is hard to be provided elsewhere.

StruBE lab.. An exceptionally coherent team! Starting from Kasia, with her warm welcoming and all-time-support (both scientifically and socially) as an elder sister, passing through Anand with his unique way of mentoring and creating fun environment, moving to Abdulrahman who taught me to keep smiling no matter what. Franceline, the sweetest person I ever met in my life! The lab was full of positive vibes and warmness in the presence of her and Kasia.. I'm sure I'm not the only person missing your presence around! I had a lovely experience with Seungbeom, the first East-Asian person I dealt with. I want to thank him for being kind and providing help each time he notices that I'm puzzled. I didn't need to ask for help! Special thanks to Raik who made no borders between students and research scientists. His easy and simple way of dealing with

people around had a positive impact on me. I learned to be always myself even in front of people higher on the horizontal hierarchy. Research was so much fun with him around where colleagues were also friends. I'm grateful for meeting Escarlet and Ana, the very sweet-hearted Latin-Americans. These two girls move in a second from being colleagues and become one's friend so smoothly! I won't forget my professional as well as personal experience with Umar, Thasneem and Shoko. Five years and half spent with these people.. My journey would have been so miserable without your kindness, good moments and endless support on the personal level before even any demand!

I was blessed to be also surrounded by extra-ordinary Arab families. I was surrounded by kind Egyptian families and for some reason they made me feel like Egypt can be my second home country even before stepping there! I want to thank the brothers Ahmad, Abdullah and Omar Dahwa. I counted them as my KAUST brothers. I was also blessed to be surrounded by amazing Saudi girls. Despite being the only intruder in their gatherings for years, they always made me feel I'm one of them, and, because of these people, staying in Kingdom was a serious option for me.

Among all the families I was surrounded by, Shaqura family was my second family. Mohammad and Manal, I've never met a couple as thoughtful and generous as them. Even their immediate family felt like my extended family. I wish that this is not the end.. I'll always consider myself as Ziad and Zeina's aunt. The warmth and tenderness created by this family will forever be carried with me.

Usually in this section, one thank people involved directly or indirectly in his/her achievement. Here, I want to apologize to my colleague, friend (and maybe a brother) Afaque! He's among the very few people who've seen me in all my states and can read me well. I was blessed to have him around during this period. With him I could talk about anything, randomly phrased thoughts or feelings, making sense or complete nonsense.. Furthermore, Afaque was the guy of mission impossible. I was less worried in his presence for whatever obstacle I face whether personal, technical, scientific, professional, official and the list never ends. I was definitely so blessed to have him around. Poor him, he had to be so patient as well. Maybe he was the most patient person I've ever met, and had the capacity to take me even during my crazy, unstable and vulnerable states. The most amazing experience I had with him is witnessing the birth of his son who chose to be born on my birthday 19th of May! I'll always carry with me the memories of being the first person to change diapers for little Muhammad and shower him. Afaque, Zikra, Muhammad and the bigger family were also a family for me. Even when they are all speaking with a language I don't understand, I felt I'm part of this family ♥.

One of Allah's big blessings on me is the amount of non-biological sisters He puts in my way. Shahad and Manar, you both helped me gain confidence in myself and taught me that differences in character cannot be an obstacle for a special relationship if the core values are the same. I had a unique experience with Shasha, my strong Algerian sister. I learned from you that one is considered dear when showing up at

hardships. Allah had put Hanin in my way during a very critical period in my life. When no one was there, she was the only one present. Then during a very critical period in her life, I found myself involved. I do not have a description for this relationship, but I cannot imagine my life without her! When I think of a nice destination for vacation or even for work, I have to think of her to be with me! Hanin, I want to go around the world with you.. share the moments of peace, crazy talks and sweet dreams… Ghada and Ikram are my unchosen dear girls. Just like sisters, we don't choose but we have unconditional love towards them. It was planned by Allah to meet at first as flat-mates and then having this relationship evolving towards sisterhood. Although I did not visit your home countries, but I really feel I have a family there, in Egypt and in Algeria. Ikram, I like the fact that with you, I don't have to talk or give hints about my mood or thoughts. It is such a nice feeling to know that there is someone out there who knows exactly how you're feeling, whether being happy, pissed off, angry, tired and so on.. While everyone else thinks that I'm good, it was very relieving to know that you can sense my state without saying a word. There is a part in my heart occupied by my sister Ikram ♥.

I thank Allah for giving me sisters for life, Rabiah and Noura. Although being miiiiiiles away, and maybe not in contact for months, you always opened your doors whenever I needed. When things get so complicated and out of my hands, I just had to return back to you, have your advice and support and proceed successfully (Al hamdulillah ☺). You both took part in every single step I take in my life even without

noticing. I pray to Allah to keep our unique friendship the way love it to be ;) ☺ Love you sis ♥.

Being away from my family for a while showed me that I have a man that I can consider as my support for life. After five years, I no longer consider Yamen as just my younger brother. I could see the real man growing in him and how he'll stand to support his elder sisters. He believed in me more than I do and I'm grateful to have such a support who can push towards what I think is impossible.

I was blessed to have my sister family around. Marwa, you've been an amazing elder sister since I was born. But this time, you even had a greater role. You were my shelter and my restaurant :P while being away from my home country. Best of all, I experienced the amazing feeling of being a second mom thanks to my nieces Hind and Haya, the light I see at the end of life hardships. I want to thank Youssef as well, without you my sister wouldn't have been able to play this role.

During this PhD journey, I have missed the daily fruity dish and breakfast from my dad and lunch and all other needs from my mom. However, I had literally felt Allah's answers to your prayers. I don't feel deserving where I stand now but I know for sure Allah wants to please you, by me! Allah bless YOU ALL ♥♥♥.

At this moment, I'm missing Uncle Abed and Uncle Adnan, who were the first to support me in my academic journeys. I dedicate this work for the soul of my beloved uncles ♥.

TABLE OF CONTENTS

LIST OF ABBREVIATIONS

2/3D	Two/three Dimensional
Å	Angstrom
aa	amino acid
AD	Alzheimer disease
Akt	Another name of Protein kinase B (PKB).
AMPK	5’ AMP-activated protein kinase
apoE3	apolipoprotein E3
Arg	arginine
Asn	Asparagine
Asp	aspartic acid
ATP	Adenosine triphosphate
BCAR3	breast cancer anti-oestrogen resistance 3
BMRB	Biological magnetic Resonance Bank
CA	Carbon α
CARA	Computer Aided Resonance Assignment
CAS	Crk-asspciated substrate
CB	Carbon β
CC	coiled-coil region
CCDC 158	coiled-coil domain-containing protein 158
CNS	central nervous system
CSP	chemical shift perturbation
DCC	Deleted in Colorectal Cancer
DTT	Dithiothreitol

ECM	extracellular matrix
EDTA	Ethylenediaminetetraacetic acid
Efs/Sin	embryonal Fyn common substrate/Src interacting
EMT	epithelial-mesenchymal transition
Erk	extracellular signal–regulated kinase
FA	focal adhesion
FAK	focal adhesion kinase
FAT	focal adhesion targeting
FERM	band 4.1 protein, ezrin, radixin and moesin
GATA4	GATA binding protein 4
GEF	guanine nucleotide exchange factor
GFP	Green Fluorescent Protein
Glu	glutamic acid
GR	glycine-arginine rich
Grb2	Growth factor receptor-bound protein 2
GST	Glutathione S-transferases
HDAC	Histone deacetylase
HEF1	human enhancer of filamentation
HEK	Human embryonic kidney cells
HEPES	4-(2-hydroxyethyl)-1-piperazineethanesulfonic acid
His	histidine
HSQC	heteronuclear single quantum coherence
IDR	Intrinsically disordered region

Ile	Isoleucine
IPTG	Isopropyl β-D-1-thiogalactopyranoside
ITC	Isothermal titration calorimetry
Kd	Dissociation constant
kDa	kilo dalton
LD motif	leucine aspartic acid-rich sequence
LDBD	LD motif binding domains
LDMF	LD motif finder
Leu	leucine
LKB1	Liver Kinase B1
LPP	lipoma-preferred partner
MAPK	Mitogen-activated protein kinase
MBD2	Methyl-CpG-binding domain protein 2
MBP	Maltose-binding protein
MDM2	Mouse double minute 2 homolog
Mg	magnesium
Mn	manganese
MST	Microscale Thermophoresis
NES	Nuclear Export Signal
Ni	nickel
NLS	Nuclear Localization signal
NMR	nuclear magnetic resonance
NOESY	Nuclear Overhauser Spectroscopy

NSP	novel Src homology 2-containing protein
NuRD	Nucleosome Remodeling Deacetylase
p-Try	phosphorylated tyrosine
p/ns	pico/nanosecond
$p21^{Cip1}$	cyclin-dependent kinase inhibitor 1
$p27^{Kip1}$	p27 cis-regulatory element
p53	Tumor protein p53
PBD	protein data bank
PBS	paxillin binding site
PEG	Polyethylene glycol
pH	Potential Hydrogen
PIN1	peptidyl-prolyl cis/trans isomerase
PIP2	Phosphatidylinositol 4,5-bisphosphate
ppm	parts par million
PR	Proline-rich
Pro	proline
PTEN	Phosphatase and tensin homolog
PTK	protein tyrosine kinase
PTP	Protein tyrosine phosphatase
PXXP	proline rich region
PWR	Proline-Tryptophan-Arginine
PYK2	Protein Tyrosine Kinase 2
Rg	Radius of Gyration

RMS	root mean square
SAXS	Small Angle X-ray scattering
SDS-PAGE	Sodium dodecyl sulfate polyacrylamide gel electrophoresis
SH2	Src (Sarcoma) homology 2 domain
SH3	Src (Sarcoma) homology 3 domain
Src	Proto-oncogene tyrosine kinase
SVMs	support vector machine
TCEP	Tris (2-carboxyethyl) phosphine
T-FAK	tense-FAK
Trp	tryptophan
Trx	thioredoxin
Tyr	tyrosine
VCAM1	Vascular Cell Adhesion Molecule 1
Vt	vinculin
Zn	zinc
$ZnCl_2$	zinc chloride

LIST OF ILLUSTRATIONS

LIST OF TABLES

Chapter 1 Cellular Functions of Focal Adhesion Kinase (FAK)

Focal adhesions (FAs) are cellular adhesion sites that connect the cytoskeleton with the extracellular matrix (ECM) to maintain the multicellular structure. FAs convey mechanical changes in the extracellular environment into intracellular signaling pathways. FAs are large and dynamic multi-protein structures with transmembrane proteins, such as integrins, in addition to cytoskeletal and signaling proteins including vinculin, paxillin, talin, focal adhesion kinase and others (Zaidel-Bar and Geiger 2010).

Focal Adhesion Kinase (FAK) is one of the key players at FAs. It is a non-receptor cytoplasmic protein tyrosine kinase (PTK) involved in the regulation of different cellular processes (mechanosensation, cell-cell signaling, cell polarization, migration, cell cycle and gene transcription) and in the maintenance of cellular structures (acto-myosin cytoskeletal dynamics, cell-cell junction formation and microtubule organization (Schaller 2010, Arold 2011)) (Figure 1-1). FAK expression and functions are precisely controlled by diverse mechanisms that include alternatively spliced forms, non-coding RNAs and an arsenal of interacting proteins. These factors directly or indirectly effect on the catalytic activity or protein stability of FAK (Armendariz, Masdeu Mdel et al. 2014, Sulzmaier, Jean et al. 2014, Tai, Chen et al. 2015, Panera, Crudele et al. 2017, Naser, Aldehaiman et al. 2018). Given its various different functions and control mechanisms, overexpression or malfunction of FAK has been associated with many diseases (Naser, Aldehaiman et al. 2018). Consequently, understanding the molecular mechanisms

coordinating the localization and activation of FAK may also open novel routes to therapeutically control FAK-driven cell metastasis and tissue invasion.

In this introduction, I survey FAK's cellular functions and involvement in human diseases, with a particular focus on the underlying structural mechanisms. This overview will help understanding the established and emerging key roles of the C-terminal focal adhesion targeting (FAT) domain, the focus of this study, in controlling FAK localization and activation.

1.1 Physiological significance of FAK

FAK is a highly versatile scaffolding protein that can regulate opposing functions in different cellular environments and tissues (Schaller 2010, Arold 2011, Naser, Aldehaiman et al. 2018). It is essential during embryonic development, but is also expressed, at low levels, in most tissues in adults. Human FAK is highly conserved among species, displaying 97% and 90% protein sequence identity compared to mouse and frog homologues, respectively (Schaller 2010). FAK exerts an essential role during embryonic development and is required for normal tissue formation in many organs (Schaller 2010, Arold 2011) (Burgaya, Menegon et al. 1995, Burgaya, Toutant et al. 1997). In adults, FAK is required for various cellular processes. FAK is involved in coordinating migration processes (Schaller 2010) (Mitra, Hanson et al. 2005, Tomar and Schlaepfer 2009) and cell proliferation (Cox, Natarajan et al. 2006). Moreover, FAK can respond to mechanical stimuli to control decisions in cell proliferation and migration (Klein, Yin et al. 2009,

Provenzano, Inman et al. 2009). FAK also plays an essential role in the assembly and turnover of FAs (Schaller 2010) and the maintenance of cellular structures (Palazzo, Eng et al. 2004) (Figure 1-1). Given that FAK is implicated in basic biomechanical processes, FAK activation affects the cellular homeostasis. Consequently, defects and overexpression of FAK can cause a wide range of diseases in humans.

Normal Tissue Development	• Required during embryonic development; angiogenesis and the development of heart during embryogenesis • Regulates hypertrophic response in the adult heart
Cell Migration	• Involved in the coordination of migration: spatiotemporal control of cell attachment, generation of leading-edge protrusions and retraction of trailing edge • Required for establishing Golgi re-localization and cell polarity in response to wounds
Cell Proliferation	• Regulates cell proliferation by affecting the expression of key cell-cycle proteins: cyclin D1, $p27^{Kip1}$ and $p21^{Cip1}$
Mechanosensation	• Required for proper adhesion on stiff matrices in fibroblasts and epithelial derived cells • Recognized as a mechano-coupler due to its influence on cellular mechanical properties.
Cellular contact sites	• Recruited to FAs primarily in response to integrin clustering • Involved in FA assembly and disassembly • Involved in epithelial-mesenchymal transition (EMT) induced by Src • Involved in formation of cell-cell junctions by regulating the expression of E- and N-cadherins
Cellular Structure	• FAK activation is crucial for disassembly of FAs induced by microtubules

Figure 1-1: Summary of Cellular Functions of FAK

1.1.1 FAK in neuronal development and brain

The detection of various neuron-specific alternatively spliced FAK isoforms has motivated research to understand the role of FAK in neuronal development (Burgaya,

Toutant et al. 1997, Menegon, Burgaya et al. 1999, Toutant, Studler et al. 2000). Consistent with FAK's role in mechanosensing and cell migration, these investigations showed that FAK mutations result in neuronal migration defects, whereas its absence produces hyperbranched migrating neurons. Additionally, absence of FAK results in decreased neuritogenesis, impaired axonal growth, and impaired actin organization and turnover (see (Navarro and Rico 2014) for review). Cell survival depends on proper cell adhesion, hence it is not surprising that FAK signaling is also implicated in this process. For example, alterations in FAK expression in rat primary neuronal cultures and cortical cells cause inhibition or suppression of FAK-mediated apoptosis (Palazzo, Eng et al. 2004, Navarro and Rico 2014).

Given its physiological role in neuronal development, FAK appears important in maintaining neuronal integrity. Indeed, dysregulation of FAK was linked to many serious neurological diseases. In schizophrenic patients, cells obtained from olfactory mucosa neurospheres are less adhesive but more motile due to defective FAK expression (Fan, Abrahamsen et al. 2013). Moreover, in autistic patients, lymphoblasts display defective adhesion, migration and proliferation due to a diminished FAK expression (Wei, Malik et al. 2011). Furthermore, although the direct role of FAK in the development of Alzheimer disease (AD) is poorly understood, many signaling pathways associated with AD development are also linked to FAK regulation. For instance, phosphatase PTEN is altered in AD, which increases its capacity to bind to FAK and to prevent its

phosphorylation and hence activation, thus leading to neurodegeneration (Gupta and Dey 2012).

1.1.2 FAK in cancer

By controlling cell adhesion, FAK protects cells from programmed cell death that would normally be induced by cell suspension in anchorage-dependent cells (anoikis). Consequently, overexpression of FAK in cellular tissues increases cell survival and allows cells to escape anoikis (Golubovskaya, Conway-Dorsey et al. 2009, Zheng, Xia et al. 2009). In addition to its cytoplasmic kinase-dependent role at FAs, FAK's capacity to override anoikis also involves kinase-independent functions in the nucleus, where FAK targets the turnover of transcriptions factors; for examples, FAK scaffolds with GATA4 and E3 ligase thus blocking VCAM1, whereas nuclear FAK binds to p53 recruiting Mdm2 that causes p53 ubiquitination (Golubovskaya, Finch et al. 2005, Lim, Chen et al. 2008, Lim, Miller et al. 2012, Aulakh, Petri et al. 2018). In addition, nuclear activated FAK can bind to various transcription factors thus regulating cancer-related gene expression (reviewed in (Zhou, Yi et al. 2019)). Whereas overriding anoikis is important for cell migration in embryonic development and wound healing, it also promotes tissue invasiveness and metastasis in cancer cells. Indeed, overexpression and activation of FAK are reported in most tumor cells and metastatic cancers (Golubovskaya, Conway-Dorsey et al. 2009, Zheng, Xia et al. 2009).

The role of FAK in brain cancer cells has been established and its overexpression is reported in astrocytoma, for instance. These studies highlight another way in which FAK contributes to tumorigenesis, namely FAK's capacity to enhance angiogenesis. FAK-associated angiogenesis increases permeability of glioma vasculature and thus increases malignancy (Haskell, Natarajan et al. 2003, Lee, Borboa et al. 2010). FAK is also involved in breast cancer development *in vivo* where deletion of FAK in breast cancer mouse models is associated with inhibition of tumorigenesis and progression in mammary cells (Fan, Zhao et al. 2013, Mierke 2013). Overexpression of FAK in malignancies and its correlation with a poor clinical outcome stress the need to fully understand the molecular details of FAK-mediated tumorigenesis and highlights FAK as a potential marker for tumor prognosis.

1.2 Structure of individual FAK domains

FAK is a 125kDa multi-domain protein that interacts with cell membrane receptors and transduces intracellular signals. It consists of an N-terminal band 4.1, ezrin, radixin, moesin (FERM) domain, a catalytic kinase domain and C-terminal focal adhesion targeting (FAT) domain. Long flexible linkers separate the central kinase domain from FERM (50 aa) and FAT (220 aa) domains (Figure 1-2). Although homologues of FERM, kinase and FAT domains are also present in other proteins, the specific combination and idiosyncrasies of these domains in FAK result in unique features (Arold 2011, Naser, Aldehaiman et al. 2018). FAK can bind to more than 50 ligands, inferring the complexity

of the mode of action and localization of FAK (major binding partners are summarized in Figure 1-2).

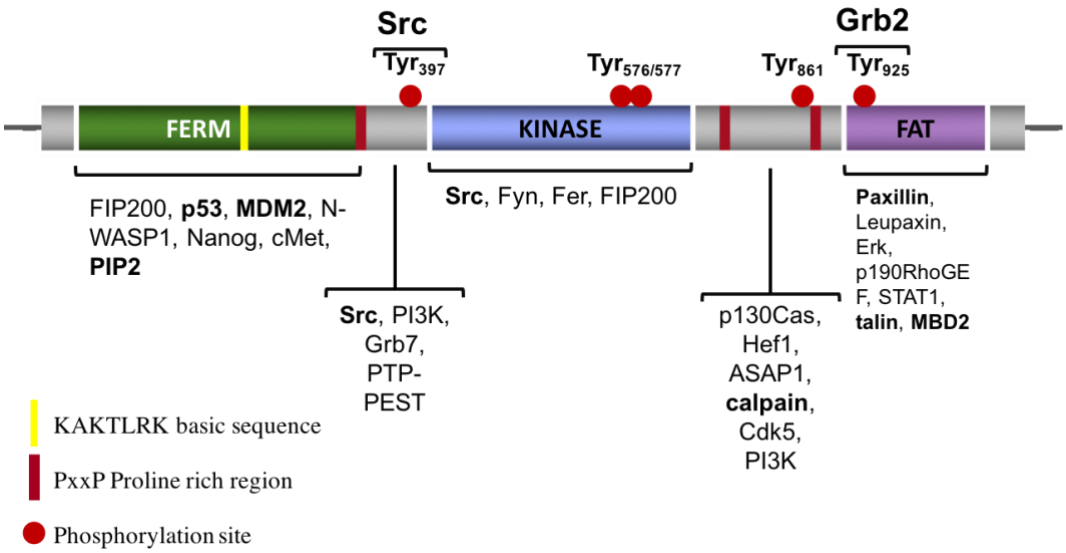

Figure 1-2: Schematic structure and function of FAK with major binding partners
Major tyrosine phosphorylation sites are indicated with red spheres. Proline-rich regions are indicated with red bars and the basic KAKTLRK patch is indicated with a yellow bar. Linker regions are colored in gray. Ligands binding to individual domains and linkers are indicated. Key ligands highlighted in the text are in bold. The color code of the FAK domains and linkers is used for all figures.

1.2.1 FERM domain

Akin to other FERM domains that commonly bind to the cytoplasmic regions of transmembrane proteins, the FAK FERM domain consists of three lobes F1, F2 and F3 (Figure 1-3). FAK FERM sequences share only 12-15% identity with other FERM domains. Akin to its homologs, FAK FERM is a scaffold for inter- and intramolecular interactions. Nonetheless, FAK FERM has evolved differential binding modes for same type of ligands (Lietha, Cai et al. 2007, Arold 2011) and features loops and unique 3_{10} helices. The F2 lobe (128-253) is mainly α-helical with three additional 3_{10} helices. It is

involved in the regulation of FAK activity as it 1) associates with the kinase domain in the autoinhibited conformation of FAK, 2) harbors a basic patch (KAKTLRK) that is important for FAK activation following growth factor stimulation and cell adhesion, and 3) binds to phosphatidylinositol that regulates activation of FAK. Lastly, the F3 lobe (254-352) forms a β-sandwich with a C-terminal α-helical cap. Compared to most homologues, it harbors an additional 3_{10} helix and a longer β5-β6 loop at the surface, creating additional opportunities for functional idiosyncrasies (Ceccarelli, Song et al. 2006) (reviewed in (Hall, Fu et al. 2011)).

The FERM-kinase linker region (352-415) comprises FAK's main phosphorylation site Tyr_{397} that, when phosphorylated, acts as a docking site for the Src SH2 domain. Additionally, this linker encompasses a proline-rich region (PXXP) that acts as a binding site for the Src SH3 domain. Jointly, the p-Tyr_{397} and the PXXP region produce a high-affinity site for the recruitment and activation of the Src kinase which, subsequently, phosphorylates FAK and bound ligands.

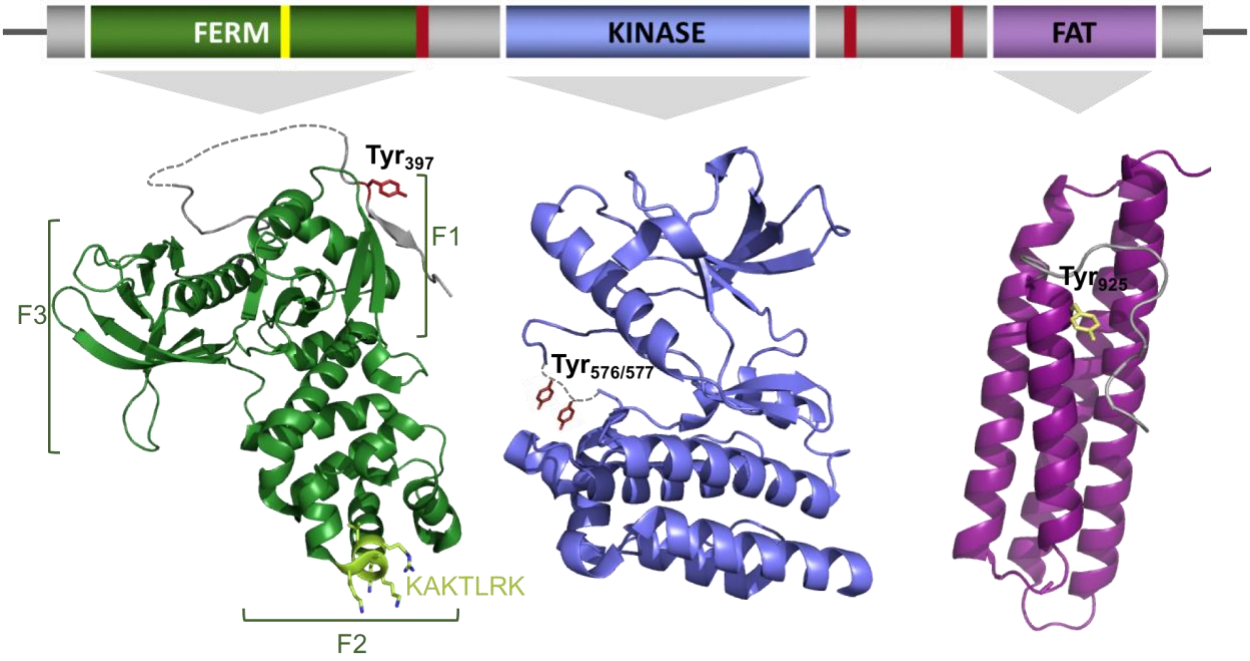

Figure 1-3: The crystal structures of the FERM, Kinase and FAT domains.
The crystal structures of FAK domains are represented color-matched below the schematic drawing structure of FAK. The 3 lobes of the crystal structure of FERM (green) are indicated. The basic residues of the KAKTLRK patch in the F2 lobe of the FERM domain are represented as light-green stick model. The crystal structure of the kinase domain is shown in blue. The dashed lines represent regions that are not included in the crystallographic structure of FERM and kinase domains. Helices 1 to 4 of the FAT domain are represented in purple. The N-terminal extension is shown in gray. The key tyrosine residue 925 is shown in yellow. Key tyrosine phosphorylation sites highlighted in the text are shown. FERM and kinase domains are prepared using PDB file 2J0J (Lietha, Cai et al. 2007) whereas the FAT domain is prepared using PDB file 3S9O (Kadare, Gervasi et al. 2015).

1.2.2 Kinase domain

The FAK kinase domain is bi-lobed with an activation loop that is disordered in its unphosphorylated state (Figure 1-3) and adapts a β-hairpin loop conformation upon phosphorylation by Src (Lietha, Cai et al. 2007). Phosphorylation on tyrosines 576 and 577 stimulates maximal catalytic activity and blocks the autoinhibitory interaction between the FAK kinase and FERM domain (Calalb, Polte et al. 1995) Lietha, Cai et al. 2007).

1.2.3 FAT domain

The FAT domain mediates recruitment of FAK to FAs by binding to LD motifs of the adhesion protein paxillin. In addition, FAT harbors docking surfaces for many ligands in different subcellular compartments and plays a role in the regulation of the catalytic activity of FAK (Arold 2011, Walkiewicz, Girault et al. 2015). FAT comprises four amphipathic α-helices arranged into an antiparallel up-down-up-down 4-helix bundle (Figure 1-3). Tyr_{925} in helix 1 is the main phosphorylation site in the FAT domain. Tyr_{925} is in a poorly accessible position within the 4-helix bundle, and helix 1 needs to adopt an 'open' conformation (where it separates from the rest of the structure) to allow Tyr_{925} phosphorylation and subsequent binding of Grb2 SH2 domain (Arold, Hoellerer et al. 2002, Arold 2011, Hall, Fu et al. 2011).

1.3 Environment-dependent activation of FAK

Full activation of FAK necessitates coordinating intra- and intermolecular interactions. In the absence of ligand binding, FAK remains in an autoinhibited conformation hindering its kinase activity. In the following sections, I will discuss FAK autoinhibition and kinase-dependent and independent functions, also highlighting the role of the FAT domain in these processes.

1.3.1 FAK autoinhibition

The kinase-dependent function of FAK involves the autophosphorylation of Tyr_{397} in the linker region between FERM and kinase domains (Ceccarelli, Song et al. 2006). In the

absence of activating ligands, FAK adopts an autoinhibitory conformation where FERM binds to the kinase domain. In this conformation, the FERM F2 subdomain binds to the C-terminal kinase lobe while FERM F1 binds to the N-terminal kinase lobe (autoinhibited form in Figure 1-4) (Lietha, Cai et al. 2007). This interaction keeps Tyr_{397} inaccessible for the kinase thus blocking its autophosphorylation. Though ATP binds to the kinase domain and stabilizes the FERM:kinase autoinhibitory conformation, Tyr_{576} and Tyr_{577} are concealed between kinase active site and FERM F1-F2 subdomains and are thus not accessible for phosphorylation by Src (Burgaya, Toutant et al. 1997, Lietha, Cai et al. 2007).

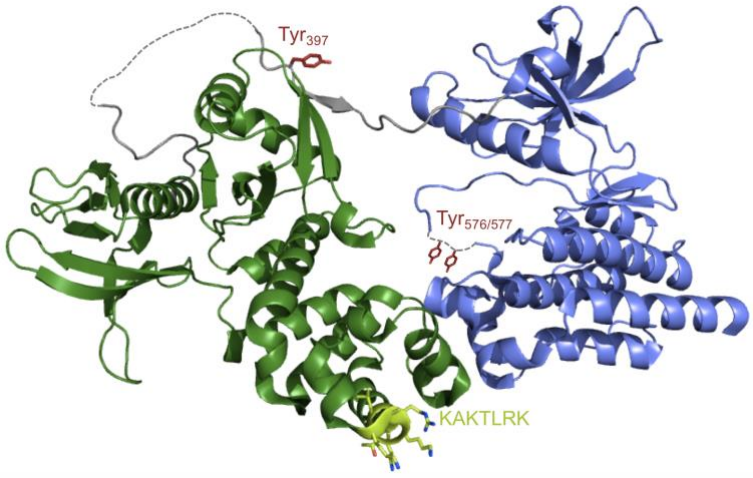

Figure 1-4: The crystal structure of FERM-Kinase domains (31-686)
The crystal structure of FERM (green) and Kinase (blue) domains in their inactive autoinhibited conformation. The linker region between the FERM and Kinase is shown in gray. This figure is prepared using PDB file 2J0J (Lietha, Cai et al. 2007).

1.3.2 FAK dimerization and autophosphorylation

An earlier model of FAK autophosphorylation was described by Lietha et al. who proposed that binding of competitive activating proteins (such as the cytoplasmic part

of ß-integrins or different growth factor receptors) to the surface of FERM F2 lobe initiates the displacement of FERM domain and thus the disruption of the FERM:kinase interface. This disruption of the autoinhibitory conformation will subsequently mediate Tyr_{397} autophosphorylation (Figure 1-5A) (Lietha, Cai et al. 2007).

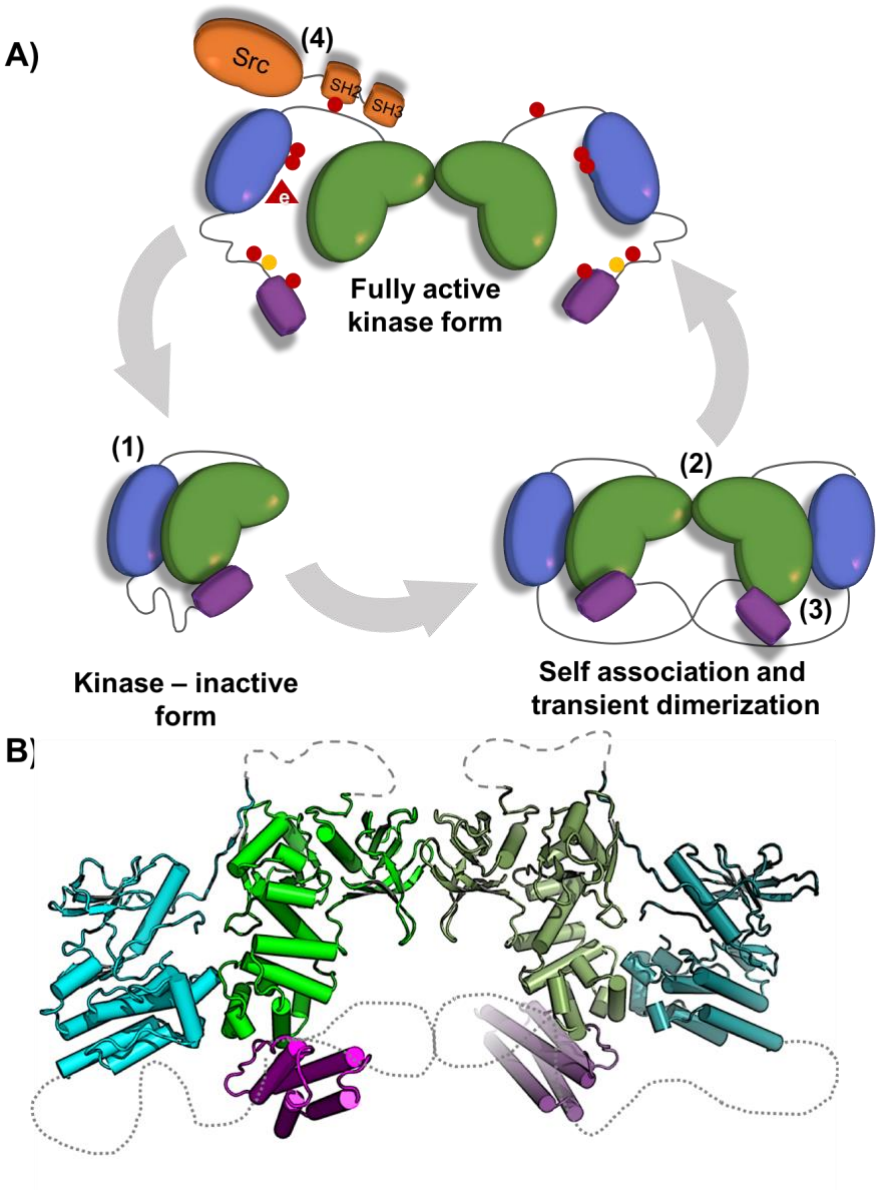

Figure 1-5: Mechanism of FAK activation and kinase-dependent function

A) 1- In the autoinhibited form, FERM binds to the kinase domain forming kinase-inactive form (FERM F2 binds to the C-terminal kinase lobe while FERM F1 binds to the N-terminal kinase lobe). 2- Upon ligand binding, transient dimerization of FERM domain in trans takes place where FAK acquires a relaxed conformation stabilized -3- by binding of FAT to the FERM domain. 4- This relaxed conformation allows the autophosphorylation of Tyr_{397} in trans where p-Tyr_{397} forms a binding site for the SH2 domain of Src. Src binding allows further phosphorylation of FAK kinase domain resulting in a fully active kinase domain (Naser, Aldehaiman et al. 2018). B) Model for dimeric FAK: model was established by combining SAXS and x-ray crystallography data. Dimeric FERM:kinase crystal structures are prepared from PDB 2J0J. The position of the FAT domain is approximate and placed using SAXS. This figure is taken from (Brami-Cherrier, Gervasi et al. 2014).

Later, our group provided evidence that FAK autophosphorylation is induced through FAK dimerization caused by dimerization of FERM and stabilized by FERM:FAT binding (Brami-Cherrier, Gervasi et al. 2014). The crystal structure of human FERM suggests that FERM dimerizes using a surface centered on Trp_{266} (Brami-Cherrier, Gervasi et al. 2014). This finding is confirmed by a recent study reporting a higher resolution crystal structure of avian FERM dimer (PDB: 6CB0) that shares 96% identity and 99% homology with human FERM (Marlowe, Dementiev et al. 2019). Full length FAK is highly flexible and unstable *in vitro*, thus, structural analysis using x-ray crystallography is not feasible. Through SAXS analysis. Brami-Cherrier et al. obtained a low-resolution ab initio beads model that supports the formation of FAK dimer in solution. This model fits well the crystallographic structure of the FERM-kinase fragment, that also contained FERM-dimers in the crystal lattice (Figure 1-5B) (Brami-Cherrier, Gervasi et al. 2014, Kadare, Gervasi et al. 2015, Walkiewicz, Girault et al. 2015). Although other domain interactions reinforce the FERM-FERM dimerization, the combined dimerization affinity (0.1-0.5 µM) is still significantly higher than the average cellular concentration of FAK (10 nM) (Brami-Cherrier, Gervasi et al. 2014). Hence, FAK dimers only form at concentrations higher

than the average cellular FAK concentrations. Local enrichment of FAK is therefore needed at the FAs for FAK dimerization. Biophysical assays show that the FERM:FERM interaction is enhanced by a mechanism where FAT is binding *in trans* to a basic patch of FERM (K_{216}AKTLRK), thus stabilizing the weak dimer (Brami-Cherrier, Gervasi et al. 2014). Dimerization of FAK allows the autophosphorylation of Tyr_{397} *in trans*, leading to activation of FAK kinase-dependent activities through recruitment and activation of Src (Figure 1-5A) (Toutant, Costa et al. 2002, Brami-Cherrier, Gervasi et al. 2014). Src-mediated phosphorylation of Tyr_{576} and Tyr_{577} of the kinase domain, Tyr_{861} in the Kinase-FAT linker region and Tyr_{925} on helix 1 of FAT domain results in maximal activation of FAK's catalytic activity as FAK adopts an open conformation (Schaller, Hildebrand et al. 1994, Schlaepfer, Hanks et al. 1994, Thomas, Ellis et al. 1998, Schaller, Hildebrand et al. 1999, Xie, Allen et al. 2008, Arold 2011).

In the absence of FAK clustering and thus Tyr_{397} autophosphorylation, monomeric FAK is thought to perform kinase-independent scaffolding functions in different subcellular compartments (i.e., nucleus) (Corsi, Houbron et al. 2009).

1.3.3 Alternative ways for FAK activation

Clustering of FAK at FAs and subsequent activation has also been proposed to result from local FAK enrichment through binding to clustered phosphatidylinositol 4,5-bisphosphate (PIP_2) (Goni, Epifano et al. 2014). PIP_2 was suggested to bind to FAK on the FERM K_{216}AKTLRK basic patch and consequently increases the enrichment of FAK at the

cell membrane. This interaction releases the FERM:kinase inhibitory conformation allowing Tyr_{397} autophosphorylation, also *in trans*. Subsequent recruitment of Src enables phosphorylation of the kinase activation loop resulting in a fully active FAK kinase that is released from the FERM domain (Goni, Epifano et al. 2014). However, the exact mechanism remains to be determined, because FERM crystals soaked with PIP2 failed to show this interaction (Goni, Epifano et al. 2014).

1.4 Environment-dependent functions of FAK

1.4.1 Interactions at the FA

After integrin clustering, enrichment of FAK at the focal adhesion sites is triggered by binding to the FA proteins paxillin and talin through the C-terminal FAT domain (Figure 1-6). The temporal regulation of these events is still not thoroughly understood. The FAK FAT domain binds paxillin on its LD motifs (in particular LD2 and LD4 out of paxillin's 5 LD motifs) and this binding stabilizes FAK dimerization and subsequent autophosphorylation (Brami-Cherrier, Gervasi et al. 2014). However, there is evidence that in nascent adhesions, paxillin binds instead to Nudel (Shan, Yu et al. 2009) hindering FAK dimerization and autophosphorylation thus explaining the presence of FAK in its inhibitory confirmation in early spreading adhesions.

1.4.2 Kinase-independent nuclear functions

FAK interactions are not only limited to FA and cytoskeletal proteins, but FAK can also translocate into the nucleus and bind nuclear proteins hence affecting gene

transcription. FAK can attenuate p53 functions in the nucleus by (i) direct binding to p53, (ii) affecting expression of p53-dependent genes, or (iii) acting as a scaffold between p53 and E3 ligase murine double minute-2 (MDM2) which promotes p53 ubiquitination and degradation thus affecting cell survival (Golubovskaya, Finch et al. 2005, Lim, Chen et al. 2008).

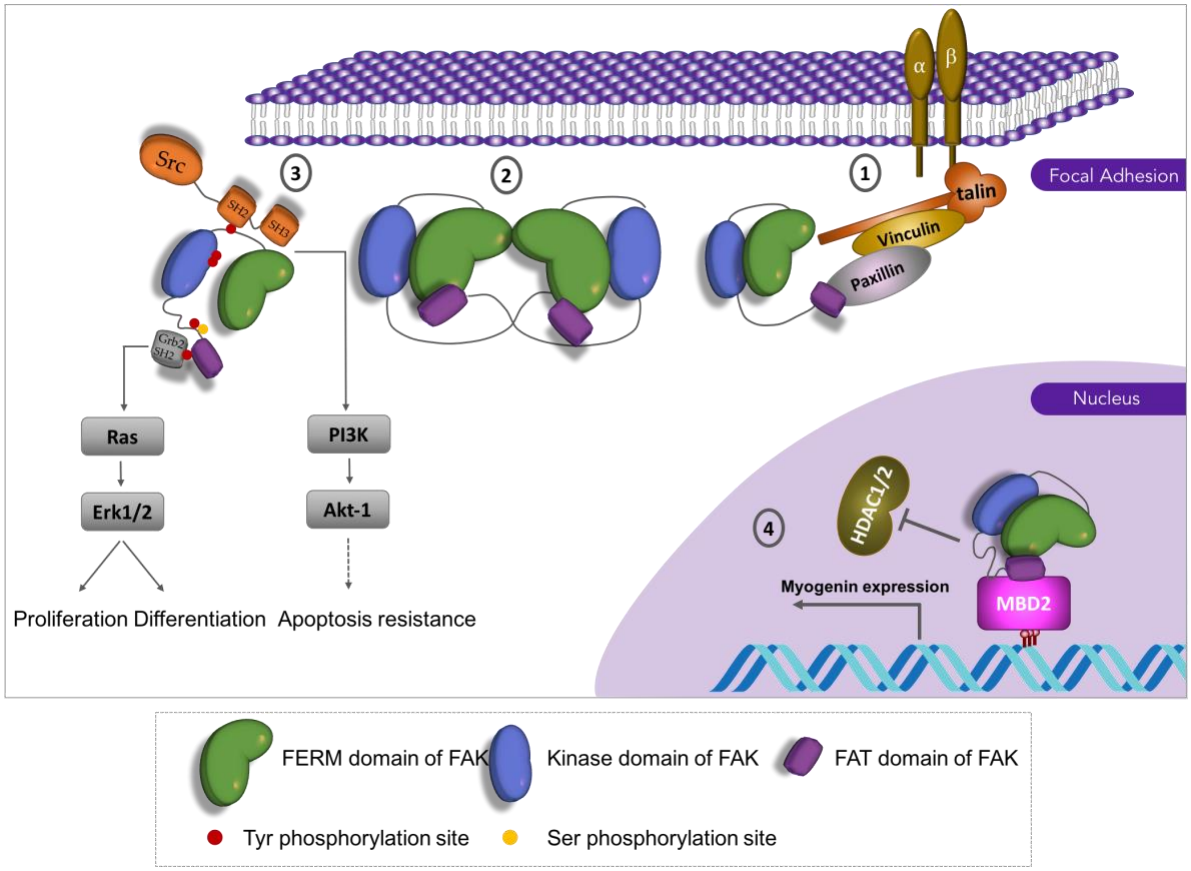

Figure 1-6: Schematic model of FAK structural rearrangement during different cellular functions

1) Activation of integrin results in the recruitment of focal adhesion proteins (illustrated here for talin, vinculin, paxillin and FAK) to the focal adhesion sites. FAK is recruited to the focal adhesions via its C-terminal FAT domain that binds to paxillin. 2) Clustering of FAK at the focal adhesion sites mediates FAK dimerization through FERM:FERM dimerization, and triggering the relaxation of the inhibitory conformation. 3) Relaxed FAK conformation mediates autophosphorylation of Tyr_{397} in trans, and p-Tyr_{397} recruits binding of Src SH2 domain. Src-mediated tyrosine phosphorylation of FAK results in a fully active FAK conformation. The FAK-

Src complex activates phosphoinositide-3- kinase (PI3K) and thus the Akt-1 survival pathway. This pathway activates downstream factors and results in apoptosis resistance. In addition, p-Tyr_{925} of the FAT domain recruits Grb2 binding and the subsequent activation of extracellular signal regulated kinase (ERK)1/2-MAPKs that is associated with both proliferation and differentiation. 4) In the nucleus, FAK interacts with the CpG-methyl binding domain protein 2 (MBD2) and disrupts the repressive binding of MBD2 to the histone deacetylase HDAC1, leading to the activation of gene expression such as myogenin.

FAK can further affect gene expression and chromatin remodeling by binding to the methyl CpG-binding protein 2 (MBD2) (Figure 1-6) (Bird and Wolffe 1999, Leonhardt and Cardoso 2000). The association between the FAT domain and MBD2 impairs MBD2-dependent recruitment of histone deacetylases thus affecting myogenin expression during muscle differentiation (Luo, Zhang et al. 2009). The molecular mechanism of this process is further explained in chapter 5.

1.4.3 Diverse roles by alternatively spliced FAK isoforms in the brain

FAK is expressed at high levels in the central nervous system (CNS), with a maximum expression during development, and also in the adult brain (Burgaya, Menegon et al. 1995). Several FAK isoforms are formed by alternative splicing, and they are selectively enriched in neuron cells (Hens and DeSimone 1995, Burgaya and Girault 1996, Burgaya, Toutant et al. 1997). Different neuronal isoforms are produced by alternative insertion of 6, 7, or 28 amino acids near Tyr_{397} while all neuronal isoforms share an insertion of 3 amino acids (Pro-Trp-Arg) in the N-terminal extension of the FAT domain (Figure 1-7) (Burgaya, Toutant et al. 1997, Menegon, Burgaya et al. 1999, Toutant, Studler et al. 2000, Toutant, Costa et al. 2002). Novel roles have been reported for these isoforms in the brain including, but not limited to, neuronal cell adhesion, FAK autophosphorylation

in cis, neurite guidance, and, yet controversial, Calmodulin-regulated adhesion (reviewed in (Armendariz, Masdeu Mdel et al. 2014)). The molecular effects on FAK regulation and function produced by these isoforms remain poorly understood. The structural outcome of the PWR insertion N-terminal to the FAT domain is the focus of Chapter 2.

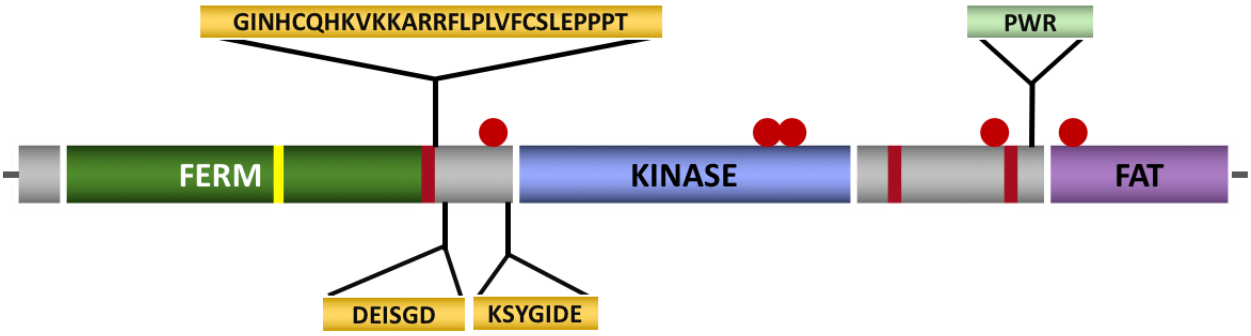

Figure 1-7: Simplified structure of FAK protein variants
This structure shows the most abundant insertions in the neuronal Isoforms of FAK. Boxes 28, 6 and 7 are inserted near Tyr_{397} (shown in mustard). All neuronal isoforms share the insertion of the three amino acids Pro-Trp-Arg in the N-terminal extension of FAT domain (shown in light green).

1.5 Research Objectives

Previous works of the Arold lab have shown that the C-terminal FAT domain of FAK plays a central role in the FAK localization and activation (Arold, Hoellerer et al. 2002, Hoellerer, Noble et al. 2003, Brami-Cherrier, Gervasi et al. 2014, Kadare, Gervasi et al. 2015, Walkiewicz, Girault et al. 2015, Naser, Aldehaiman et al. 2018). Nonetheless, the intricate connection between the localization, ligand binding and site-specific activation of FAK remains poorly understood. In this thesis, I aim to enhance the understanding of the FAT's role in site-specifically controlling activation and biological functions of FAK.

- As a first step, I wish to assign FAT Nuclear Magnetic Resonance (NMR) chemical shifts using ^{13}C,^{15}N-double labelled FAT. Then, I will use this information for binding studies and as a guide for biochemical and functional experiments.
- FAT assignment will be used to compare site-specific structural and dynamic differences between FAT isoforms.
- Moreover, I wish to use information gained from NMR studies to identify novel binding partners.
- In combination with other biochemical methods, NMR studies will be also used to investigate the structural basis of FAT binding to cytoplasmic and nuclear ligands for a better understanding of FAT-mediated temporal regulation of FAK.
- In parallel, I'll describe how I identified zinc ion as a new co-factor for FAK activation, and investigated the structural and functional implications of this interaction.

The results obtained are expected to enhance our understanding of the complicated interplay between the intramolecular and intermolecular interactions of FAT, and to help understand how FAK integrates various stimuli into a site-dependent activation. Thus, this work might also provide a stepping stone for the design of drugs that selectively inhibit distinct FAK functions.

Chapter 2 Structural Analysis of the FAT domain by NMR

As mentioned in the introduction, the FAT domain is an important determinant for localization and activation of FAK. In addition to targeting FAK to the FAs, FAT binds to various binding partners in different cellular localizations owing to its dynamic nature. I aim, in this chapter, to use NMR to investigate FAT dynamics and its interaction with cytoplasmic and nuclear ligands.

2.1 Structural features of FAT: what is known in the literature

In the following, I will briefly introduce what is currently known about the structural basis of FAT-mediated localization and signaling of FAK.

2.1.1 Structural properties of special residues of the FAT domain

The first insights about FAT domain dynamics came from crystallographic analysis of two crystal forms of FAT (Figure 2-1A) (Arold, Hoellerer et al. 2002, Hayashi, Vuori et al. 2002). Crystallographic analysis of crystal form I comprising residues 892-1052 showed that residues 892-907 form a disordered flexible region for which no electron density can be found. Ile_{909} within the N-terminal extension of FAT (residues 908-916) binds to a hydrophobic pocket of either the same molecule or a symmetry-related FAT molecule in the crystal lattice. Residues 923 to 1047 constitute the anti-parallel four-helix bundle domain. FAT helices are linked by short loops and N-terminal residues 917 to 922 aid in connecting helix 1 to helix 4 by two salt bridges built between Arg_{919}-Asp_{1039} and Asp_{922}-Arg_{1042} (Figure 2-1B) (Arold, Hoellerer et al. 2002). In unliganded FAT, the IS_{910}PPP motif

binds to the paxillin binding site (PBS) at the interface between helix 1 and 4 (Arold, Hoellerer et al. 2002, Kadare, Gervasi et al. 2015). When Ser_{910} is phosphorylated by Erk1/2, the peptidyl-prolyl cis/trans isomerase (PIN1) binds to $pS_{910}PPP$ and recruits the protein tyrosine phosphatase (PTP-PEST) that subsequently dephosphorylates FAK Tyr_{397}, thus resulting in an increased FA turnover (Zheng, Xia et al. 2009, Zheng, Yang et al. 2011).

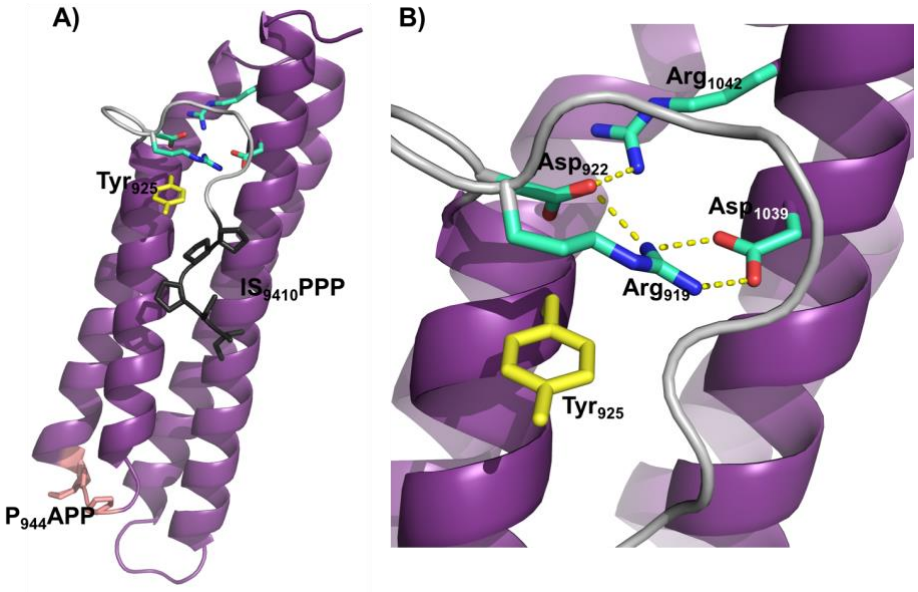

Figure 2-1: Crystal form I of FAT domain
A) The four helices of FAT are colored in violet and the N-terminal extension is shown in gray. The $IS_{910}PPP$ motif is indicated in black stick model. The side chains of Tyr_{925} in the first turn of helix 1 (colored yellow) and the residues involved in tethering helix 1 to helix 4 (Arg_{919}, Asp_{922}, Asp_{1039}, and Arg_{1042}; colored green) are shown. The hinge $P_{944}APP$ motif is shown as pink stick model. B) An expanded view of the residues connecting helix 1 and 4. This figure was prepared using PDB accession 3S9O.

The first turn of FAT helix 1 harbors Tyr_{925} that, when phosphorylated, acts as a binding site for the SH2 domain of the adaptor protein Grb2 (Arold, Hoellerer et al. 2002). Bound Grb2 then activates the Erk2/MAPK pathway (Schlaepfer, Hanks et al. 1994).

2.1.2 Comparison with structurally related proteins

Using the DALI algorithm, Hayashi et al. 2002 identified three closely related structural homologs in the Protein Data Bank (PDB). Akin to FAT, all these proteins share an amphipathic 4-helical bundle; Helices 2-5 in the N-terminal fragment of α-catenin, helices 1-4 of the C-terminal tail of vinculin (Vt) and helices 1-4 of apolipoprotein E3 (apoE3). Vt is the closest homolog to FAT with an N-terminal extension that tethers Helix 1 and 4 to the bundle (Figure 2-2) (Arold, Hoellerer et al. 2002, Hayashi, Vuori et al. 2002). Additionally, FAT and Vt share functional homology; they are both FA proteins, bind to paxillin and can recruit other proteins to FAs. However, unlike Vt, FAT doesn't bind to actin nor to phospholipid vesicles (Hayashi, Vuori et al. 2002).

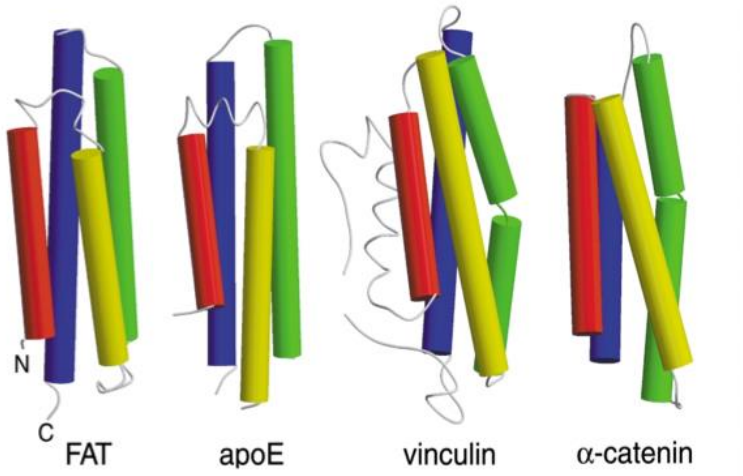

Figure 2-2: Structural comparison with structurally related protein
FAT structural homologs show similar helical structures. Helix 1 after the N-terminus is colored in red, helix 2 in yellow, helix 3 in green and helix 4 in blue. This figure is taken from Hayashi et al. (Hayashi, Vuori et al. 2002).

Subsequently, sequences homologous to the FAT domain were identified in three proteins of the CAS family, namely CAS (Crk-associated substrate), Efs/Sin (embryonal

Fyn common substrate/Src interacting) and HEF1 (human enhancer of filamentation 1). Structure-based alignment showed 42% identity of the C-termini of these proteins with FAT domain (especially FAT helix 2 and 3) (Arold, Hoellerer et al. 2002). Though the function of the C-termini of these proteins is not fully elucidated, the C-terminus of both CAS and HEF1 target the protein to the FAs. Moreover, HEF1 C-terminus was shown to harbor a binding site for breast cancer anti-oestrogen resistance 3 (BCAR3, a family member of novel Src homology 2-containing protein (NSP)). Small Angle X-ray scattering analysis proposes that the C-terminus of HEF1 binds to a Cdc25-like guanine nucleotide exchange factor (GEF) fold on BCAR3 structural insights provided by Small Angle X-ray scattering analysis proposes that the C-terminus of CAS proteins can regulate the function of NSP GEF domains (Garron, Arsenieva et al. 2009). The mapping of this interaction partially overlaps with the crystal structure of the complex NSP-p130Cas (another CAS family protein) (Mace, Wallez et al. 2011).

2.1.3 FAT conformational dynamics

Arold et al. reported FAK crystal form II that grew in conditions similar to the first crystal form but appeared only after 3 months (Figure 2-3A) (Arold, Hoellerer et al. 2002). This analysis identified a domain exchange between two FAT molecules, where the N-terminal extension and helix 1 were swapped with the symmetry-related molecule forming an arm-exchanged FAT dimer (Figure 2-3B). Based on the slow growth of the crystals, this domain may represent an ‘open’ population of FAT with low occupancy. This hypothesis is supported by the observation that Tyr_{925}, located on helix 1 of FAT_{892-}

$_{1052}$, is a poor substrate for Src phosphorylation *in vitro*, and that p-Tyr$_{925}$-FAT fails to bind to the SH2 domain of Grb2 under native conditions. Binding occurred only with denatured FAT$_{892\text{-}1052}$, suggesting that a rare open conformation is required for Tyr$_{925}$ phosphorylation and subsequent Grb2 binding (Arold, Hoellerer et al. 2002).

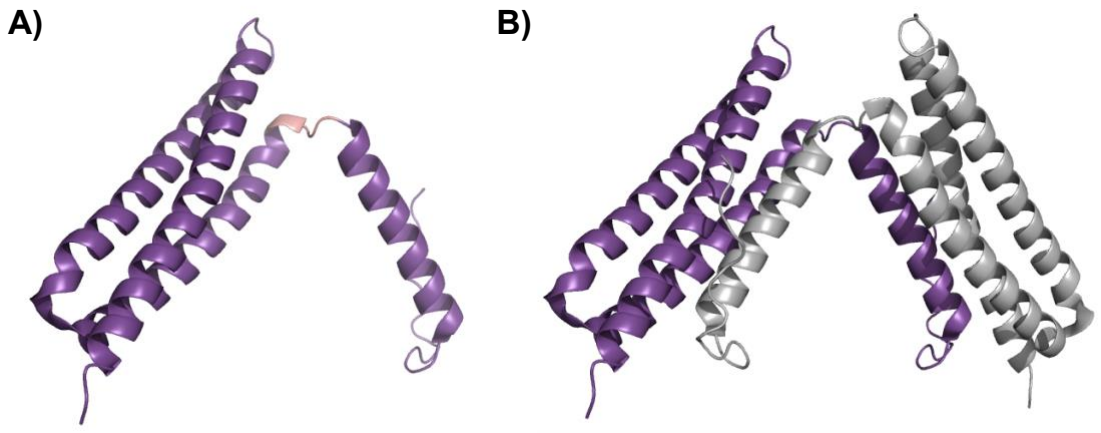

Figure 2-3: Dynamic changes of FAT domain
A) Crystal form II of FAT domain intermediate with unfolded helix 1 separated from the helical bundle. The hinge P$_{944}$APP motif is shown in pink. B) Domain-swapped FAT dimer where the N-terminal extension and helix 1 of molecule one is exchanged with symmetry-related molecule (shown in gray). This figure is prepared using PDB file 1K04.

Helix 1 arm exchange in FAT is reported in a recent study in a crystal structure of FAT bound to the cytoplasmic P3 motif of Deleted in Colorectal Cancer (DCC). Helix 1-swapped FAT dimerizes with DCC-P3 in 2:2 ratio and this dimeric binding is stabilized in the presence of calcium. The study suggests a calcium-aided DCC-P3 and FAT binding in the growth cones of axons, a step that initiates PIP2-induced FAK clustering and thus activation (Xu, Liu et al. 2018).

Helix 1 is tightly connected to the helical bundle through hydrophobic interactions (Figure 2-1B), thus forming a high-energy barrier for a domain exchange event to

happen (Arold, Hoellerer et al. 2002). However, discrete molecular dynamics simulation following NMR hydrogen exchange experiments propose a FAT domain intermediate where helix 1 is losing its helical structure and separates from the helical bundle (Dixon, Chen et al. 2004). Opening of helix 1 from the rest of the bundle may be facilitated by the hinge motif P_{944}APP that is conserved among vertebrate FAK (Arold, Hoellerer et al. 2002). In confirmation, a mutation that promotes the open helix 1 conformation by increasing the strain in the helix 1- helix 2 loop (named T-FAK, where T stands for 'tense') shows less association with paxillin (which requires a compact 4-helical FAT to bind) and is less recruited to FAs. However, those T-FAK recruited to FAs (presumably through paxillin-independent mechanisms such as Talin) show increased p-Tyr_{925} and decreased FA adhesion stability. These results suggest that FAT domain may undergo dynamic conformation changes in mature FAs promoting FA turnover (Kadare, Gervasi et al. 2015).

2.2 NMR assignment of the FAT domain

To further investigate the dynamics and interactions of the FAT domain with its ligands, I used NMR as a robust technique for studying protein dynamics. In this part of the project, I aimed at obtaining residue assignments of the NMR chemical shifts on ^{15}N, ^{13}C-double labelled FAT. I then used these assignments to investigate binding of the FAT domain to its ligands.

The biophysical *in vitro*-based approach chosen requires large amounts of purified recombinant protein. To obtain a construct with the most native-like behavior possible, I chose the human FAK fragment residues 892-1052 as the FAT construct for my analysis. This fragment had initially been identified as a stable proteolytic cleavage product of $FAK_{852-1052}$. $FAT_{892-1052}$ was expressed and purified as reported by Arold et al. (Arold, Hoellerer et al. 2002). For details please see the Materials and Methods section 7.2.

2.2.1 Backbone assignment of the FAT domain

2.2.1.1 Projection of available FAT assignments

Although NMR chemical shifts of this human FAT construct had been assigned previously, these assignments are not deposited in the BMRB data bank, and only reported in the thesis of Dr. Maria Höllerer. Deposited assignments are only available for avian forms of FAT (95% sequence identity). Previously, Dr. K. Walkiewicz of the Arold lab had recorded NMR data on ^{15}N-labelled FAT in collaboration with Dr. MacKenzie (Baylor College of Medicine, USA). Based on the available published and unpublished data, Dr. MacKenzie had succeeded in assigning 128 out of 158 resonances.

The initial step towards assigning the chemical shifts was based on compiling and transferring the chemical shift information from Dr. MacKenzie, Dr. Höllerer and the avian deposited assignments. Collectively, I first projected these assignments (128 peaks) on FAT ^{1}H-^{15}N HSQC spectrum. Using SPARKY NMR analysis tool that calculates the maximum amplitude of a peak, I centered the peaks to create a peak list that corresponds to our FAT ^{1}H-^{15}N HSQC spectrum. Jointly, I identified 112 peaks, however, I

failed to assign the following peaks: 1) 902, 915, 917 and 921 on the N-terminal tail, 2) 933 on the Helix 1, 3) 957 on the Helix 2, 3) 980, 987, 988, 1002 and 1004. on the Helix 3, and 4) 1018, 1020, 1029, 1037, 1043 and 1044 on the Helix 4.

2.2.1.2 ^{15}N, ^{13}C-labelled FAT, towards complete chemical shift assignment

To achieve a more complete chemical shift assignment of the FAT domain, human $FAK_{852-1052}$ construct was produced in minimal media in the presence of ^{13}C-labeled glucose as the main carbon source. Using Bruker 950 MHz NMR spectrometer, 3D triple resonance experiments were carried out on 100µM of double labelled FAT sample. In addition to the two-dimensional HSQC spectrum, backbone assignment was obtained using these 3D resonance experiments; HNCA, HN(CO)CA, HNCO, HN(CA)CO, HNCACB and CBCA(CO)NH. Spectra were analyzed using CARA software (**C**omputer **A**ided **R**esonance **A**ssignment) which is a tool specially dedicated for backbone and sidechain assignment of biomacromolecules.

At pH=6.5, labeled FAT ^{1}H, ^{15}N-HSQC showed sharper and less broadened peaks in comparison with FAT at pH=7.5, and, hence, I went further with the backbone assignment of FAT at pH=6.5. First, the initial 112 assigned peaks were confirmed using the 3D experiments. Triple resonance experiments were then used to pick new peaks.

Except for residue A1004, the 16 residues mentioned in section 2.2.1.1 that I could not previously assign, were successfully assigned using 3D NMR experiments. These residues are V902, A915, L917, N921 on the N-terminal tail, K933 on the Helix 1, V957 on the

Helix 2, H980, Q987, K98 and K1002 and on Helix 4 residues K1018, M1020, V1029, V1037, L1043 and K1044. Nevertheless, I failed to identify residues V928, V954 and L965 on our spectrum. In the unpublished data of Dr. MacKenzie and Dr Höllerer, 20 residues remained unassigned. In this project, I assigned 15 out of these 20 residues (11 with high confidence and 5 with low confidence). Work is in progress to confirm uncertain assignments using 3D-NOESY experiments on a higher concentrated FAT sample. Residues newly assigned using the double labeled FAT are summarized in Table 2-1. The chemical shift resonances with the updated assignments are represented in Figure 2-4 and the detailed chemical shift values for the FAT domain residues are reported in Appendix Table 1. In the following section, I explain the verification of our peak assignment by testing the binding of FAT to known ligands.

Table 2-1: Progress of human FAT domain assignment after 3D NMR experiments

	N-terminus	**Helix1/Loop1**	**Helix2/Loop2**	**Helix3/Loop3**	**Helix4**
failed to match with previous unpublished data		V928	V954, L964		A1004
Newly assigned residues	S892, S893, Q905, Q907			L975	Q1006, V1008, M1009, L1012
Newly assigned with low confidence	E908, I909, S910			Y1007, T1010, S1011	
Unassigned		Q943	V951	A977, S978	Q1013

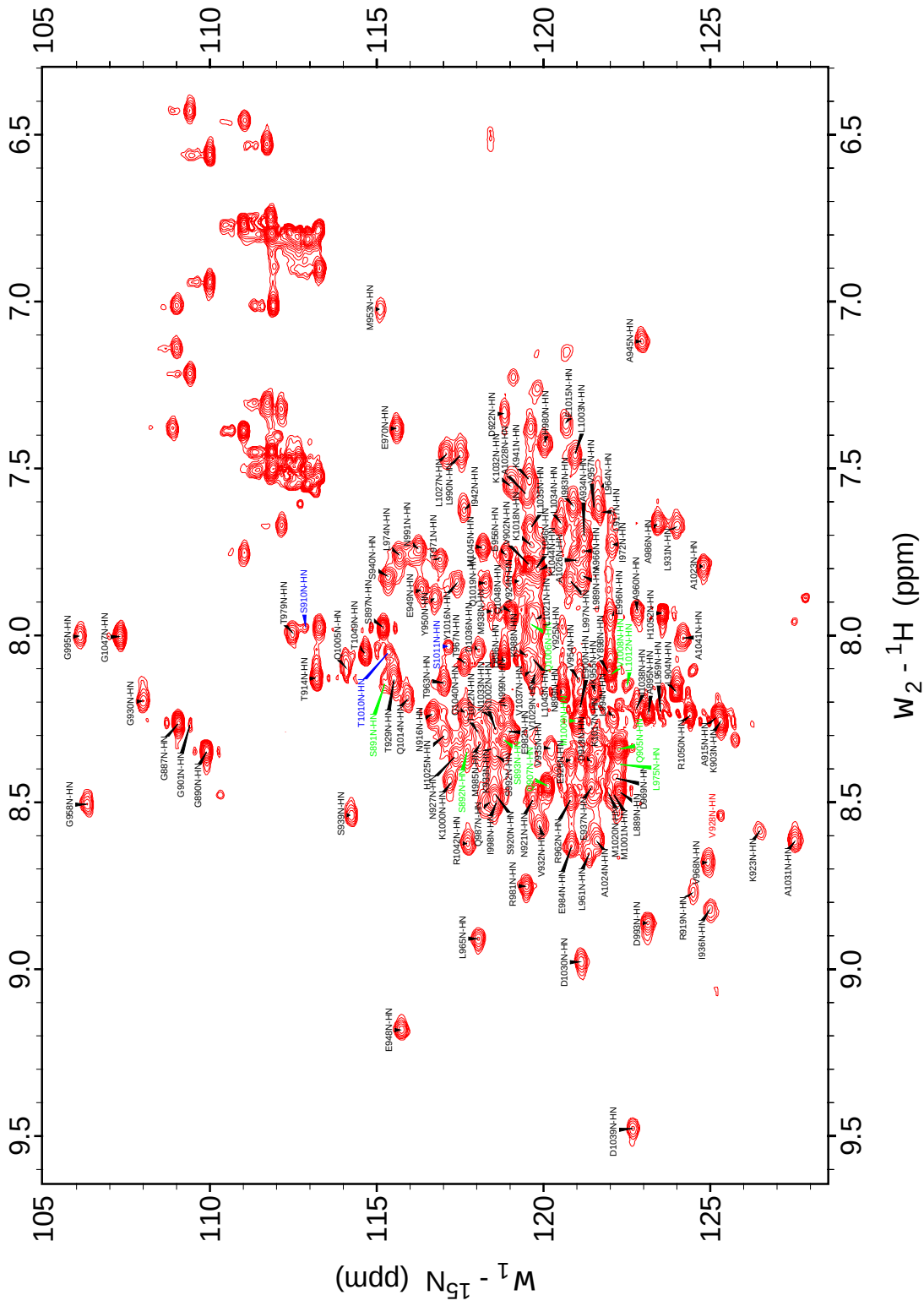
105
110
115
120
125
6.5
7.0
7.5
8.0
8.5
9.0
9.5
W2 - 1H (ppm)
W1 - 15N (ppm)

Figure 2-4: ^{1}H-^{15}N-HSQC of FAT after 3D NMR experiments
Chemical shift resonances with updated assignments are labeled in black. Newly assigned residues are labeled in green and uncertain assignments are shown in blue.

2.2.2 Comparative titration analysis with LD motifs of paxillin

The NMR structure of the chicken FAT domain complexed with Paxillin LD2 and LD4 has been previously determined and deposited in the PBD (2L6G). In addition, the $^{1}H^{15}N$-HSQC spectra of human $FAK_{852\text{-}1052}$ titrated with these peptides and the changes in the CSPs are reported in the thesis of Dr. Höllerer. To verify peak assignments, I titrated ^{15}N-labeled FAT with LD4 and LD2 peptides and compared our peak shifts to those previously observed by others.

LD motifs were dissolved in FAT gel filtration buffer, and titrated with 100 µM of ^{15}N-labeled FAT. The $^{1}H^{15}N$-HSQC spectra of the titration experiments were superimposed, and the changes in chemical shifts for ^{1}H and ^{15}N were measured in ppm (δH and δN). ^{15}N shift changes were then multiplied by a scaling factor of α = 0.2. The summed Euclidean distance moved was calculated following this equation: $\text{total change in chemicl shift pertubation } (CSPi) = \sqrt{\frac{1}{2}[\delta_H^2 + (\alpha.\delta_N^2)]}$ Figure 2-5 (Williamson 2013). The standard deviation σ was subsequently evaluated.

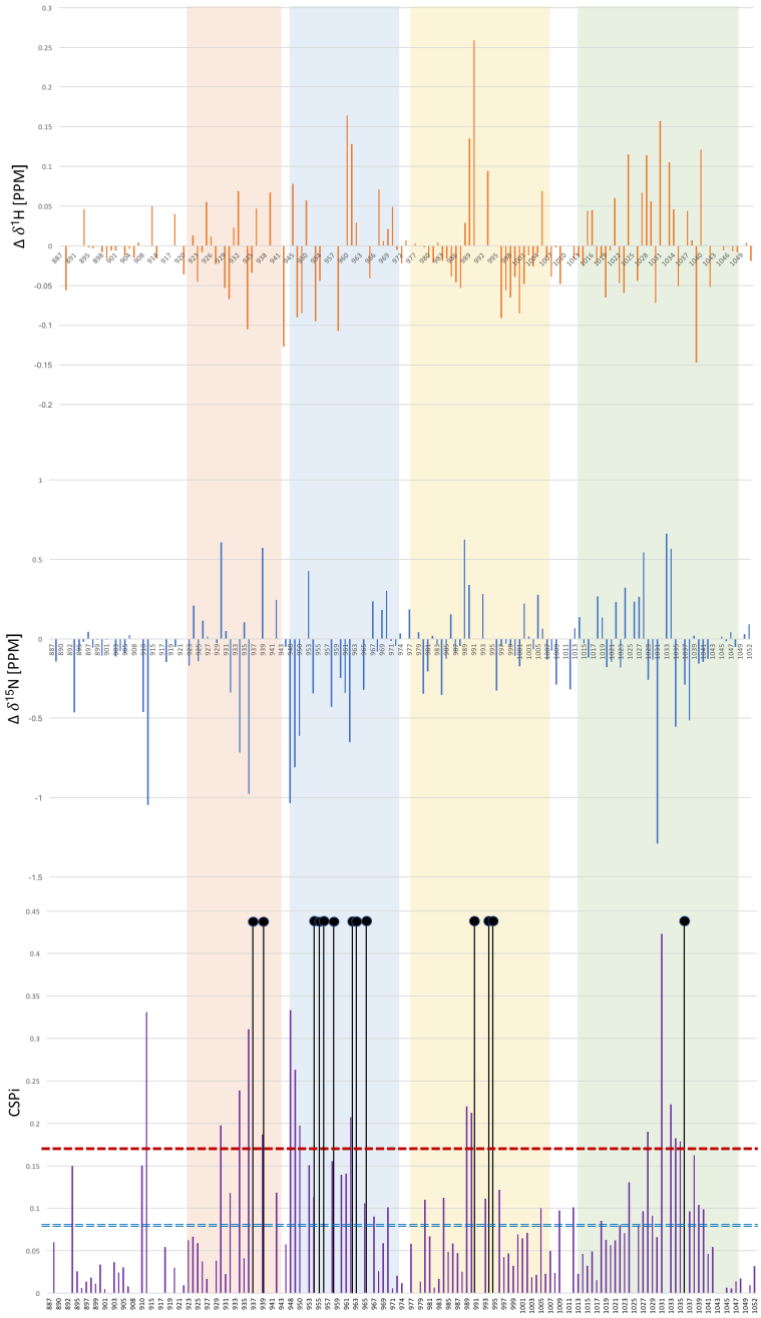

Figure 2-5: HSQC Chemical shift differences for ^{1}H and ^{15}N

Chemical shift differences in ppm where calculated for ^{1}H (top panel), ^{15}N (middle panel) and the weighted combined ^{1}H,^{15}N (lower panel) chemical shift perturbation of FAT in the presence of a four times molar excess of LD2 peptide. Red dashed line indicates the upper threshold of 2σ= 0.16 and the blue double-dashed line indicates the lower threshold of σ= 0.08. Others that disappeared upon LD2 addition are marked by full black circles. The shaded areas represent the helices (red for helix 1, blue for helix 2, orange for helix 3, green for helix 4).

In this section, I only discuss the comparative analysis of LD2 titrations onto FAT. Dr. Höllerer had previously detected broadening or disappearance of resonances of key residues upon titrating LD2 onto FAT. These residues were K933, M938 and I942 in Helix 1, K955, E956, V957, G958, L959, T963, L964 and A966 in Helix 2, N991 and G995 in Helix 3 and L1035 in Helix 4. These titration experiments were also able to detect CSP changes for residues that were previously marked with a small CSP changes and residues that showed increased amide exchange protection (Dr. Höllerer, thesis) (Appendix table 2). The high correlation between affected residues from our assignment and previous assignments strongly suggested that the transfer of peak assignments had been carried out with high confidence.

2.2.3 Application of FAT assignments to identify novel binding partners: LD-motif containing proteins

Having assigned the backbone of the human FAT domain, I used this information to identify new FAT-binding LD motifs. As explained earlier, recruitment of FAK to focal adhesion sites requires, in part, its interaction with paxillin LD motifs. LD motifs are named after the first two amino acids, Leu and Asp, in their consensus sequence LDXLLXXL, and form short α-helical amphipathic structures acting as protein-protein interaction sites (Brown, Curtis et al. 1998). Owing to their biological importance and the discovery of multiple proteins with LD Motif Binding Domains (LDBD), the prevalence and function of these LD motifs outside the paxillin family were addressed in our lab. In the following section, I will first briefly discuss the *in silico* identification of

new LD-motif containing proteins and then report the application of our FAT NMR assignment to test their binding.

2.2.3.1 In silico identification of novel LD-motif containing proteins by the Arold group

To expedite searching for LD motifs on a proteome-wide level, our group collaborated with the groups of Prof. V. Bajic and Prof. X. Gao (CEMSE, KAUST) to develop a computational search tool, the LD Motif Finder (LDMF). LDMF employs supervised machine learning models based on Support Vector Machines (SVMs), to predict the occurrence of LD motifs in protein sequences. The final LDMF model was obtained through an iterative and integrated combination of computational, biophysical and structural methods. LDMF predicts novel LD motifs with low false positive rates. When used on the human proteome, LDMF identified twelve new human LD motif-containing proteins. All these proteins were found to be involved in cell adhesion and migration, and play a role in regulating cell morphogenesis (Alam, Alazmi et al. 2019).

2.2.3.2 FAK can bind to newly identified LD motifs; LPP and CCDC158

Out of these twelve identified LD motifs, two were highly interesting and unexpected. The predicted sequences found within the Lipoma-preferred partner (LPP) and the Coiled-coil domain-containing protein 158 (CCDC 158), stood out because they did not contain a classical LD motif (Figure 2-6). Nonetheless, these motifs still bound to FAT in our *in vitro* binding experiments. Intriguingly, predicted LD motifs of both CCDC 158 and LPP exhibited an opposite orientation of the consensus $L^{0}D/E$ motif (**$D/E^{+6}L$**) (Figure 2-6). Peptides that correspond to the predicted LD motifs were synthesized and their

consequent binding to FAT was quantitatively measured by fluorescence anisotropy by F. Huser from the Arold group. Binding assays indicated a binding affinity (K_d) of 100µM for FAT:LPP and 50µM for FAT:CCDC 158. These results were further confirmed by Differential Scanning Fluorimetry (Alam, Alazmi et al. 2019).

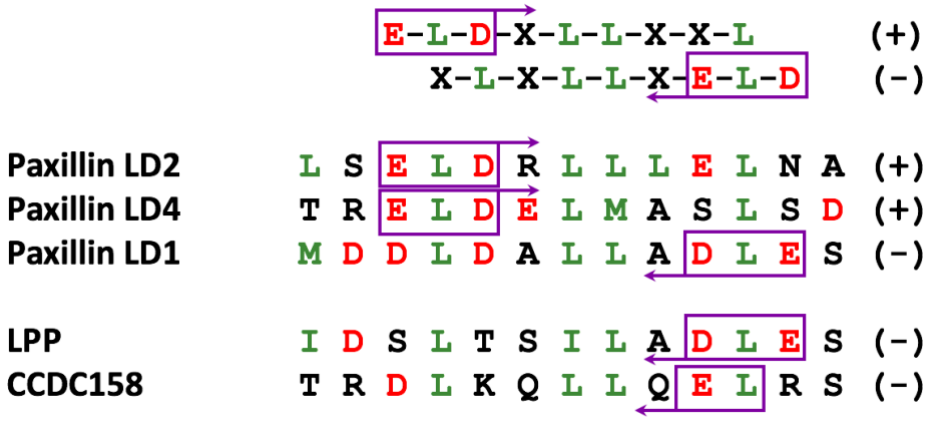

Figure 2-6: LD motifs of paxillin, LPP and CCDC158 proteins
Purple boxes represent ELD/E residues of position -1 (E), 0 (L) and +1 (D/E) characteristic of the LD consensus sequence. (+) represent the forward orientation and (-) represent the reverse orientation.

The most likely explanation for the inversed sequence is that the pseudo-palindromic nature of the helical LD motif conformation allows interactions in two opposite directions. Such opposite binding has already been observed in the interaction between the LD1 motif and α-parvin (Lorenz, Vakonakis et al. 2008). If such reverse LD motif interactions were experimentally proven, they would not only add to the complexity of the multi-functional characteristic of FAK, but would also provide novel insights about mechanisms for regulation and localization of FAK.

LPP is a scaffolding protein that plays an important role in the assembly and disassembly of cell adhesions, and it may be involved in signal transductions from adhesion sites to the nucleus, hence regulating gene transcription (Petit, Fradelizi et al. 2000, Petit, Meulemans et al. 2003). To the best of my knowledge, the cellular function of CCDC158 has not yet been investigated. Our research work predicted a potential LD motif located in a flexible region between its second and third coiled-coil domain. To assess whether the predicted LPP (SLTSILADLE) and CCDC158 (DLKQLLQELR) motifs bind to FAT on its canonical binding sites (in support of opposite binding directionality), or if these atypical LD motifs bind in a completely different manner, I chose NMR $^{1}H^{15}N$-HSQC titration analysis. Peptides were dissolved with FAT buffer (20 mM HEPES pH=7.5, 150 mM NaCl and 1 mM TCEP) and titrated with 100 µM of ^{15}N-labeled FAT. $^{1}H^{15}N$-HSQC spectra of the titration experiments were superimposed (Appendix Figures 1 and 2) and chemical shifts changes for ^{1}H and ^{15}N were measured in ppm (Appendix Figures 3 and 4) similar to LD2 and LD4 (data not shown) measurements. Analysis of changes in chemical shift perturbations upon LPP and CCDC 158 titrations indicated significant resonance changes for residues of the canonical LD2/LD4 binding sites on FAT despite their reversed LD motif orientation. To corroborate the inverse binding orientation, I used NMR-derived data to dock LPP and CCDC158 on the FAT domain (collaboration with A. Momin from the Arold group). *In silico* docking (HADDOCK) produced reversely-orientated LPP:FAT and CCDC158:FAT models that achieved confident lowest-energy binding poses. LPP was

bound with more preference for site 2/3, while CCDC158 interacted specifically with the 1/4 site of FAT in NMR (Figure 2-7).

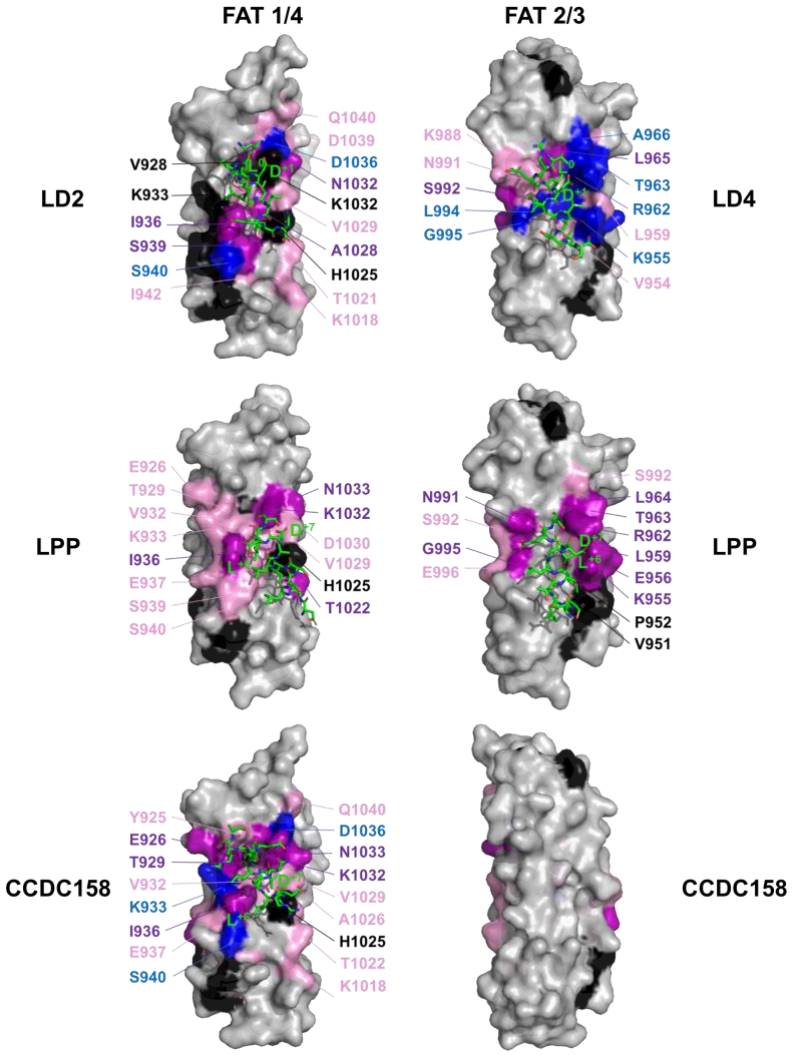

Figure 2-7: NMR binding site mapping of LD motifs onto the FAK FAT domain
NMR chemical shift changes introduced by titrations with LD motif peptides were mapped onto the molecular surface (grey) of the FAT structure in blue (resonances disappeared), purple (shift changes great than 2 σ) and pink (chemical shift changes between 1 and 2 σ). Unassigned residues and prolines were coloured black. Two sides of the FAT domain are shown: the side composed of helices 1 and 4 (1/4) and the side composed of helices 2 and 3 (2/3). LD motifs are shown as stick models, with carbons coloured in green. Paxillin LD2 and LD4 peptides were taken from the crystal structures 1ow8 and 1ow7, respectively. Positions of LD motifs of LPP and CCDC158 were obtained by NMR-data guided docking. Positions 'L^{0}' and 'D^{+1}' of the canonical class I consensus, and positions 'L^{+7}' and 'D/E^{+6}' of the inverse class II are labelled.

2.2.4 Discussion

In this chapter, I had presented how I used NMR analysis to investigate the FAT dynamics and its interaction with ligands. I had experimentally identified the binding sites of novel LD motif-containing peptides to the FAT domain. Remarkably, the consensus L^0D/E motif was not detected in the predicted LD motifs of LPP and CD158 but in the opposite orientation $D/E^{+6}L$. This may imply binding to their corresponding sites in an opposite orientation compared to LD2 and LD4.

Indeed, NMR analysis strongly corroborates that these atypical LD motif peptides use the same binding sites as the canonical motifs to associate with FAT, supporting the possibility of an interaction of the LD motifs in the opposite direction compared to LD2 and LD4. This is not the first time such opposite binding orientations have been detected for the same type of motif. Paxillin LD1 ($DL^0DXLLXD^{+6}L^{+7}E$) binds α-parvin in the opposite orientation compared to LD2 and LD4. Binding of the same type of motif in two opposite orientations also occurs in interactions of PR peptides (Ladbury and Arold 2011) and NES (Fung, Fu et al. 2015). Akin, docking data infer that the consensus L^0D/E motif binds FAT in the opposite orientation $D/E^{+6}L^{+7}$ in LPP ($L^0TSILAD^{+6}L^{+7}$) and CCDC158 ($L^0KQLLQE^{+6}L^{+7}$) (see Figure 2-8 for comparison of LD motif sequences). These findings proposed new FAK binding partners that may be involved in regulating FAs. However, the spatial and temporal control of these binding events is yet to be determined. Such understanding will help us reveal how FAK and other binding partners orchestrate the dynamics at the focal adhesion sites.

I had, therefore, established the conditions for using NMR as a tool to study interactions and dynamics of our human FAT construct. In the next chapters, I report how I used these NMR assignments, in conjunction with other methods, to investigate FAK regulation and interactions through FAT.

	0	+1	+2	+3	+4	+5	+6	+7
LD2	L	D	R	L	L	L	E	L
LD4	L	D	E	L	M	A	S	L
LD1	L	D	A	L	L	A	D	L
LPP	L	T	S	I	L	A	D	L
CCDC158	L	K	Q	L	L	Q	E	L

Figure 2-8: Alignment of sequences of paxillin LD2, LD4, LD1, LPP, CCDC158 peptides.
Characteristic leucine of the consensus LDXXLLXL motif is referred to as position and subsequent C-terminal residues referred to as +1, +2, etc. Consensus L0D of LD2 and LD4 and in the opposite orientation in LD1, LPP and CCDC158 represented as D/E+6L.

Chapter 3 Specific Regulations of FAT$^+$, the Neuronal Isoform of FAT

Neuronal FAK isoforms are produced by alternative splicing and characterized by the insertion of amino acid boxes in FERM-Kinase and Kinase-FAT linker regions (Figure 1-7). Insertions in neuronal FAK isoforms are expected to create neuronal-specific functions (Armendariz, Masdeu Mdel et al. 2014). However, the molecular effects on FAK regulation and function produced by these isoforms remain poorly understood. My objective is to study the structural–and possibly functional–differences between FAT and the FAT domain of the major neuronal isoform of FAK.

3.1 Introduction to FAT$^+$, the major brain isoform of FAT

Contrary to non-neuronal cells, neurons are devoid of focal adhesion but rather evolve 'focal points' that contain disperse integrins and actin fibers. Focal points are characterized by relatively low vinculin content and no talin. Mature adhesion site or non-focal points comprise integrins, vinculin and the neuronal FAK isoforms (Armendariz, Masdeu Mdel et al. 2014). FAK are found at growing tips of growth cones where it is required for point contact formation and axon guidance; it regulates actin cytoskeleton organization and facilitates forward growth cone movement (Burgaya, Menegon et al. 1995, Grant, Karl et al. 1995). Brain-specific isoforms of FAK share an insertion of PWR (Pro-Trp-Arg) amino acids in the N-terminal extension of the FAT domain (termed FAT$^+$ of FAK$^+$) (Burgaya, Toutant et al. 1997, Toutant, Studler et al. 2000). Simplified FAK$^+$ structure and the structure prediction of human FAT$^+$ are shown in Figure 3-1A and C.

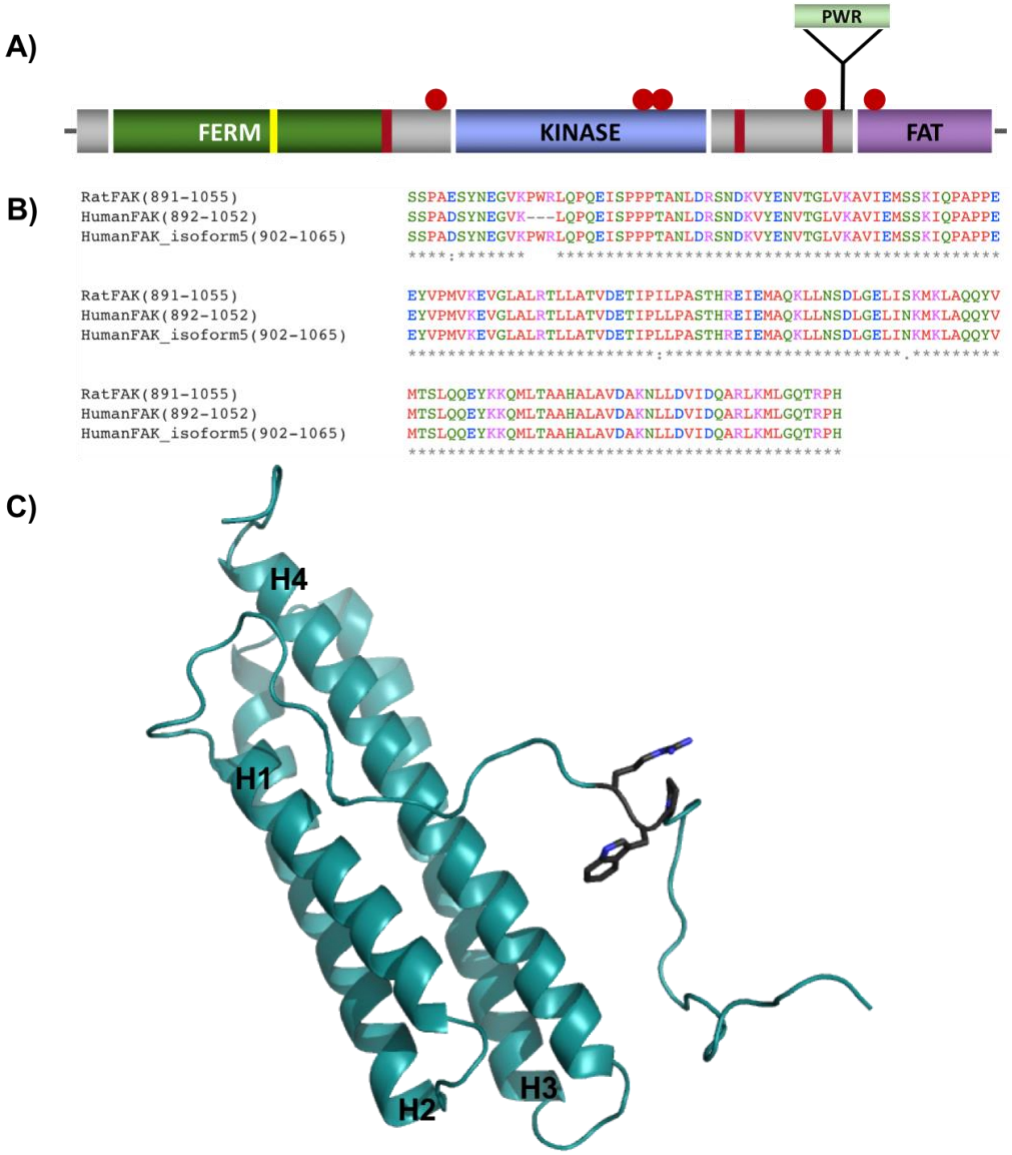

Figure 3-1: Comparison of FAT isoforms and representation of FAT^{+} structure predicted by RaptorX

A) Domain structure of FAK^{+} showing the PWR insertion with respect to other domains. B) sequence alignment of rat FAT^{+}, human FAT^{0} and human FAT^{+} (FAT isoform 5). C) Ribbon model of human $FAT_{892\text{-}1055}$ predicted by RaptorX. The PWR insertion in the N-terminal extension is represented in black stick model in the computational theoretical model.

The biological outcome of this insertion is not fully understood. However, its location between FAT and important binding sites on the kinase-FAT linker region suggests that it

may influence FAK regulation and interactions on or in the proximity of the FAT domain, to allow neuron-specific cell spreading and migration.

3.1.1 Localization of FAK$^+$ in neuronal and non-neuronal cells

Both FAK and FAK$^+$ display the same subcellular localization; both isoforms localize at the FAs when transfected in non-neuronal cell while they are concentrated in the growth cones when transfected in hippocampal neurons (Contestabile, Bonanomi et al. 2003). Hence, it is anticipated that the PWR insertion is not directly responsible for the differential distribution of FAK isoforms in different cell types. Moreover, FAT and FAT$^+$ sequences were sufficient to direct their intracellular distribution similar to that of FAK and FAK$^+$ (Contestabile, Bonanomi et al. 2003). This finding suggests that specific ligands in the neuronal environment are responsible for FAK subcellular distribution or that the insertion does not affect the conformation of LD motif binding sites on the FAT domain.

3.1.2 Possible effects on protein conformation and cellular functions of the PWR insertion

In unpublished research, our collaborators Dr. G. Kadaré (group of J.-A. Girault, INSERM, France) used biochemical and molecular biology methods to test the effect of the PWR insertion on the overall conformation of FAK using a conformation-specific antibody (anti-FAK 2A7). Although the anti-FAK antibody pulled down both FAK^0 and FAK$^+$, anti-FAK 2A7 failed to pull-down FAK$^+$ implying that PWR motif introduces sufficient conformational consequences to alter a conformation-specific antibody recognition. Dr. G. Kadaré also reported an increase in the phosphorylation of Tyr_{925} in FAT helix 1 and

Tyr_{861} in the kinase-FAT linker of FAK^+, similar to the functions reported for T-FAT. This increase may enhance the activation of the ERK/MAPK signaling pathway. Nevertheless, and unlike T-FAT, FAK^+ did not exhibit differential binding to the FA proteins paxillin and talin, possibly due to the presence of paxillin and talin binding sites away from the PWR insertion.

3.2 Structural analysis of the FAT^+ domain

To date, the structure of the FAT^+ domain has not been studied. Since the PWR insertion is adding a charged residue, a bulky hydrophobic residue, and a proline residue to the N-terminal extension of FAT domain, this insertion could affect the interactions and flexibility of this region (Figure 3-1C). In this section, I studied the effect of the PWR insertion on the structure of the FAT^+ domain with the aim to link my observations to neuronal-specific functions of FAK^+. Here, the 'standard' FAT domain of FAK, devoid of additional exons, will be annotated as FAT^0 of FAK^0.

3.2.1 Analysis of the crystal structure of FAT^+

I initially used the rat $FAT_{891\text{-}1055}$ fragment, obtained from our collaborators (group of J.-A. Girault, INSERM, France) to study the change in domain dynamics caused by the PWR insertion. The rat sequence has two amino acid substitutions compared to the human FAT and FAT^+ isoforms (L974I and N999S) (Figure 3-1B). I determined the structure of rat FAT^+ by X-ray crystallography method to investigate structural changes due to rat-specific mutation and/or the PWR insertion. FAT^+ crystal screening was carried out by

Alois Bräuer in the Technical University of Munich (TUM) at 14mg/ml protein concentration. Protein samples mixed with well solution of 0.1M HEPES pH=7.2, 0.01M Zn^{2+}, 20% PEG 6000 produced crystals (Figure 3-2A) of the space group P 2_1 2_1 2_1 that diffracted to a maximum resolution of 2.2Å. Interpretable electron density was obtained for residues 915 to 1052. Despite being present in the protein sequence, no clear electron density was observed for the PWR region, indicating that it was probably flexible (data analyzed by Professor S. Arold).

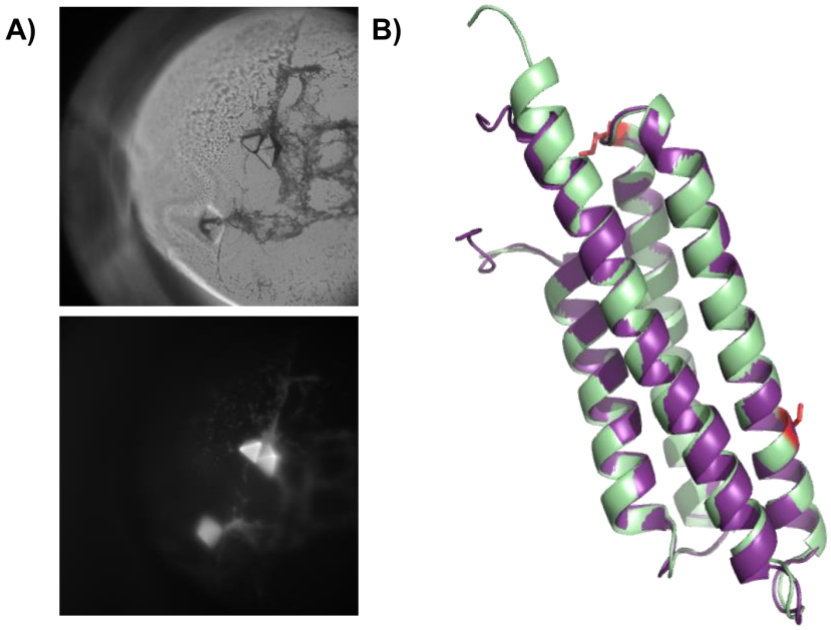

Figure 3-2: FAT$^+$ crystal structure
A) Crystal observed for FAT$^+$ with well solution of 0.1M HEPES pH=7.2, 0.01M $Zn^{2+,}$ 20% PEG 6000. Upper panel is the crystal observed under bright field light. Lower panel is observed under UV light. B) Alignment of the crystal structure of FAT$^+$ with FAT^0 (3S9O PDB file). Rat FAT$^+$ is represented in green and FAT^0 is represented in violet. The rat-specific substitutions L974I and N999S are shown as red sticks.

The FAT$^+$ structure was highly similar to the structure of FAT^0 crystallized previously in C 2 2 2_1 (3S9O PDB file), and can be superimposed with an RMS of 0.424 Å (Figure 3-2B).

Having shown that the folded regions of FAT^{+} and FAT^{0} are very similar in terms of adapted conformation, my next strategy was to compare the dynamics of both isoforms through NMR analysis.

3.2.2 NMR chemical shift assignment analysis of $^{13}C,^{15}N$-labeled FAT^{+}

To eliminate a possible influence of the rat-specific residues I974 and S999, I mutated them back into the human Leucine and Asparagine, respectively. $^{13}C,^{15}N$-labeled FAT^{+} was produced and prepared for the NMR experiments using the same conditions as for the FAT^{0} domain. For FAT^{+} assignment, the available chemical shift values of the FAT^{0} domain (explained in section 2.2.1) were transferred to the 2D HSQC spectrum of FAT+, and 3D experiments were used to correct the assignment (Figure 3-3). Akin to the assignment of the FAT domain, and in addition to the unassigned residues (Q943, V951 A977, S978, Q1013), chemical shifts of I909, S910, V928, V954, L964, Y1007 and L1012 were either not assigned or ambiguously assigned. Moreover, resonances for residues A1005, T1010 and S1011 were very weak. Nonetheless, analysis of the FAT^{+} spectra added confidence to the chemical shift assignments on FAT^{0}. For instance, chemical shifts of Q907 and L975 were sharper in FAT^{+} and thus confirmed while Q905 showed a weaker chemical shift on the HSQC. Whereas the chemical shift of L904, just after the PWR insertion, disappeared from the HSQC of FAT^{+} in comparison to FAT^{0}, I was able to find the chemical shift of the inserted Arginine R903 (chemical shift values are detailed in Appendix Table 3.

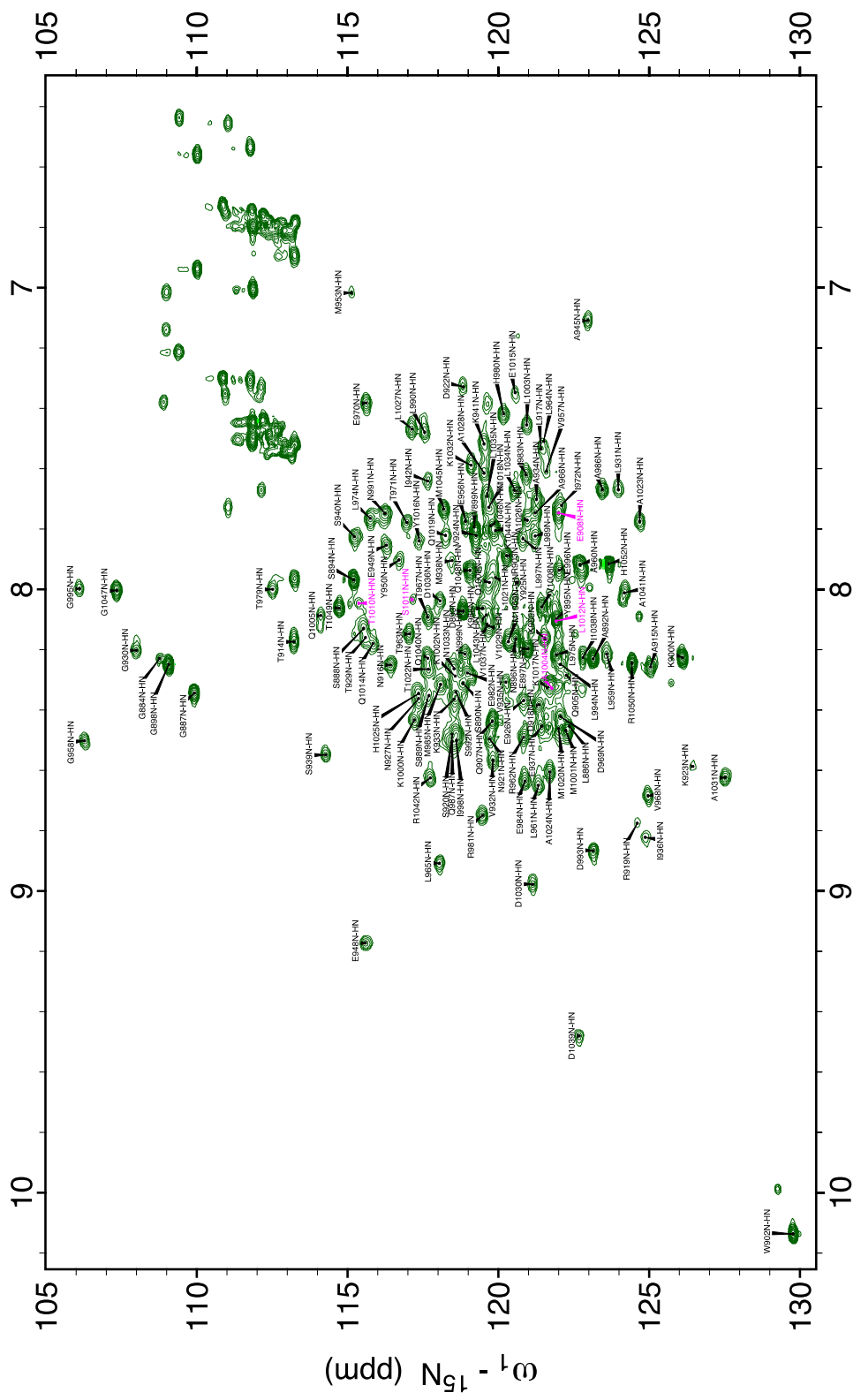
105
110
115
120
125
130
7
8
9
10
ω1 - 15N (ppm)
ω2 - 1H (ppm)

Figure 3-3: ^{1}H-^{15}N-HSQC of FAT^{+} after 3D NMR experiments
Chemical shift resonances are labeled in black and uncertain assignments are shown in magenta.

The 2D ^{1}H-^{15}N HSQC of FAT^{+}, that has only one Trp residue, shows two signals for HN group of the Trp sidechains of two different intensities. The signal with larger intensity displays the HE1/NE1 signal on the ^{1}H-^{15}N HSQC correlation map at 10.14 ppm/129.8 ppm and represents 87% of Trp sidechain population detected. This chemical shift is typical for the solvent embedded Trp side chains (10.1 ppm/129.3 ppm) (Fenwick, Oyen et al. 2018) indicating that it is exposed to the solvent and not involved in any stable iterations.

In addition, this signal is sharper and more intense compared to the amide H/N correlations from residues within the 4-helix bundle core of FAT^{+}. The second low-intensity signal (13% of Trp sidechain population) shows a chemical shift change and thus, I speculate that the tryptophan of the PWR motif is in two conformationally different states that undergo slow exchange on ms-s NMR timescale.

3.2.3 Comparative analysis of ^{1}H-^{15}N HSQC spectra of FAT^{0} and FAT^{+}

To test whether the PWR insert tethered to the FAT domain leads to changes in protein dynamics and interactions, we compared the ^{1}H-^{15}N HSQC spectra of both ^{15}N-labeled FAT^{0} and FAT^{+}. We first noticed that the center part of the ^{1}H-^{15}N HSQC spectra for both isoforms does not show large changes in the chemical shift changes (Figure 3-4). This part represents the ordered region of the FAT domain indicating that the secondary and tertiary structure of the helical bundle were preserved. However, new signals appeared

in the FAT^{+} spectrum which may be directly associated with changes caused by this insertion. To check the consistency of the chemical shift assignments between both isoforms, the chemical shift values of ^{1}H, ^{15}N and ^{13}C (CA and CB) of FAT^{+} were plotted against those of FAT^{0} (Figure 3-6A) which showed no huge differences implying that chemical shifts were properly transferred on FAT^{+} ^{1}H-^{15}N HSQC spectrum.

For the subsequent analysis, I removed residues that are not assigned on one or both isoforms (residues are 908, 909, 910, 928, 943, 951, 977, 978, 1004, 1007, 1012 and 1013), in addition to the 13 proline residues. Residues that showed ΔHN chemical shift changes greater than 2*σ (σ =0.025) (Figure 3-5 and Appendix Table 4) were mapped on the predicted structure of human FAT^{+} (Figure 3-6B). In addition to residues flanking the PWR insertion, significant $\Delta\mathrm{HN}$ chemical shift changes occurred primarily in the loop N-terminal to helix 1, specifically, residues 915 to 921 (Figure 3-6C). These changes may reflect altered dynamics of the loop that tethers helix 1 and helix 4 to the bundle. Higher dynamics in the FAT^{+} form may lower the unfolding energy barrier created by hydrophobic interactions at this interface.

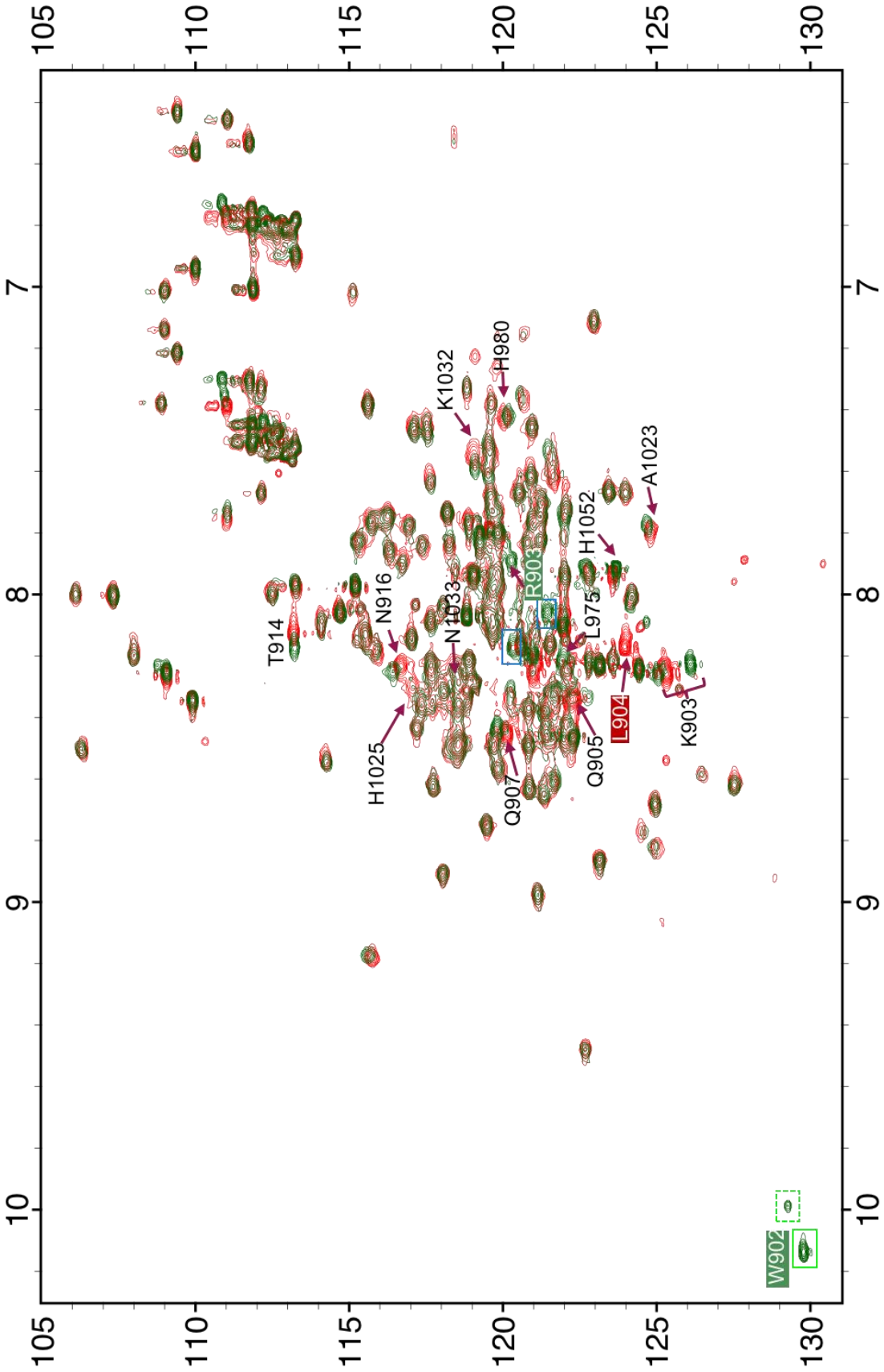
105
110
115
120
125
130
7
8
9
10
ω1 - 15N (ppm)
T914
N916
H1025
N1033
K1032
H980
R903
L975
H1052
A1023
Q907
Q905
L904
K903
W902

Figure 3-4: An overlap of 2D ^{1}H-^{15}N HSQC spectra of FAT (red) and FAT^{+} (green)
Residues with chemical shifts showing significant changes are indicated by arrows. The green boxes show the chemical shifts for the two populations of Trp side chain. The new chemical shift of the inserted R903 is labeled in a green box while the disappearing L904 is shown in a red. The blue boxes indicate the new unassigned signals that appeared on FAT^{+} spectrum.

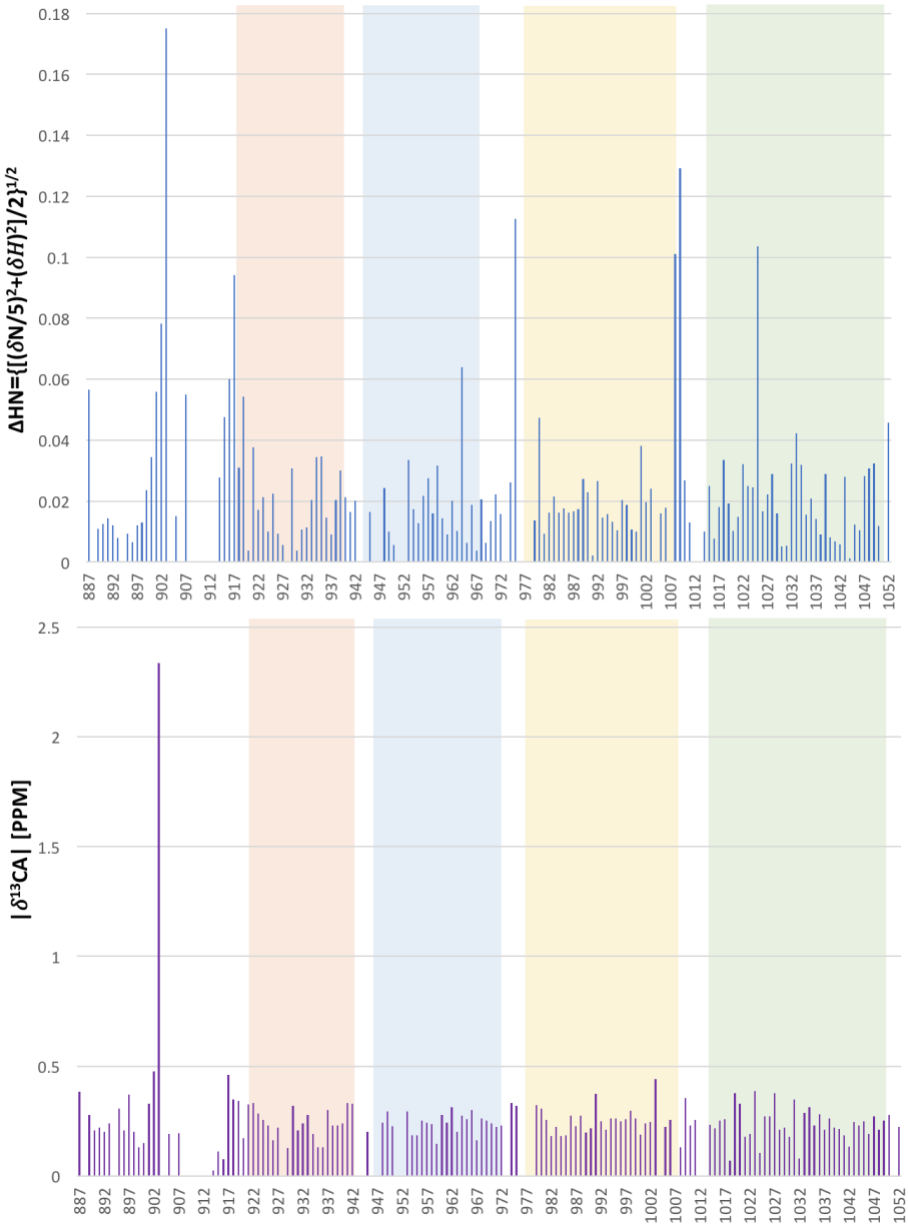

Figure 3-5: Chemical shift perturbations differences between FAT^{0} and FAT^{+}.
The weighted combined changes in ^{1}H and ^{15}N (upper panel) and ^{13}C (lower panel) chemical shift perturbations of FAT^{0} and FAT^{+}. The shaded areas represent the helices (red for helix 1, blue for helix 2, orange for helix 3, green for helix 4).

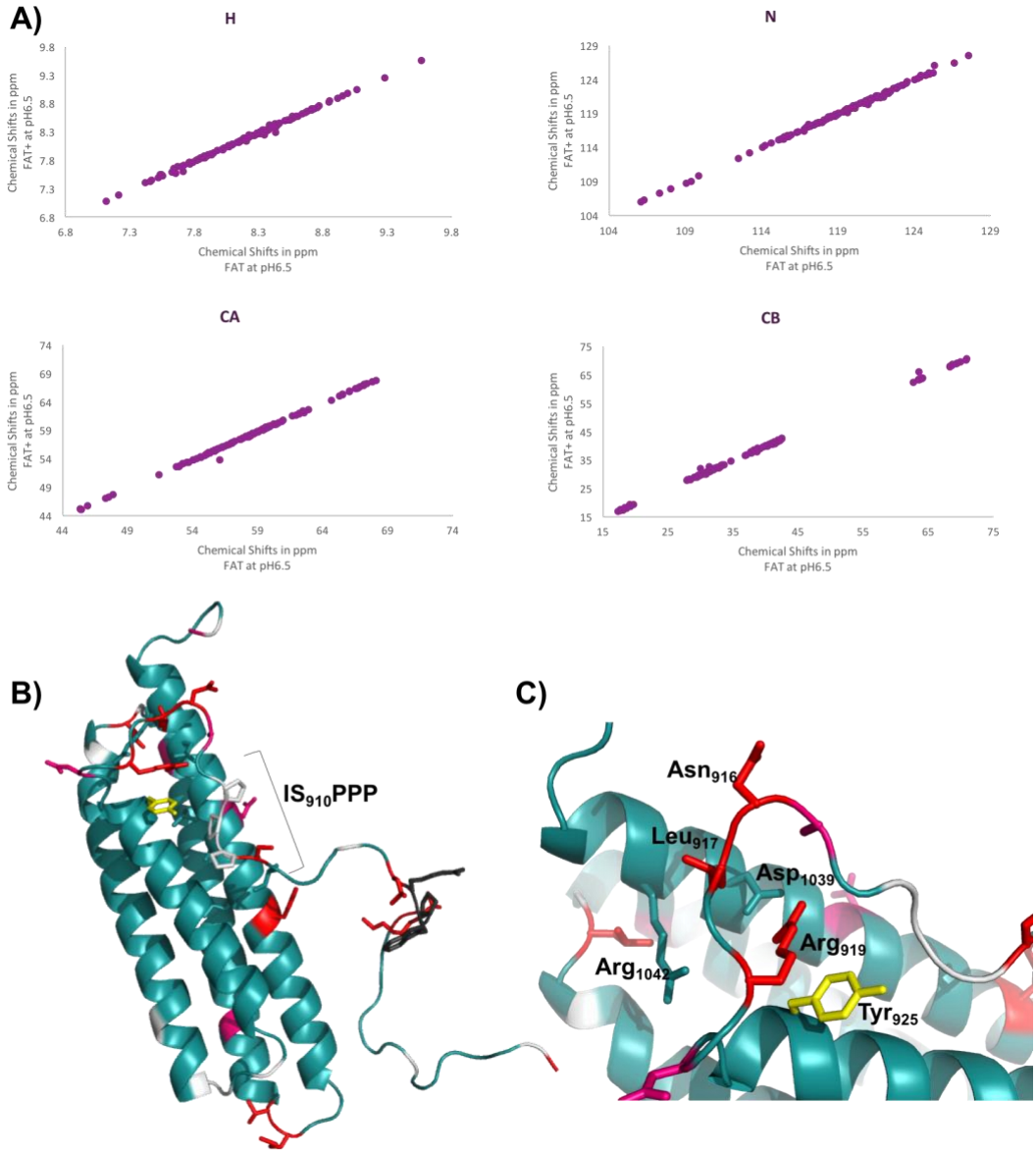

Figure 3-6: ΔHN changes of PWR insertion of the structure of FAT^{+}

A) Plot of chemical shift values for ^{1}H, ^{15}N and ^{13}C (CA and CB) for FAT^{+} against FAT^{0}. B) Human FAT^{+} structure is shown in dark green. PWR insertion is represented in stick model in black. Disappearing and most significantly changed residues (greater than 2σ) are indicated in red while those with chemical shift changes greater than 1.5σ are indicated in pink. $IS_{910}PP$ motif is indicated. C) An expanded view of the affected residues in the loop N-terminal to Helix 1. Changes in chemical shifts for ^{1}H, ^{15}N and ^{13}C were measured in ppm (δH, δN and δC). The summed Euclidean distance moved by both ^{1}H and ^{15}N was calculated following this equation: total change in chemical shift perturbation $(\mathrm{CSPi}) = \Delta\mathrm{HN} = \sqrt{\frac{1}{2}[\delta_{\mathrm{H}}^{2} + (\alpha.\,\delta_{\mathrm{N}}^{2})]}$ where the scaling factor α = 0.2 is multiplied to the ^{15}N shift changes (Williamson 2013)

3.3 Functional analysis of the FAT^{+} domain

The differences identified by these NMR studies motivated further studies to examine differences in the mode of action of FAT isoforms *in vitro*. Therefore, I combined biochemical and biophysical approaches to test the binding of FAT^{+} to known FAT^{0} ligands such as FERM FAK and paxillin LD motifs.

3.3.1 FAT^{+} binds with higher affinity to the FERM domain of FAK

According to her unpublished data mentioned above, Dr. G. Kadaré suspected that the PWR produced insertion conformational changes in FAT, because a conformation-specific antibody of FAK failed to recognize FAK^{+}. I thus wondered whether PWR induces changes in intermolecular interactions of FAT with the FAK domains. FAT binds *in trans* to the basic patch of FERM (K_{216}AKTLRK) stabilizing FAK dimer which is in turn brought by FERM:FERM dimerization (Brami-Cherrier, Gervasi et al. 2014). Hence, I tested the effect of the PWR insertion on FAT:FERM binding.

In order to test binding of FAT isoforms to FERM, I first produced chFERM which is a mutated human FERM with two mutations from chicken FERM, F85L and W181G,

present on lobe 1 and lobe 2 respectively, to increase protein solubility (Brami-Cherrier, Gervasi et al. 2014). W181 mutation lies in a region preceding the basic patch on which FAT is suggested to bind to and, thus, does not influence FERM:FAT binding. N-terminal His-tagged FAT^0 and FAT^+ were produced from plasmids synthesized by TWIST bioscience ltd. To carry out MST experiments, His-tagged FAT^0 and FAT^+ proteins were labeled with NT647 fluorescence dye (from NanoTemper technologies). 50 µM of chFERM was serially diluted 50 nM final concentration of FAT isoforms. MST data analysis showed that FAT^+ binds with 3 fold higher affinity to chFERM compared to FAT^0 (Figure 3-7). This finding suggests that PWR-induced structural changes of FAT^+ can increase its binding affinity to FERM. Given that the autoinhibited FAK conformation required FERM:FAT binding, these results suggest possible increased stability of FAK autoinhibited form.

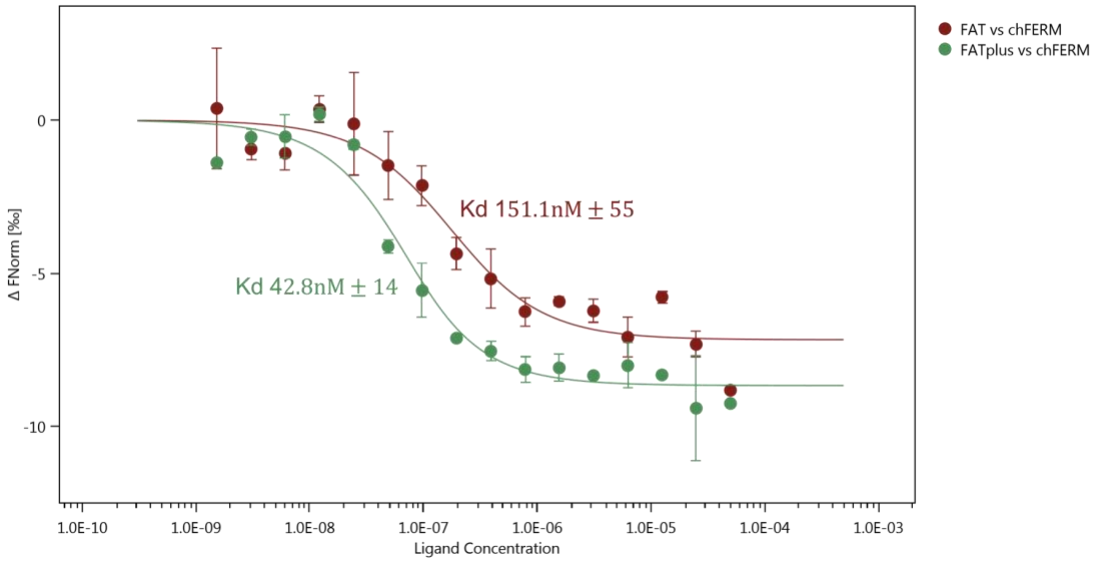

Figure 3-7: Binding of chFERM to FAT^0 and FAT^+

3.3.2 FAT^{+} did not exhibit differential binding to LD motifs

Localization of FAK molecules at FAs is initiated by binding to paxillin LD motifs as discussed earlier. I used MST assays to compare binding of FAT^{0} and FAT^{+} to LD4 and two of the novel LD-motif containing peptides E41L5 and CCDC 158 (Alam, Alazmi et al. 2019). Labeled peptides with FITC-Ahx N-terminal modification were used at 50 nM and serial dilutions of FAT^{0} and FAT^{+} were prepared starting from 330 µM. LD motifs have differential binding affinity to the two binding sites on FAT and, accordingly, I observed two binding curves within one dilution series (except for CCDC158, which has only one binding site). Therefore, data analysis was divided into two: binding at high FAT concentration (from 330 µM to 2.5 µM) and binding at low FAT concentration (from 2.5 µM). These results showed no significant difference between both isoforms for binding to the selected LD motifs (Figure 3-8). This finding suggests that the PWR insertion does not affect the binding of the FAT domain to LD motifs and thus explains the similar pattern of FA localization for both isoforms (Contestabile, Bonanomi et al. 2003).

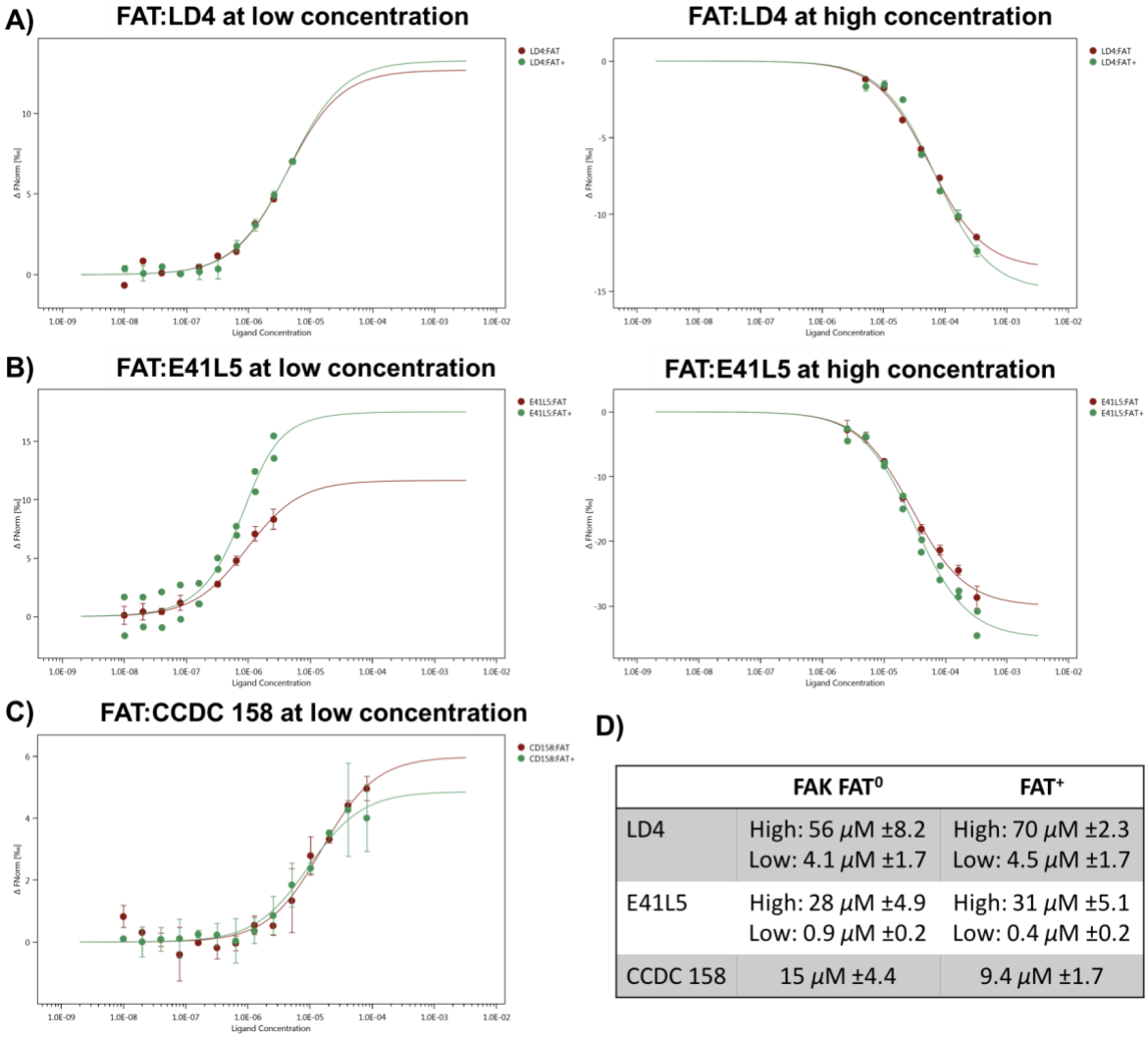

	FAK FAT^0	FAT$^+$
LD4	High: 56 μM ±8.2 Low: 4.1 μM ±1.7	High: 70 μM ±2.3 Low: 4.5 μM ±1.7
E41L5	High: 28 μM ±4.9 Low: 0.9 μM ±0.2	High: 31 μM ±5.1 Low: 0.4 μM ±0.2
CCDC 158	15 μM ±4.4	9.4 μM ±1.7

Figure 3-8: Figure 3. Binding of LD motifs to FAT^0 and FAT$^+$
MST results of FAT^0 and FAT$^+$ binding to LD4 (A), E41L5 (B) and CCDC 158 (C). Red binding curves corresponds to LD motifs binding to FAT^0 whereas green curves correspond to those binding to FAT$^+$. D) summary table of the binding affinities measured in µM.

3.4 Discussion

The vast majority of FAK neuronal isoforms has the PWR insertion N-terminal to the FAT domain. To date, there are no reports that describe the effect of this insertion on the structure and dynamics of FAT. Moreover, FAK$^+$ exhibits the same pattern of autophosphorylation and subcellular localization of FAK^0 when transfected in neuronal

and non-neuronal cells (Toutant, Studler et al. 2000, Toutant, Costa et al. 2002, Contestabile, Bonanomi et al. 2003). Here, I investigated the structural and dynamic differences between FAT^0 and FAT^+ through NMR studies.

X-ray crystallographic analysis showed that FAT^+ and FAT^0 are structurally similar. I then compared NMR backbone assignment and ^1H-^{15}N HSQC spectra of both isoforms and observed subtle changes indicative for changes in protein dynamics.

Major changes in chemical shifts were detected in residues N-terminal to helix 1. As discussed in the previous chapter (section 2.1.1), the N-terminal residues 917 to 922 aid in connecting helix 1 to helix 4 by salt bridges built between Arg_{919}-Asp_{1039} and Asp_{922}-Arg_{1042}. Moreover, FAT, in its native conditions, exhibits a conformation not accessible for Tyr_{925} phosphorylation and Grb2 binding (Arold, Hoellerer et al. 2002). Here, I reported significant dynamic changes in residues 915 to 921 upon PWR insertion in addition to changes in residues between 1039 and 1043. I speculate that these changes may reflect alteration in the stability of salt bridges formed around Tyr_{925} thus resulting in exposing Tyr_{925} for phosphorylation. Arold et al. 2002 reported that phosphorylation of Tyr_{925} and subsequent Grb2 binding requires structural rearrangement (Arold, Hoellerer et al. 2002) that may be initiated by displacement of N-terminal loop from the helical bundle (Mohanty and Bhatnagar 2017). These findings may thus explain the increased Tyr_{925} phosphorylation of FAT^+ reported by Dr. G. Kadaré, and suggest this would lead to increase in Grb2 binding and turnover of adhesion sites (Ezratty, Partridge et al. 2005).

Analysis of FAT^{+} ^{1}H-^{15}N HSQC spectrum showed the appearance of two populations of Trp sidechains of two different intensities. Here, I propose that the population with larger intensity is solvent exposed whereas that of lower intensity may be involved in some interactions resulting in significant chemical shift changes. For example, it is possible that the FAT^{+} N-terminal loop undergoes conformational changes bending back to the helical bundle. Such effect would explain the changes in chemical shifts detected in hydrophobic residues of helix 4 (M1020, A1023 and A1024) that may be directly affected by the contact with Trp. This hypothesis might be confirmed by analysis of 3D-NOESY experiments. The observed differences may therefore suggest that the N-terminal dynamically exchanges between two detectable populations: (A) is more abundant and exposed to the solvent whereas (B) interacts with hydrophobic residues on helix 4. This finding goes in line with the observation made by our collaborators from the group of J.-A. Girault who previously showed that the PWR insertion changes the recognition of FAK by a conformation-specific antibody. I therefore propose that the PWR insertion induces possible dynamic associations between the PWR sequence and the FAT core leading to a change in the epitope recognition site of a conformation-specific antibody.

My results suggest an increase in binding affinity of FAT^{+} to the FERM, compared to FAT^{0}. Given that integrins are not clustered in neurons, these finding proposes a neuronal-specific regulation of FAK that may help clustering and stabilizing the FAK dimer formation. More binding experiments are needed to confirm this finding and to

conclude about the affinities. In unpublished data, Dr. MacKenzie, from Baylor College of Medicine, USA, mapped the changes of FAT^0 ^1H-^{15}N HSQC spectrum upon FERM binding. As of now, I could not reproduce his results possibly due to differences in experimental design and/or constructs used. I provided evidence that the PWR insertion does not affect the binding of the FAT domain to LD motifs (Paxillin LD4, and LPP and CCDC 158 LD motifs) akin to findings provided by our collaborators who showed that the PWR insertion does not influence binding to Paxillin. This agrees with an earlier study reporting that FAK^0 and FAK^+ (but also FAT^0 and FAT^+) follow the same intracellular targeting (FA in non-neuronal cells and growth cones in neurons) (Contestabile, Bonanomi et al. 2003).

The proposed dynamic changes triggered by the PWR insertion and possible increased intermolecular binding affinities may be important for neuronal-specific regulation of FAK activity. Unlike FAK^0, FAK^+ is regulated by depolarization, lipid extracellular messengers (cannabinoids) and neurotransmitters (glutamate and acetylcholine) (Derkinderen, Toutant et al. 1996, Derkinderen, Siciliano et al. 1998). Increased intermolecular interactions may provide an alternative way for FAK regulation at adhesion sites in neurons. In addition, FAK is enriched in the motile compartments of neurons where motility over a substrate necessitates fast turnover of adhesion sites (Suter and Forscher 1998). As already reported, tyrosine phosphorylation exerts an important role in this adhesion remodeling process (Felsenfeld, Schwartzberg et al. 1999). Results of this section suggest that the PWR insertion of FAK neuronal isoforms

may provide conformational flexibility essential for structural rearrangements. Moreover, it is also probable that the addition of charged and bulky residues adjacent to PR regions facilitate binding of neuronal cytoplasmic or nuclear poly-protein binding ligands or other proteins. It is thus interesting to investigate potential association of neuronal molecules mediated by FAK neuronal-specific insertions.

Chapter 4 Zinc as a Potential Novel Co-factor for FAK Activation

Specific protein residues such as Histidine, Lysine, and Cysteine are known to interact with metal ions (Ca^{2+}, Mg^{2+}, Mn^{2+}, Ni^{2+}, Zn^{2+} and other bivalent metal ions). Metal interactions can contribute to protein stabilization, to protein-ligand interactions or to protein catalysis. Hence, metal coordination plays an important role in many biological processes (Christianson 1991, Predki, Harford et al. 1992, Harford and Sarkar 1995). According to a recent estimate more than half of all proteins are associated with metal ions in their active form (Lu, Yeung et al. 2009). It is therefore important to understand the factors that govern metal binding and reactivity in biological systems. FAK and the Protein Tyrosine Kinase 2 (PYK2) share a similar organization of their domains (Lev, Moreno et al. 1995, Girault, Labesse et al. 1999, Walkiewicz, Girault et al. 2015) , however, and among FAK family, PYK2 has a unique capacity of sensing calcium (Ca^{2+}) ions (Walkiewicz, Girault et al. 2015). PYK2 thus acts as a central transducer of the calcium signal in focal adhesion turnover (Hashido, Hayashi et al. 2006) in addition to functions outer of focal adhesions (Andreev, Simon et al. 1999). To date, there is no evidence for an interaction between FAK and Ca^{2+} or any other metal ion.

In the preceding Chapter, I have described the crystal structure of FAT^{+}. Close inspection of the electron density and structural arrangement of FAT^{+} molecules in the crystal lattice revealed that the molecules were mainly contacting each other via a non-bonded atomic entity. The electron density and coordination of this entity was not compatible with it being a water molecule. This FAT^{+} crystal grew with a well solution that

contained 10 mM Zn^{2+} (0.1M HEPES pH=7.2, 0.01M Zn^{2+} and 20% PEG 6000). Indeed, accordingly placed zinc ions refined well, and its coordination by FAT residues (histidines and aspartic acids) was compatible with zinc ions (Figure 4-1A). Zinc has either a catalytic, structural or regulatory function when bound to a protein. Average concentration of zinc in human cells is around 200–300 µM (Maret 2015). Zinc coordinates with four chemical moieties to form a distorted tetrahedral geometry (Sousa, Lopes et al. 2009). This coordination comprises N, O, and S donors in the side chains of the protein ligands such as histidine, glutamate, aspartate, and cysteine. Three to six protein ligands, originating from one to four proteins, may interact with one zinc ion (Sousa, Lopes et al. 2009). My intriguing finding raised the question if the zinc-coordinated FAT multimers were a crystallization artefact or were also occurring in vitro, with potential biological implications.

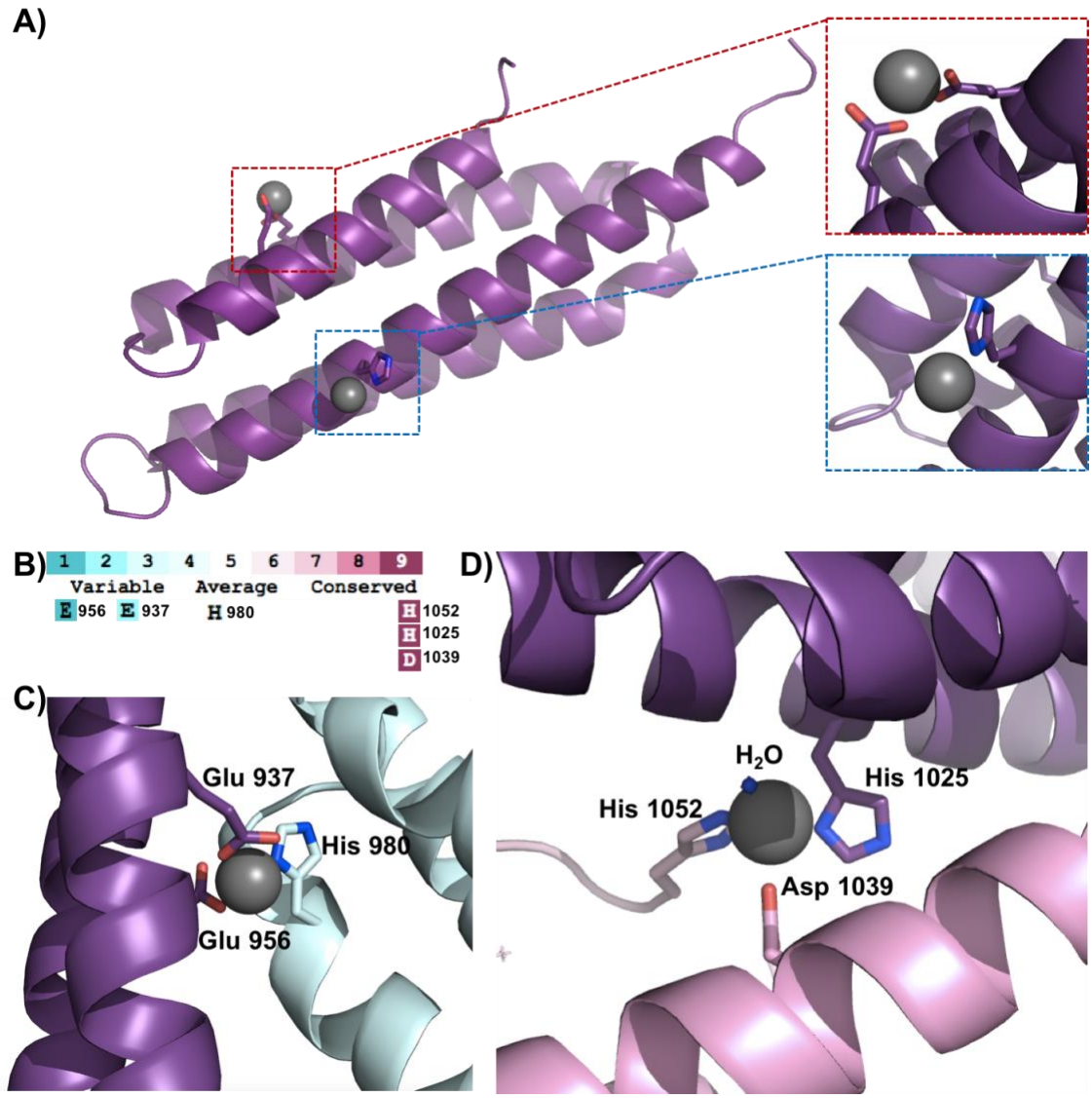

Figure 4-1: Two zinc ion co-crystallizing with FAT domain

A) The crystal structure of one rat FAT^{+} molecule comprising two of zinc ions. Closer of Zn1 (red box) and Zn2 (blue box) are shown. Zinc ion is represented as a gray sphere. In the crystal lattice, coordination of both zinc ions is completed by symmetry-related FAT residues. B) The score of residue conservation among species with 1 is the lowest score and 9 is the highest score. C) Zn1 is interacting with Glu_{937} and Glu_{956} of one FAT molecule (in violet) and His_{980} of another FAT molecule (in cyan). D) Zn2 is interacting with His_{1025} (helix 4 of molecule 1, in violet), Asp_{1039} (helix 4 of molecule 2, in pink), and His_{1052} (C-terminal tail of molecule 3, in another shade of pink). Zinc ion is represented as a gray sphere.

4.1 Results

4.1.1 Potential clustering of the crystallized FAT molecule driven by zinc

The observation that well-ordered zinc ions were present in rat FAT^{+} crystals motivated us to try to crystallize the human FAT domain under the same conditions, to test if the interactions with zinc were preserved. Indeed, I obtained crystals of human FAT under the same conditions and in the same space group as FAT^{+} ($P2_12_12_1$ and cell parameters are 47.05, 52.65, 52.57 for FAT^{+}, 47.82, 53.97, 54.86 for FAT^{0}, all angles are 90˚). I obtained 2.2Å diffraction data, and solved the structure using FAT as molecular replacement template. Although not yet fully refined, the structure shows the same zinc coordination as FAT^{+}.

For a single FAT molecule, the zinc molecule (1) (referred to as Zn1) was found in close proximity to Glu_{937} of helix 1 and Glu_{956} of helix 2, whereas zinc molecule (2) ((referred to as Zn2) interacted with His_{1025}. In order to complete the coordination of zinc-ligand interaction, I used Pymol to visualize the crystal symmetry-related molecules FAT. Interestingly, the majority of the protein contacts that stabilized the crystal were made through Zn^{2+}. Zn1 was interacting with Glu_{937} (helix 1) and Glu_{956} (helix 2) of one FAT molecule and His_{980} (helix 3) of another FAT molecule. However, these residues were not conserved among species (Figure 4-1B and C). Zn2 interacted with three highly conserved residues of three clustered FAT molecules; 1) Asp_{1039} (helix 4 of FAT molecule A), 2) His_{1025} (helix 4 of FAT molecule B), and 3) a C-terminal His_{1052} (FAT molecule C) and a water molecule (Figure 4-1B and D). The generation of symmetry-related molecules

based on the conserved interactions of Zn2 alone showed FAT domains arranged in a rod-like pattern that was brought together by Zn^{2+} (Figure 4-2A).

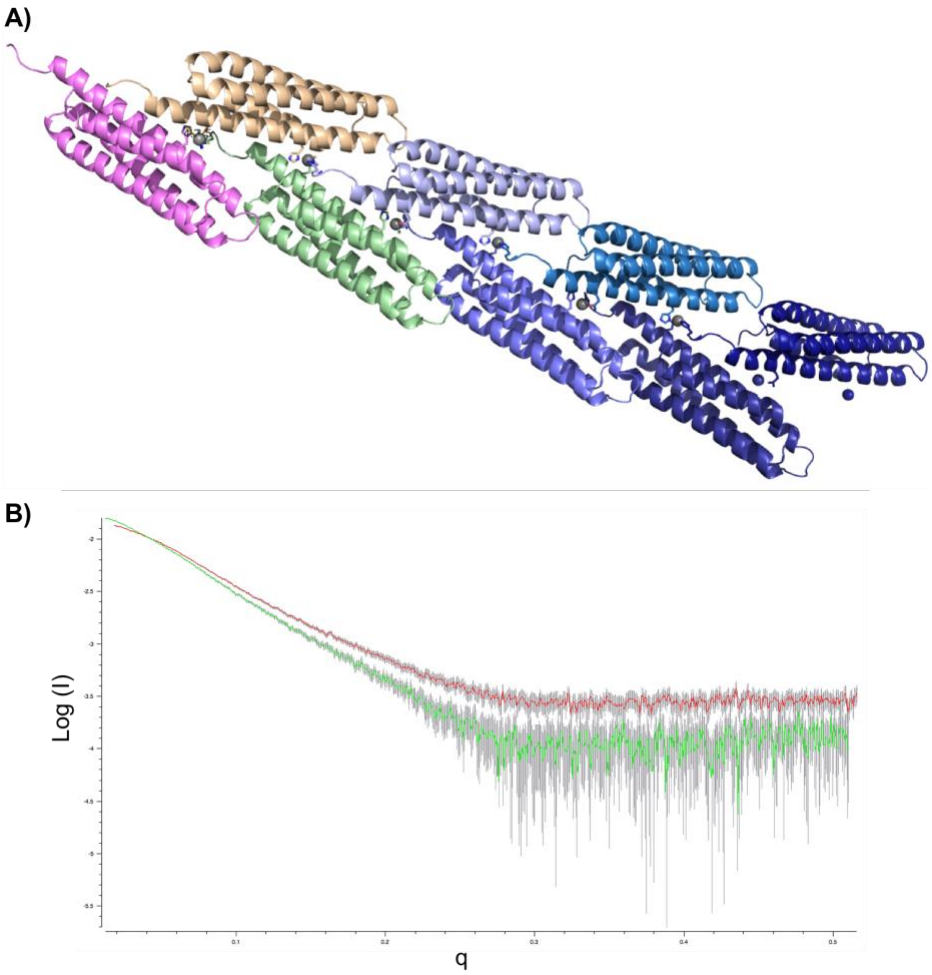

Figure 4-2: Multimerization of FAT molecules by Zn2
A) *In crystallo* multimerization of FAT. The Zn2 (gray), interacting with the conserved FAT residues, connects FAT molecules into a rod-like shape. B) SAXS data analysis using Primus showing the plots for FAT at 1 mg/ml (red) and FAT at 1 mg/ml with 50 uM of Zn^{2+} (green).

The interaction between zinc ions and the FAT domain and the consequent clustering was further examined by Small-angle X-ray scattering (SAXS) data for FAT samples incubated with Zn^{2+} at different concentrations. SAXS measurements were done for FAT at 1mg/ml with and without 50 uM of Zn^{2+}. Rg calculated for FAT at 1mg/ml was 22.60 ±

0.25 whereas upon addition of 50uM Zn^{2+} the Rg value increased to 30.81 ± 0.56 supporting the multimerization of FAT driven by Zn^{2+}. Further 3D structural data analysis for the rod-like structures is in progress (Figure 4-2B).

4.1.2 Zinc-driven clustering of FAT *in vitro*

In order to check if this multimerization occurs *in vitro*, I carried out a gel shift assay, in which increasing concentrations of FAT were incubated with 0.1mM Zn^{2+} for 2 hours and then analysed on 18% native gels with 0.1mM Zn^{2+} added to the running buffer. I did not observe significant shifts in the migration of FAT samples incubated with Zn^{2+} in comparison to the control FAT sample incubated with 2 mM EDTA (Figure 4-3).

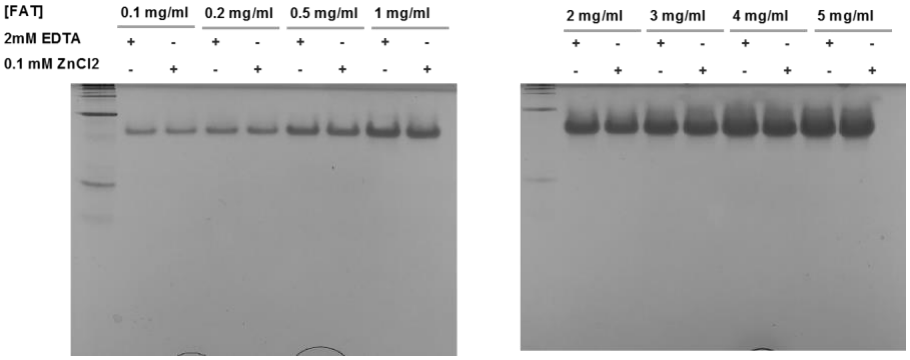

Figure 4-3: Gel-shift assay for FAT incubated with Zinc
Different concentrations of FAT were incubated with or without Zn^{2+}.

I reasoned that the visualization of non-covalent Zn-induced FAT multimerization is not strong enough to persist during the gel shift assay. I therefore attempted to capture the association using a crosslinker. I chose glutaraldehyde to crosslink the FAT molecules; it covalently produces intermolecular as well as intramolecular crosslinked FAT molecules. I carried out a crosslinking experiment in which 1 mg/ml of FAT solution was incubated

with 0.25, 0.5, and 1 mM of Zn^{2+}. Using a procedure similar to a hanging drop crystallization experiment, one drop of protein sample was applied on a coverslip adjacent to a drop of a 8% glutaraldehyde. The crosslinked protein samples were collected after 10, 20, 30, 40, and 60 minutes incubation. Samples that were analyzed on a native gel without being boiled showed that bigger protein species started to appear after 20 minutes when incubated with 1 mM Zn^{2+}. Multimers in samples incubated with 0.5 mM Zn^{2+} at pH=7.5 appeared after 30 minutes, while those incubated with 0.25mM Zn^{2+} appeared after 60 minutes. (Figure 4-4A).

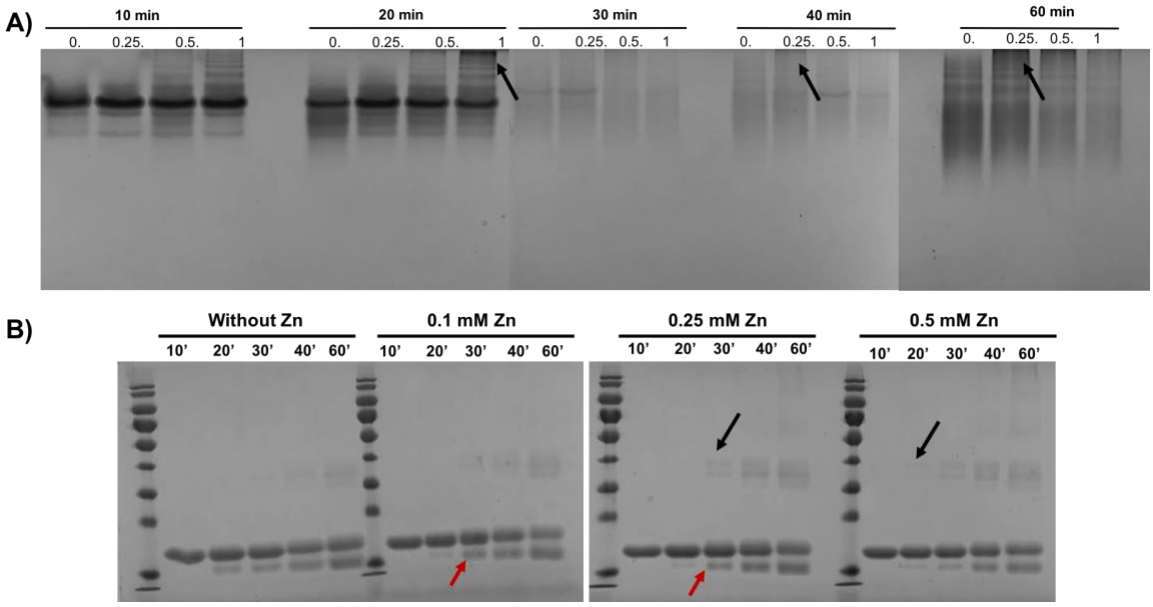

Figure 4-4: Effect of zinc on clustering FAT molecules shown in crosslinking experiments
A) Crosslinked FAT samples incubated with 0, 0.25, 0.5 and 1 mM of Zn^{2+} and run on native gel. B) Crosslinked FAT samples boiled and ran on SDS-page gels. Black arrows indicate the appearance of aggregation and red arrows indicate intramolecular crosslinking.

The same results were obtained when I incubated 0.5mg/ml of FAT with a lower range of Zn^{2+} concentrations (0.1, 0.25 and 0.5 mM) for better gel resolution. Crosslinking of

FAT molecules started to appear after 30 minutes when incubated with 0.25 mM Zn^{2+} and after 20 minutes when incubated with 0.5 mM Zn^{2+} (Figure 4-4B). These results showed that the presence of Zn^{2+} induces clustering of FAT molecules in vitro, with takes place faster when incubated with higher concentrations of Zn^{2+} increasing the association rate. Hence, findings here support the capacity of zinc to cluster FAT *in vitro*.

I next asked if FAT clustering was specific to zinc, or could also be induced by the presence of other divalent metal ions. To verify the specificity of zinc binding to FAT, I incubated 1 mg/ml of FAT with 0.5 mM of Ca2+, Mg2+ and Mn2+, and compared the result to incubation with 0.5 mM Zn^{2+}. All tested metal ions produced a crosslinking pattern similar to the control FAT incubated with 2 mM EDTA (Figure 4-5). These results demonstrated that FAT clustering is specifically induced by Zn^{2+}.

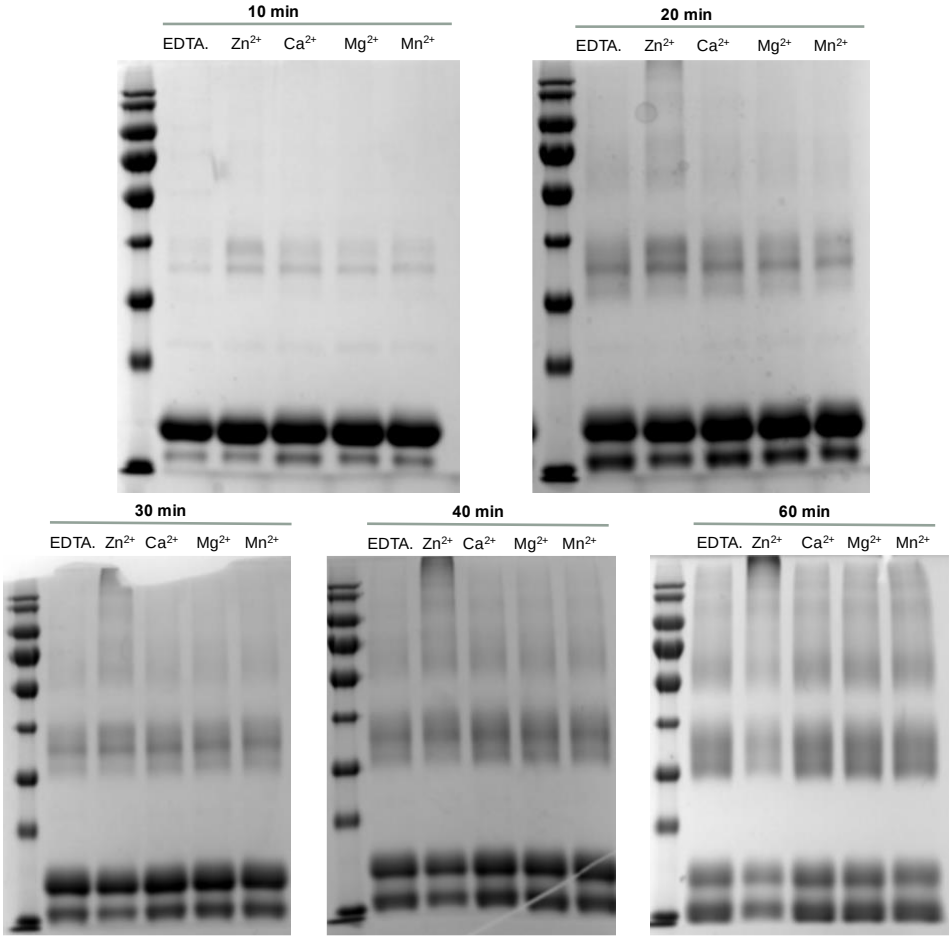

Figure 4-5: Crosslinking FAT incubated with bivalent metal ions
FAT samples incubated with zinc, calcium, magnesium and manganese of 0.5mM at pH=7.5

4.1.3 Zinc-driven clustering of FAT^{+} occurs at a lower rate at pH=7.5

I also tested the effect of zinc on the FAT^{+} domain, by incubating 1 mg/ml of protein with 0.5mM of Zn^{2+} at pH=6.5 and 7.5. In parallel, I also incubated FAT+ with other divalent metal ions to assess the specificity of Zn^{2+} binding. Crosslinking FAT^{+} samples with 8% glutaraldehyde showed that Zn-driven oligomerization of FAT molecules occurred faster for FAT^{0} than for FAT^{+}. FAT^{0} showed increased crosslinking already 10 minutes after incubation with 0.5 mM of Zn^{2+}. Conversely, FAT^{+} showed no significant

difference 10 minutes after crosslinking. The effect of zinc on FAT^{+} oligomerization started after 30 minutes where I detected less 'intramolecularly' crosslinked FAT^{+} molecules while FAT^{+} oligomerized could not penetrate the gel (Figure 4-6). Additionally, this comparative crosslinking experiment showed that the effect of zinc is more prominent at pH=7.5 compared to 6.5. I therefore propose a pH-dependent role for zinc in FAT clustering.

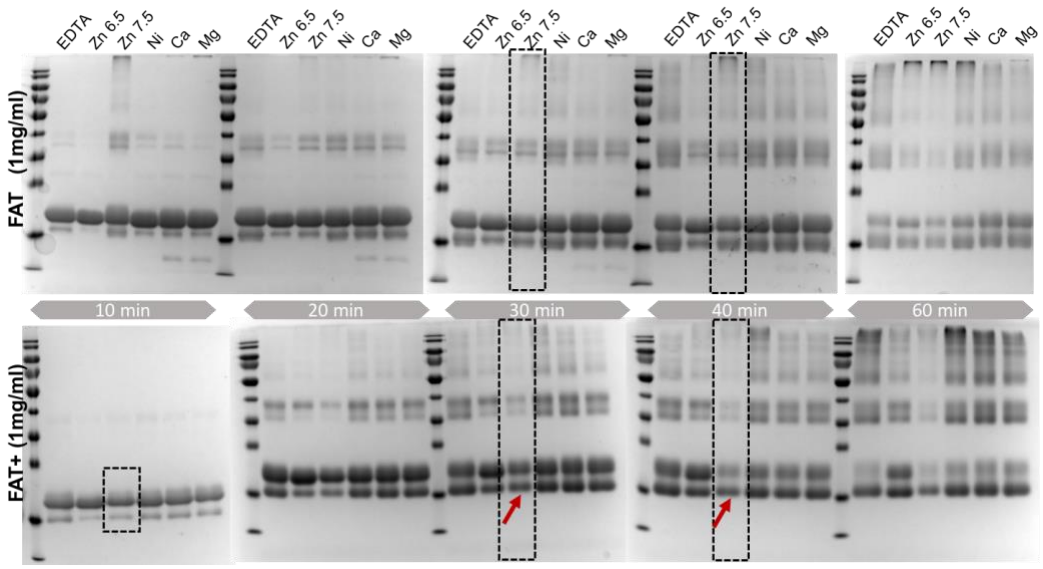

Figure 4-6: Crosslinking FAT^{0} and FAT^{+} incubated with 0.5 mM of bivalent metal ions
FAT is incubated with Zn^{2+} at pH=6.5 and pH=7.5, and with other metal ions at pH=7.5. Red arrows indicate intramolecular crosslinked FAT.

While Ca^{2+} and Mg^{2+} metal ions showed no difference in the crosslinking pattern for both FAT and FAT^{+} compared to control groups (EDTA-incubated fractions), it is worth noting that Ni^{2+} exhibited increased crosslinking compared to negative control. The capacity of nickel for inducing crosslinks is however reduced compared to zinc. This residual Ni-induced oligomerization of FAT may explain the false-positive results

(discussed later in section 5.1.2) where I observed non-specific binding of GST-FAT to Nickel beads.

4.1.4 Zinc increases autophosphorylation of FAK *in vitro*

Given that clustering of FAK molecules at the FA sites is required for FAK dimerization and autophosphorylation (Brami-Cherrier, Gervasi et al. 2014), my observations suggest that zinc may act as a cofactor for FAK activation. Both, crystallization and crosslinking require fairly high FAT concentrations. Therefore, I designed an autophosphorylation assay of full-length FAK in the presence of zinc. In this experiment, Dr. S. Hong and P. Yu, from Professor Arold's group, designed a mammalian wild type FAK separated from its GST tag by a 3C protease cleavage site. GFP-tagged FAK was transfected and expressed in HEK cells by I. Isaioglou from Professor Jasmeen Merzaban group. Cell lysate was incubated with nano-bodies (prepared by Dr Hong) and then cleaved by 3C protease overnight. Purified FAK was later incubated with kinase buffer (50 mM HEPES pH 7.5, 0.01% Brij, 10 mM $MgCl_2$, 2 mM $MnCl_2$, 0.05 mM DTT, 100 uM ATP) to test autophosphorylation of FAK. Four samples of equal volumes were prepared, to which either Zn^{2+} or EDTA were added. Phosphorylation experiment was done at 30°C for 1 hour. Then, from each sample, two equal volumes were loaded on two separate gels for western blotting with FAK antibody and p-Tyr_{397} antibody (labeled as pY397 on the figure). Full-length FAK is not very stable at 30°C and, thus, I observed FAK cleavage products. Western blot analysis showed that FAK autophosphorylation activity is increasing with increasing concentration of Zn^{2+} (Figure 4-7).

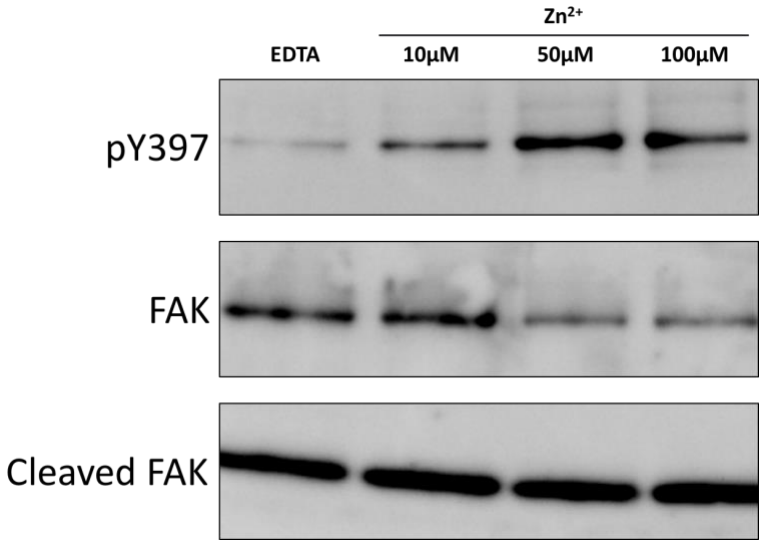

Figure 4-7: Autophosphorylation of FAK in the presence of zinc
Increasing concentration of Zn^{2+} were added onto FAK. Cleaved FAK products are presented here to indicate equal loading of protein samples.

4.2 Discussion

The crystal structure of zinc-bound FAT, and crosslinking experiments propose a novel function for Zn^{2+} in clustering the FAT domain. This finding was also supported by SAXS data which showed the appearance of larger structures in presence of zinc. Given that clustering of FAK molecules at the FA sites is required for FAK dimerization and subsequent autophosphorylation (Brami-Cherrier, Gervasi et al. 2014), these observations suggest that zinc may act as a cofactor for FAK activation.

The pH-dependency effect of zinc binding is most likely explained by the (de)protonation of the zinc coordinating residues, in particular histidines. This is not the first time a pH-dependent behavior of FAK is observed. At the level of full-length FAK, autoinhibitory FERM:kinase interactions and the catalytic activity of the kinase domain were reported to be pH sensitive (Ritt, Guan et al. 2013).

My preliminary data proposed that Zn^{2+} enhances the autophosphorylation of full-length FAK. This is not the first-time zinc is shown to influence protein kinases. The role of intracellular zinc in the activation of protein kinases has been studied especially in brain tissues. In cortical neuronal cells, zinc induces the serine/threonine liver kinase B1 (LKB1) activity stimulating AMP-activated protein kinase (AMPK) (Eom, Lee et al. 2016). In another study, researchers found that increasing exposure of Zn^{2+} induces the phosphorylation of Src family kinase which is a tyrosine protein kinase (Manzerra, Behrens et al. 2001). More recently, Anson et. al 2018 used fluorescent biosensors and single cell imaging to explore the changes of intracellular kinase signaling in neurons and detected an increase in Erk kinase activity upon increase in intracellular Zn^{2+} (Anson and Palmer 2018). In this study, I propose that zinc may play a role, along with other FA proteins, in recruiting and clustering FAK facilitating its autophosphorylation and activation.

Chapter 5 Structural Basis of FAT Binding to Ligands

Controlled activation and localization of FAK functionally links adhesion, migration and survival of the cell. To accomplish its numerous different functions, FAK acts as a versatile nanomachine that exhibits both similar functions in different cellular environments as well as different functions in similar environments. FAT domain plays an important role at the focal adhesion sites as well as in the nucleus. In this section, I aim to investigate the structural basis of FAT binding to cytoplasmic and nuclear ligands, namely Talin and MBD2.

5.1 Binding to Cytoplasmic ligands

FAK interacts with different partners at the FAs in response to extracellular stimuli. Talin is a cytoskeletal adapter protein that functions at the cell–matrix attachment sites and binds to FAK. Although paxillin was considered to be the first protein that recruits FAK to the focal adhesion sites, transfected FAK was found to also co-immunoprecipitate with cellular Talin (Chen, Appeddu et al. 1995, Zheng, Xing et al. 1998, Wang, Ballestrem et al. 2011), and depletion of Talin disrupts the localization of FAK at FAs (Wang, Ballestrem et al. 2011). These findings suggest that Talin plays a role in recruiting FAK mediating its phosphorylation and subsequent activation and localization. Conversely, Lawson et al. proposed that FAK is responsible for the recruitment of Talin to nascent adhesions (Lawson, Lim et al. 2012). The exact binding model of these two proteins is not entirely understood. In this study, I aim to investigate the interaction between FAK and Talin at the molecular level.

5.1.1 Cloning Talin F2F3

Talin is composed of a N-terminal head region (Talin-H_{1-433}) and a highly elongated C-terminal rod domain (Talin-$R_{434-2541}$) (Figure 5-1A). Talin-H comprises a FERM domain consisting of three lobes, F1, F2, and F3 (Rees, Ades et al. 1990, Garcia-Alvarez, de Pereda et al. 2003). Studies have shown that the minimal binding site of FAK lies in the F2F3 domain of Talin (Borowsky and Hynes 1998, Lawson, Lim et al. 2012), whereas other studies have presented that C-terminal 41 amino-acids of the FAT domain are sufficient for binding to Talin (Hayashi, Vuori et al. 2002). Accordingly, $Talin_{206-405}$ was cloned comprising F2 and F3 lobes of Talin, into m-pET32a. Talin F2F3 construct had the C336S mutation to improve protein stability (de Pereda, Wegener et al. 2005). Cell lysate was purified via Nickel affinity column chromatography and gel filtration (Figure 5-1A). This construct displayed a high expression yield and a size exclusion chromatography elution profile corresponding to a 25 kDa protein (data not shown) The protein was stable up to concentrations of 4 mg/ml.

5.1.2 Results

I first performed ITC titrations in which Talin and FAT samples were dialyzed in the same ITC buffer. The titration of 500µM of FAT (placed in the syringe) onto 25µM of Talin (in the measurement cell) showed no variation in the peak size over the range of injections, which indicated that there was no binding under this condition (Figure 5-1B).

In collaboration with Dr Amal Ali from Professor Merzaban group(KAUST), I then tested the ability of his-tagged Talin F2F3 to pull down FAT in an assay in which Ni-beads and His-tagged Talin were incubated with FAT for 1 hour at room temperature. A control experiment was

carried out without Talin where we expected to see no binding of FAT to Ni-beads. After several washes, Talin bound to Ni-beads failed to pull down FAT (Figure 5-2). We next performed a further analysis through immunoprecipitation assay. GST or Ni-Beads were washed with the corresponding buffer (CHAPS and Triton x-100) and incubated with both proteins overnight. We tested the ability of GST-FAT to retain His-Talin in the presence of GST beads (Figure 5-3A, left panel), and the ability of His-Talin retain GST-tagged FAT in the presence of Nickel beads (Figure 5-3A, right panel). Proteins were stained with SYBRORUBY for better sensitivity. Gel analysis revealed co-immunoprecipitation of GST-FAT with Talin bound to Ni-beads. We repeated the same experimental set-up and detected the precipitants by western blot. Using anti-His antibody, GST-FAT protein was not strongly efficient in retaining Talin from the supernatant (Figure 5-3B). However, His-Talin was able to retain FAT from the supernatant using anti-GST antibody (Figure 5-3C). To clarify the contradictory results between the simple, pull down assay and co-immuoprecipitation and western blot, we tested whether GST-FAT would bind to Ni-beads even in the absence of Talin. Ni-beads (in triton x-100 buffer) and GST-FAT were incubated with and without His-Talin and immunoprecipitation was checked by western blot using anti-GST antibody. In both samples, with and without Talin, anti-GST antibody was able to detect GST-FAT immunoprecipitated with Ni-beads (Figure 5-3C). Hence, GST-FAT bound non-specifically to Nickel beads, an observation made earlier in section 4.1.3.

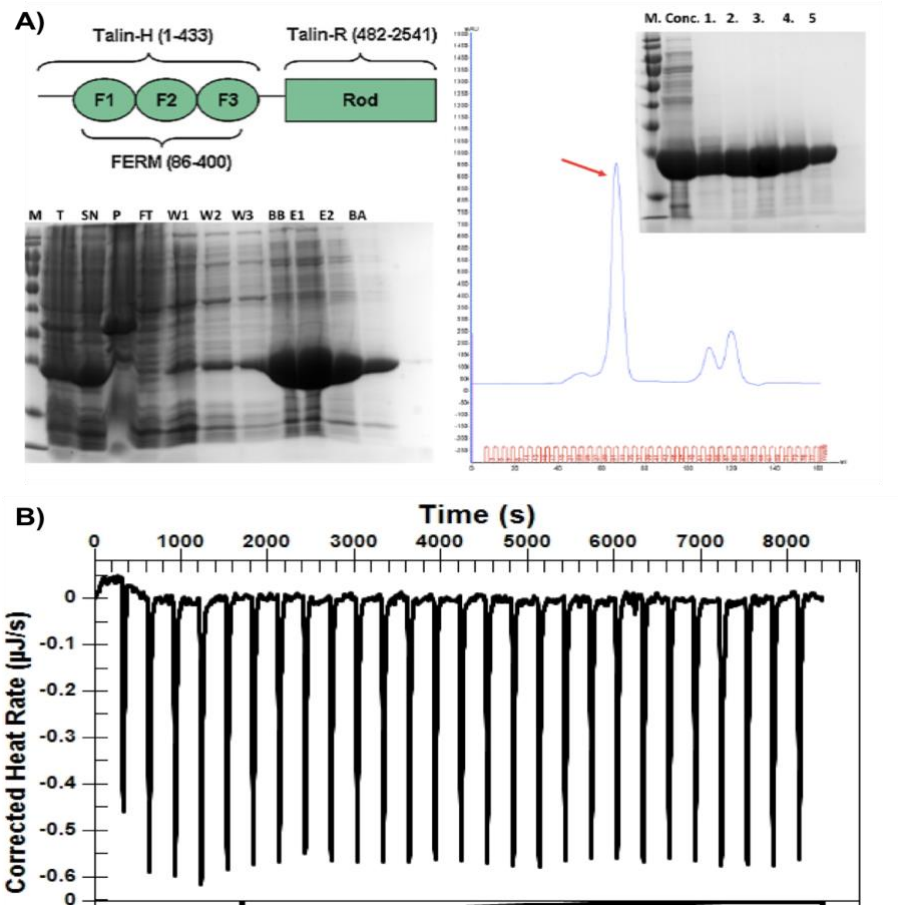

Figure 5-1: Purified Talin does not bind to FAT

A) Purification of Talin F2F3 fragment cloned into m-pET32a. domain organization of Talin full length protein. SDS-PAGE gel showing the affinity purification of MBD2 fragment 3 (M: marker, T: total cell lysate, SN: supernatant, P: pellet, Ft: flow through of proteins not bound to Ni-beads, W1-W3: washes from 1 to 3 with wash buffer, BB: sample of beads before cleavage, E1-2: eluted protein fractions 1 and 2, BA: samples of beads after cleavage). Top panel: SDS-PAGE gel showing protein fractions collected after gel filtration (lanes 1 to 5 are fraction of the peak). Lower panel: Gel filtration chromatogram, red arrow showing the protein peak. B) Plot of raw heat data shows that there is no change in the heat peaks implying no binding interactions.

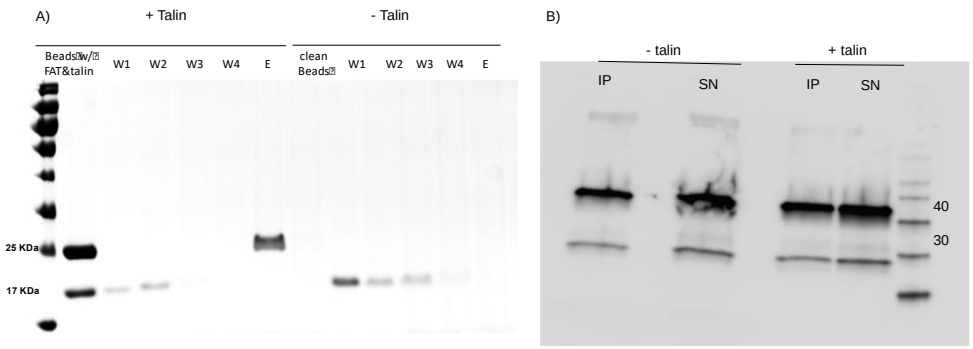

Figure 5-2: Pull down assay failed to detect binding between FAT and Talin

A) The pull-down assay was carried out by incubating Nickel beads with either his-tagged Talin and FAT or with FAT alone. Beads were directly washed 4 times and then bound protein was eluted with 400mM imidazole. B) Immuno-precipitation of Ni beads and GST-FAT incubated with and without His-Talin and detected by anti-GST antibodies revealed the unspecific binding of GST-FAT to Ni-beads (IP: immunoprecipitants, SN: supernatant).

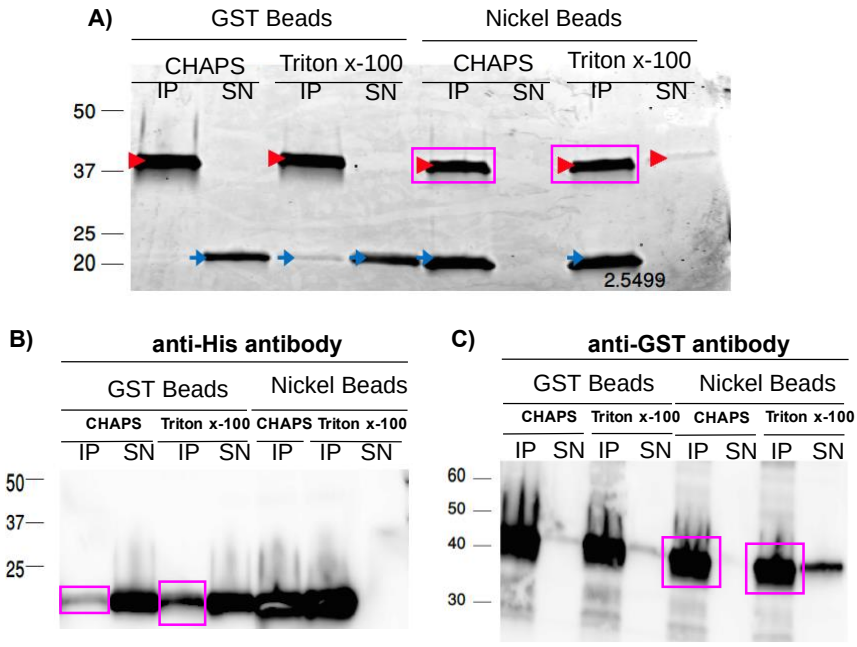

Figure 5-3: Co-immunoprecipitation experiments for FAT and Talin

A) Immuno-precipitation: Beads were washed with the corresponding buffer and incubated with proteins overnight. GST-tagged FAT was used to retain His-tagged Talin in the presence of GST beads (left panel) and His-tagged Talin was used to retain GST-tagged FAT in the presence of Nickel beads (right panel). Proteins were stained with SYBRORUBY. Red arrow is GST-FAT, blue arrow is His-Talin, and magenta boxes indicate GST-FAT immunoprecipitate with Talin. B) Western Blot using anti-His antibody shows that GST-FAT protein was not strongly efficient in fishing Talin (bordered with magenta box) while C) shows that using anti-GST antibody, His-Talin incubated with Ni-beads was able to fish FAT from the supernatant (bordered with magenta box) (IP: immunoprecipitants, SN: supernatant).

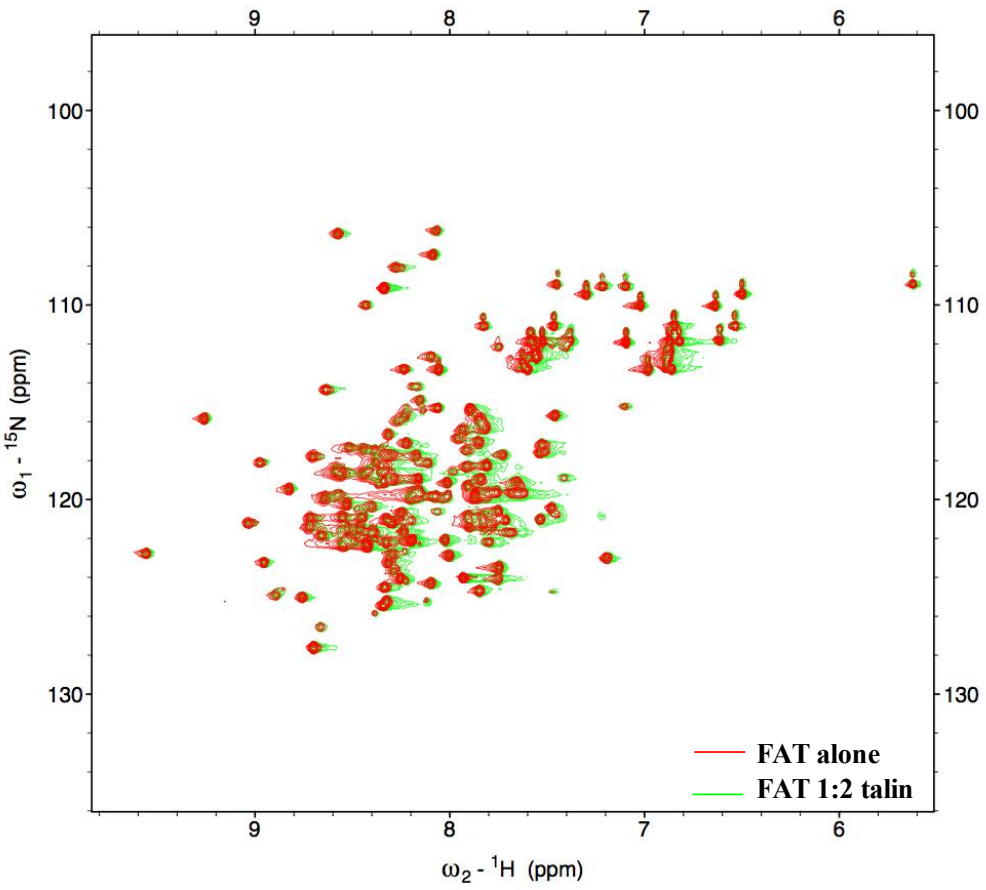

Figure 5-4: ^{1}H-^{15}N HSQC spectra for apo-FAT and FAT with Talin
The overlap of ^{1}H-^{15}N HSQC experiments shows no significant changes in the chemical shifts of FAT incubated with Talin at ratio 1:2 (red spectrum for apo FAT, green spectrum for FAT with Talin at ratio 1:2).

Collectively, these assays did not support that Talin and FAT interact under the conditions tested. Finally, I assessed the Talin-FAT interaction by NMR, through monitoring the change in CSPs of ^{15}N-labelled FAT incubated with Talin in ^{1}H-^{15}N HSQC experiments. 90µM of ^{15}N-labeled FAT was incubated with Talin at molar ratios of 1:0.5, 1:1 and 1:2. Consistent with the pull-down and ITC experiments, ^{1}H-^{15}N HSQC did not exhibit significant changes in the chemical shifts of FAT that was incubated with Talin when compared to apo-FAT (Figure 5-4, only 1:2 ratio is shown here).

5.2 Binding to Nuclear ligand: MBD2

In addition to its roles at the cellular adhesions, FAK translocates into the nucleus where it binds to nuclear proteins and affects gene expression. By shuffling between the nucleus and the cell membrane, FAK can rely signals from the extracellular matrix and focal adhesions into the nucleus and affecting gene regulation (Lim 2013). Several physiological and chemical nuclear localization signals allow shuttling of FAK from the cytoplasm to the nucleus. Stress signals (such as oxidative stress), cell de-adhesion from the matrix and FAK inhibition are the main factors promoting FAK nuclear localization (Zhou, Yi et al. 2019). FAK encompasses a lysine-rich nuclear localization signal (NLS) in the F2 lobe of the FERM domain and leucine-rich nuclear export signal (NES) in the kinase domain. FAK in its kinase inactive form exposes its NLS while the NES is masked by the FERM:Kinase interaction thus allowing FAK retention in the nucleus (Lim 2013). Upon FERM-mediated transfer into the nucleus, FAK binds to p53 transcription factor and recruits E3 ubiquitin-protein ligase Mdm2 promoting p53 degradation thus inhibiting p53-mediated gene regulation (Golubovskaya, Finch et al. 2005, Lim, Chen et al. 2008). In addition, nuclear FAK exerts anti-inflammatory effects by mediating the degradation of GATA4 and thus inhibiting the expression of vascular cell adhesion factor-1 (VCAM-1) (Lim, Miller et al. 2012). While binding to p53 and GATA4 is mediated via direct binding to the FERM domain of FAK, binding to another nuclear protein, MBD2, is mediated through FAT (Luo, Zhang et al. 2009).

Another nuclear FAK ligand is the methyl CpG-binding domain protein 2 (MBD2) that binds to FAK through its FAT domain. MBD2 binds methylated CpG-islands on the DNA and recruits HDAC1, thus regulating histone acetylation and chromatin structure (Bird and Wolffe 1999, Leonhardt and Cardoso 2000). Binding of FAK to MBD2 is thought to reduce HDAC1 recruitment and, therefore, may influence regulation of chromatin structure and, subsequently, gene expression (Luo, Zhang et al. 2009). The molecular basis of this interaction is not fully understood. Expression of different fragments of MBD2 in yeast, *in vitro* and in mammalian cells revealed that the GC-rich region and the methyl binding domain (MBD) are sufficient to bind to the FAT domain (Luo, Zhang et al. 2009).

5.2.1 Cloning MBD2 fragments

To unveil the structural basis of this interaction, I designed MBD2 fragments of different lengths to test their binding affinities to FAT. MBD2 full length protein comprises a highly-disordered N-terminus with (glycine-arginine) GR repeats, a methyl binding domain (MBD) and a C-terminal coiled-coil (CC) region. I designed different MBD2 fragments to check the minimal binding site to FAT. MBD2 fragment 1 ($MBD2_{39-216}$) covers most of the GR-rich N-terminus and MBD, fragment 2 ($MBD2_{121-216}$) contains a shorter GR-rich region along with MBD, whereas fragment 3 ($MBD2_{146-216}$) constitutes solely the MBD (Figure 5-5 presents the fragments).

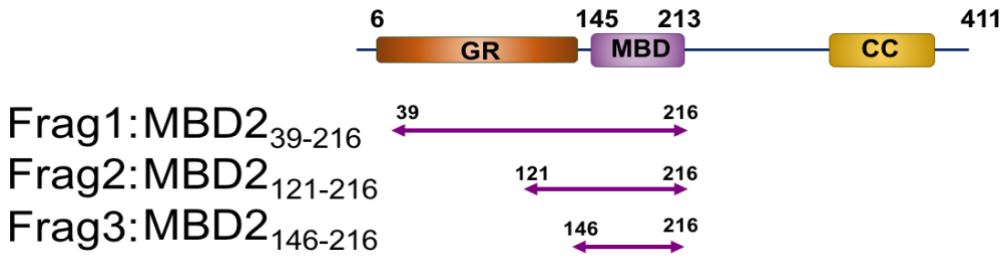

Figure 5-5: Design of MBD2 fragments

Cloning these fragments and the full-length protein proved to be difficult. Initially, constructs were cloned into pET28b vector with a His-tag. Only fragment 2 was successfully cloned, expressed and purified.

I next cloned the full-length protein into a pGEX6P1 vector with a GST-tag. The full-length clone was successfully transformed into BL21 cells, but expression tests failed. Cloning the full-length protein into MBP vector failed. The molecular weight of the resulting expressed full length MBD2 (≈42 KDa) was very close to that of MBP (38 KDa). The mass spectrometry analysis detected MBP protein for the band that was expected to be the targeted full length MBD2 expressed after inducing the cells.

The following approach was to clone MBD2 fragments and full length into pET32a vector as conducted by Desai et al. in (Desai, Webb et al. 2015). This approach was more successful and I was able to clone MBD2 full length and shorter fragments (Table 5-1 presents the details of these constructs). Four constructs have now been cloned, yet only MBD2 fragment 2 and 3 showed good expression yields and were purified. After cell lysis and centrifugation, the lysate was incubated with Nickel beads. Elution was

done by incubating cell lysate with 3C-protease to cleave MBD2 fragment from bound thioredoxin (Trx) and His-tags. For further purification, eluted protein was then applied to a gel filtration column (fragment 2 purification profile is shown in Figure 5-6).

Table 5-1: Molecular parameters of MBD2 fragments and full length

Protein	length	# of amino acids	Molecular weight	Extinction coefficient	Ip	Special amino acids
Full MBD2	1272	413	43390	26470	10.06	6C, 4W
MBD2 frag1	576	182	18431	15470	11.79	3C, 2W
MBD2 frag2	330	100	10840	9970	10.33	1C, 1W
MBD2 frag3	258	85	9430	9970	9.81	1C, 1W

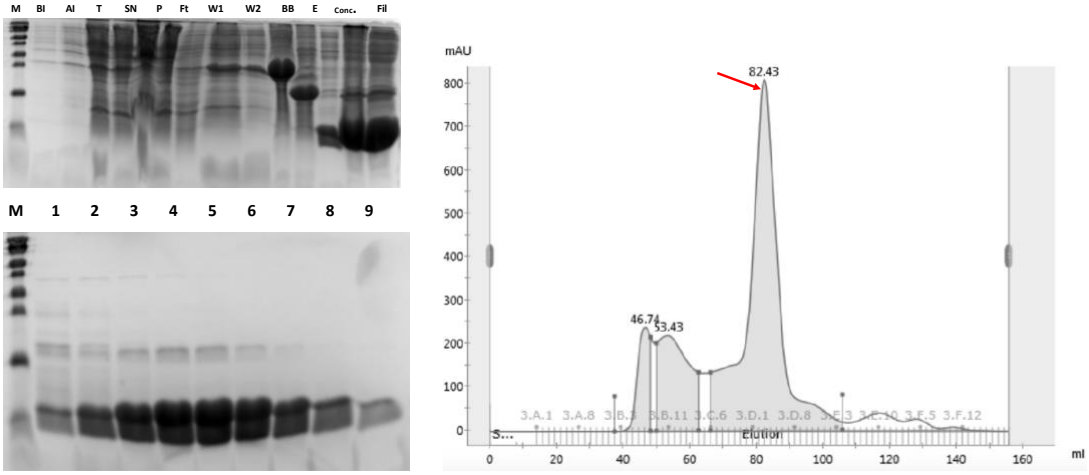

Figure 5-6: Purification of MBD2 fragment 3 cloned into pET32a vector

A) SDS-PAGE gel showing the affinity purification of MBD2 fragment 3 (M: marker, BI: before induction, AI, after induction, T: total cell lysate, SN: supernatant, P: pellet, Ft: flow through of proteins not bound to Ni-beads, W1-W3: washes from 1 to 3 with wash buffer, BB: sample of beads before cleavage, BA: samples of beads after cleavage, E: eluted protein, Conc: concentrated eluted protein, Fil: sample of filtered protein before gel filtration run. B) SDS-PAGE gel showing protein fractions collected after gel filtration (lanes 1 to 9 are fraction of the peak). C) Gel filtration chromatogram, red arrow showing the protein peak.

5.2.2 MBD does not bind to $FAT_{892\text{-}1052}$ in vitro

I first performed ITC titrations in which MBD2 fragments 2 and 3 were dialyzed in the same ITC buffer with $FAT_{892\text{-}1052}$. The titration of 100 µM MBD2 fragments onto 10 µM FAT showed no variation in the peak size over the range of peptide injections (Figure 5-7), which indicated that there was no binding with an affinity higher than ~10-20 µM under my experimental conditions. To test if binding between FAT and MBD2 constructs occurred at lower affinities, I used NMR ^{1}H-^{15}N HSQC titration experiments as a robust and sensitive tool for testing low-affinity protein-protein interactions. However, the titration of MBD2 fragments 2 and 3 into 100 µM FAT showed no significant changes in the overlapped ^{1}H-^{15}N HSQC spectra (Figure 5-8).

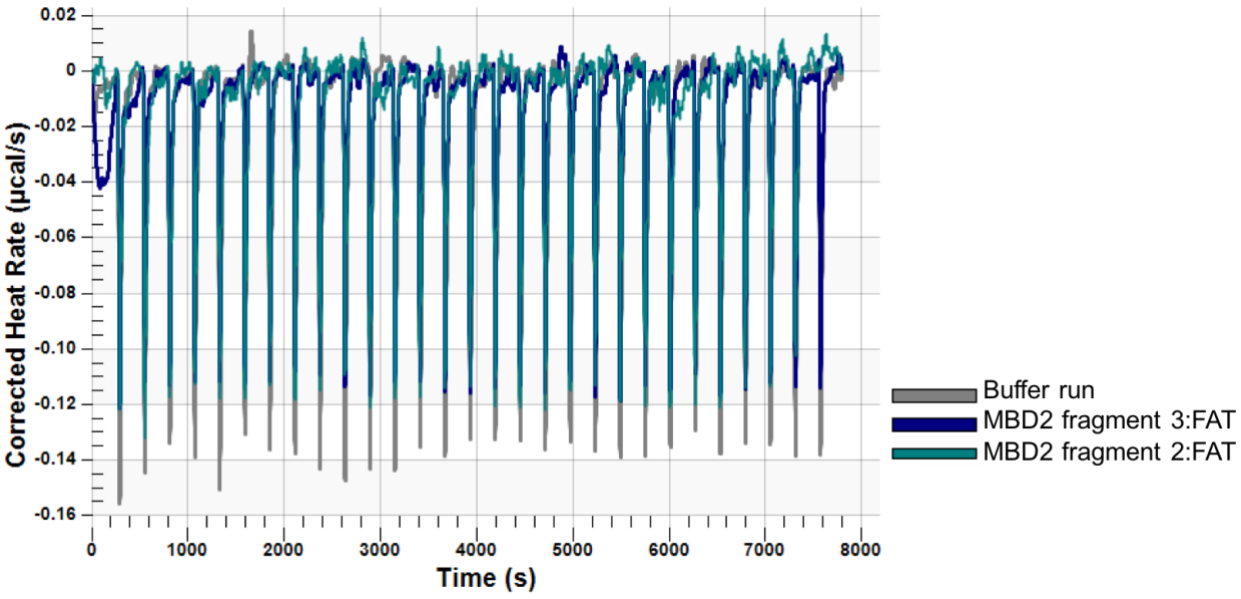

Figure 5-7:Figure 5 7: ITC shows no binding between MBD2 fragments 2 and 3 with the FAT domain.

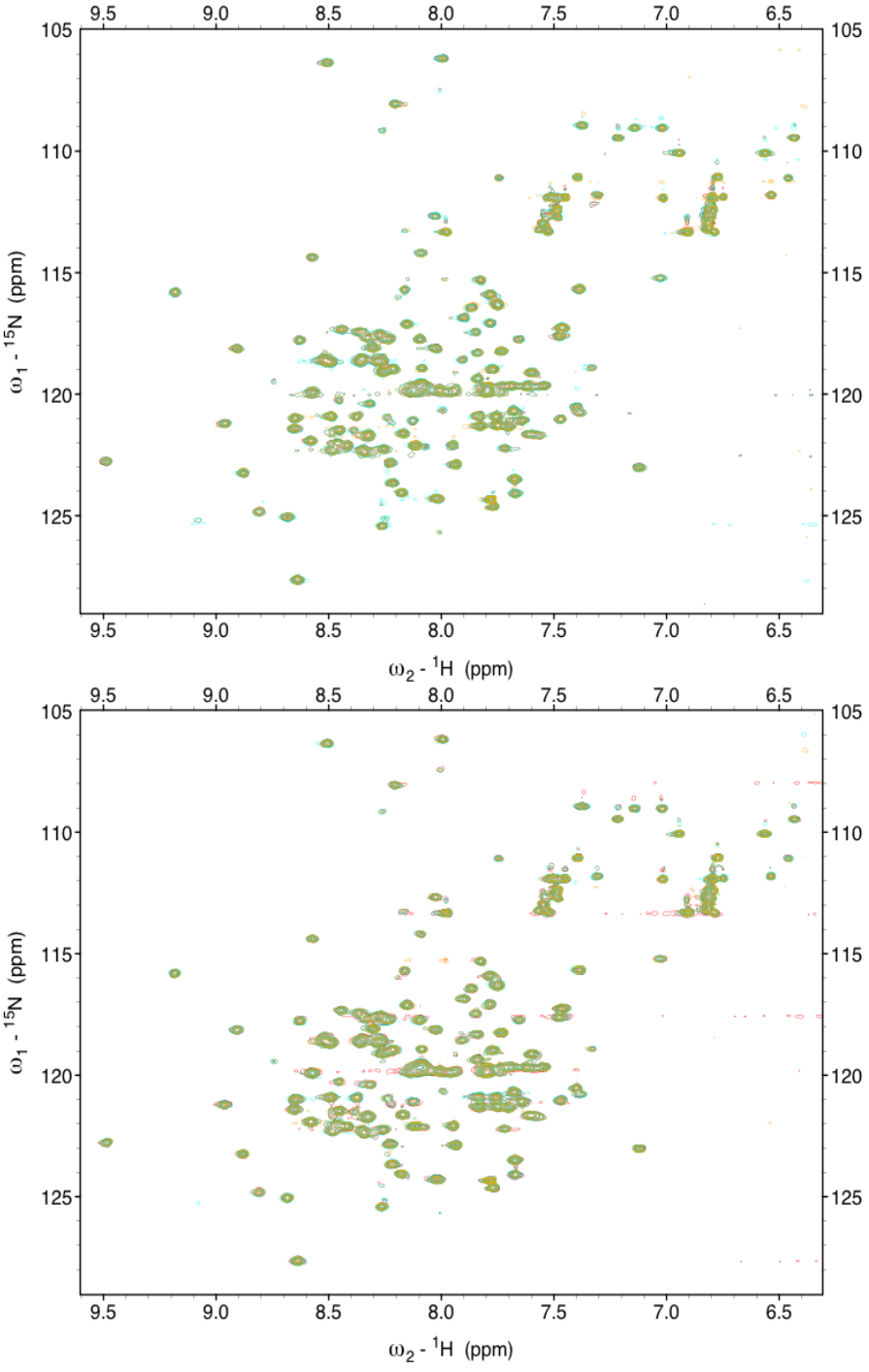

Figure 5-8: NMR Titrations of FAT and MBD2

Overlay of ^{1}H-^{15}N-HSQC spectra of 100 µM ^{15}N-FAT in the absence (red) and presence of 0.2 (green), 1 (cyan) and 4 (yellow) times molar excess of MBD2 fragments. Top panel shows titrations of MBD2 fragment 3 and bottom panel shows titrations of MBD2 fragment 2 into the FAT domain.

Luo and his group have shown evidence of the FAT domain interaction with MBD2 both in yeast cells as well as *in vitro*. However, the shortest FAT construct used in their assay included the proline rich regions (PR) in the Kinase-FAT linker (Luo, Zhang et al. 2009). I, hence, questioned whether the longer FAT constructs expressed using BL21 expression system is essential for FAT:MBD2 interactions. Accordingly, $FAT_{849\text{-}1052}$ containing PR2 and $FAT_{800\text{-}1052}$ containing both PR1 and PR2 were cloned into pJEx41 vector. Preliminary ITC titrations of these longer FAT constructs with MBD2 fragment 2 and 3 did not show binding (Figure 5-9). However, more experiments would be needed to conclude on the role of PR regions in the interaction between FAT and MBD2.

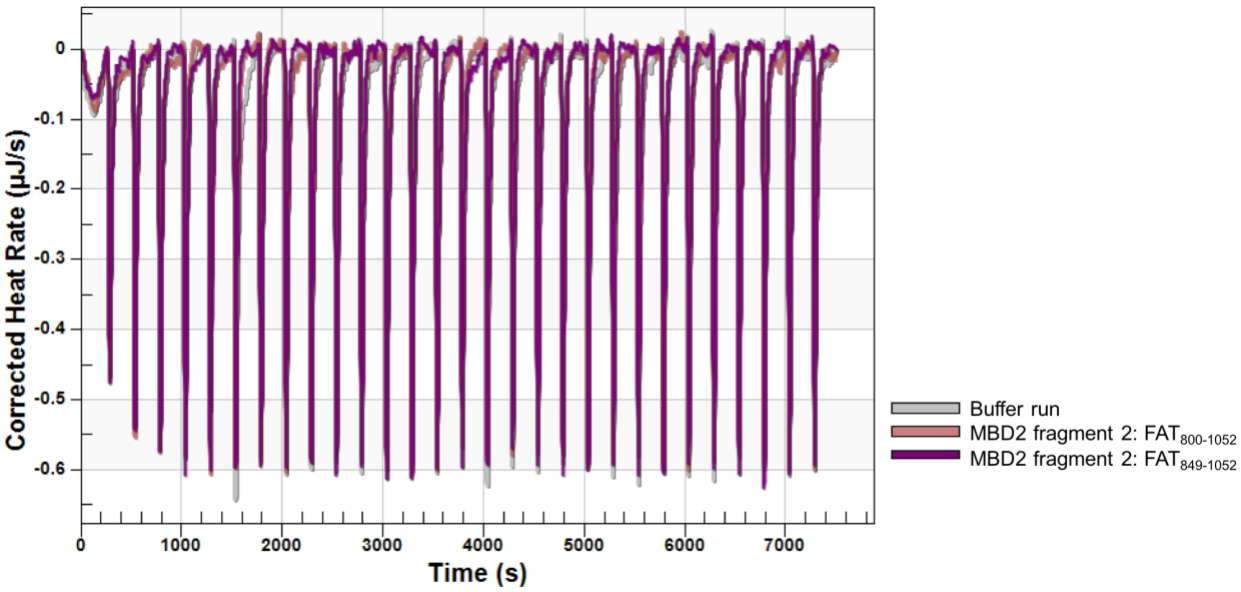

Figure 5-9: ITC shows no binding between MBD2 fragment 2 with longer FAT constructs

5.3 Discussion

In this chapter, I aimed at deciphering the interaction between the FAT domain and two of its ligands, cytoplasmic talin and nuclear MBD2. These binding partners are described in the literature; however, the structural basis of these interactions is not fully understood.

First, in *vitro* co-immunoprecipitation, ITC and HSQC titrations failed to detect an interaction between our recombinant FAT domain and the Talin F2F3 head. Although these findings were not consistent with previous published work, *in vitro* binding experiments for FAK and Talin, in which both were recombinant proteins, were not performed previously. Rather, the interaction between FAK and Talin was detected through binding assays carried out in cell cultures, or involving proteins obtained both from cellular lysates, or from the transfection of one recombinant protein in cells that endogenously express the other protein (Chen, Appeddu et al. 1995, Borowsky and Hynes 1998, Zheng, Xing et al. 1998, Hayashi, Vuori et al. 2002, Wang, Ballestrem et al. 2011, Lawson, Lim et al. 2012). These studies have also tentatively mapped the FAT:Talin interaction. Initially, Chen et al. proposed the C-terminal residues 965 to 1012 of the FAT domain are sufficient for binding to Talin (Chen, Appeddu et al. 1995). Later, Lawson et al. showed that FAT E1015A mutation disrupts recruitment of Talin to nascent adhesions (Lawson, Lim et al. 2012). Additionally, $Talin_{225-357}$ has been described as the minimal FAK binding site on Talin, while a Talin construct containing additional residues, $Talin_{186-357,}$ binds to FAK with higher affinity (Borowsky and Hynes 1998).

Conversely, Cooley et al. were not able to detect an interaction between FAK and Talin using co-immunoprecipitation techniques for cellular proteins nor using *in vitro* binding assays with GST-fusion proteins (Cooley, Broome et al. 2000). Interestingly, the only *in vitro* binding assay reporting FAK:Talin interaction involved *in vitro* translated FAK and GST-fusion Talin fragments (Lawson, Lim et al. 2012). These observations may indicate that the interaction requires additional cellular partners. It is also possible that post-translational modification necessary for protein-protein interaction. To address these possibilities in future experiments, we plan to carry out co-immunoprecipitations with our recombinant proteins that were incubated with cell lysate. In addition, in vitro translation of Talin and/or FAT can be performed using eukaryotic machinery to account for post-translational protein modifications.

On the other hand, I was also unable to reproduce binding between the FAT domain and MBD2 fragments. Using pull-down and co-immunoprecipitation assays, Luo and his group provide evidence of FAK:MBD2 interactions through binding of the FAT domain of FAK to the MBD domain of MBD2. In this study, I used BL21-expressed recombinant proteins to study this interaction at the atomic level and for binding site mapping. *In vitro* biophysical binding assays showed that $FAT_{892-1052}$ does neither bind to $MBD2_{146-216}$ nor to a longer MBD2 construct containing a short GR-rich region along with MBD ($MBD2_{121-216}$) under the experimental conditions used. These observations may be explained by two hypotheses. Firstly, the prokaryotic expression system used does not allow post-translational modifications needed to allow binding between the two

domains since Luo et al. used the mammalian expression system in their assays (Luo, Zhang et al. 2009). In addition, it is probable that the domain boundaries considered in this study do not harbor the minimal binding surface of interaction needed. Based on a single type of ITC experiment, we cannot rule out completely a role of the PR regions of the linker N-terminal to FAT, and other binding experiments are needed to confirm my observation. Equally important is the intrinsically disordered region (IDR) of MBD2 which is connecting MBD to the CC domain of MBD2. IDRs can act as a center for various protein interactions (Tompa 2012). Intriguingly, IDR of MBD2 is vital for the recruitment of histone deacetylase core components of the Nucleosome Remodeling and Deacetylase complex (NuRD) (Desai, Webb et al. 2015). Indeed, all MBD2 constructs used by Luo et al. encompassed the IRD. Consequently, I hypothesize that FAT, with the N-terminal PR motifs, binds to the MBD and IRD of MBD2, thus competing for the binding site of HDAC1, hampering its recruitment and inhibiting heterochromatin formation and gene repression.

Within a role of FAK in cancer, it will be interesting to identify the surface of interaction between FAT and nuclear MBD2 to have better understanding of the regulatory mechanisms of FAK on gene expression. Moreover, answering these research questions would help us understand the sequence of FAT binding events and thus the decision between regulation of focal adhesion dis/assembly and gene expression.

Chapter 6 Concluding Remarks

Owing to its crucial functions in embryogenesis and tumorigenesis, FAK is the center of attention for many research groups, including the Arold group. FAK acts primarily as a scaffold protein that bridges protein complexes but possesses a kinase-dependent set of activities. Different regulation mechanisms tightly control each of the many functions of FAK. The FAT domain of FAK, the focus of my study, adapts different conformational structures and is thus implicated in inter- and intramolecular interactions that control FAK localization and activation. In the present study, I combined biophysical and structural methods to understand site-specific dynamics of FAT and to investigate binding of key FAT ligands embedded at focal adhesion sites or in nuclear complex structures. The tentative molecular dynamics that are proposed by my NMR studies for alternatively-spliced FAT isoforms, combined with G. Kadaré et al. findings, suggest mechanistic insights about environment-dependent FAK functions. I here suggest that the proposed change in the flexibility of the loop N-terminal to FAT domain may add a level of control neuronal activation of FAK. These functions may also require the engagement of small second messengers. My findings suggest that FAT interaction with zinc may provide an enigmatic alternative way for clustering and thus activation of FAK in specific environments. Conversely, and in the absence of FAK clustering, FAK is expected to adopt a kinase-inhibitory conformation and serve as an assembly platform. This regulatory mechanism could explain the roles of FAK in the nucleus. My results suggest that binding of FAK to the nuclear MBD2 protein is more complex than the

involvement of only the FAT and MBD domains, and that IDR may be crucial for this interaction. More studies are needed to decipher the means of this interaction at the atomic level in order to explain whether this binding disrupts the FERM:FAT interaction and enhances FAK translocation into the nucleus. By describing the temporal interaction between FAK and cytoplasmic and nuclear ligands, we can help dissecting some facets of FAK functional heterogeneity and interactions. In this project, we add to the emerging understanding of how a competition of ligands can lead to site-specific modulation of FAT's interactions and affect its capacity to dimerize/cluster FAK, contributing to site-specific FAK activation. These understandings pave the way for well-defined targeting of FAK:ligand inhibitors and drug designs that selectively disrupt site-specific interactions in FAK-overexpressed cancer cell types.

Chapter 7 Materials and Methods

7.1 Cloning

The F2F3 lobe (206-405) of Talin FERM domain and full length MBD2 genes were codon optimized for bacterial expression and synthesized by Invitrogen (Thermo Fisher Scientific). Talin F2F3 domain had C336S mutation to improve protein stability and was cloned into a modified pET32a-m vector using the following oligonucleotides 5'-AAAACCTATGGTGTTAGCTTTTTTCTG-3' and 3'-ATAACTGTAATAAGACTTTTTCTTTTTTAGTATT-5' then transformed into *E. coli* BL21 (DE3). MBD2 Full length and smaller fragments were cloned into pET23a vector via Gibson cloning method using the following oligonucleotides: 5'-ATTGGATCCCTGGAAGTTCTGTTCCAGGGGCCCCTGCGTGCACATCCGGGTGGTGGT-3' and 5'-ATTCTCGAGTTATCATGCTTCATCACCGCTATCCATTT-3' for full length, 5'-ATTGGATCCCTGGAAGTTCTGTTCCAGGGGCCCCTGAGCGCACTGGCACCGAGTCCG-3' as a forward primer for fragment 1, 5'-ATTGGATCCCTGGAAGTTCTGTTCCAGGGGCCCCTGGCACCGCGTCGTGAACCGGTT-3' a forward primer for fragment 2, 5'-ATTGGATCCCTGGAAGTTCTGTTCCAGGGGCCCCTGGAAAGCGGTAAACGTATGGAT-3' a forward primer for fragment 3 and 5'-ATTCTCGAGTTATTTGCTCGGCATCATTTTACCGGTAC-3' as a reverse primer for the three fragments. Plasmids of MBD2 full length and smaller fragments were transformed into *E. coli* BL21 (DE3). His-tagged FAT (892-1052), FAT+/FAT isoform5 (892-1055), FAT (849-1052) and FAT (800-1052) were cloned by Twist Bioscience supplier in pJEx411c vector.

7.2 Protein expression and purification

FAT domain of human FAK (892-1052) and FAT-plus domain of rat FAK (891-1055) were expressed as GST-fusion proteins in *E. coli* BL21 using the expression vector pGex-6P2. Bacteria were grown in LB medium. FAT and FAT-plus were expressed at 37°C for 3h

while FAT (849-1052) and FAT (800-1052) were expressed at 30°C for 6h. MBD2 fragment 2 and 3 were expressed at 20°C overnight.

For purification, cells were thawed and lysed by mild sonication. Cell debris was removed by centrifugation. Lysates containing FAT and FAT-plus GST-fusion proteins were incubated with Glutathione Sepharose 4B beads (GE healthcare). The beads were thoroughly washed with 20 mM Tris-HCl (pH 8.0), 1 M NaCl, 2 mM EDTA, and 2 mM DTT. Beads were resuspended in 20 mM Tris-HCl (pH 8.0), 150 mM NaCl, 2 mM EDTA, and 2 mM DTT. Bound protein was incubated for 2 hr at room temperature with recombinant 3C protease.

Lysates containing His-tagged proteins were incubated with Ni-NTA agarose (invitogen). The beads were thoroughly washed with 20 mM HEPES (pH 7.5), 500 mM NaCl and 10mM imidazole. Beads were resuspended in 20 mM HEPES (pH 7.5) and 350mM NaCl and bound protein was incubated for 2 hr at room temperature with recombinant 3C protease. Eluted protein was dialyzed overnight with 20 mM HEPES (pH 7.5), 350mM NaCl and 2mM EDTA. Protein eluted from the affinity columns was further purified by size-exclusion chromatography using a Superdex 75 column (GE healthcare).

7.3 Peptides

Peptides were purchased from GenScript with the following sequences: PWR (EGVKPWRLQPQE), LD4 (SASSATRELDELMASLSD), LD2 (NLSELDRLLLELNAVQ), LPP (AEIDSLTSILADLESS), CD158 (DPTRDLKQLLQELRSVIN), DLC1(PEL0DDILYHVKGMQRIVNQWSEK) and Scramble (LSDAMETSSLRDALE).

7.4 Isothermal titration calorimetry

To titrate PWR peptide onto FAT, protein was dialysed in ITC buffer (100 mM HEPES pH 7.4, 150 mM NaCl, 2mM EDTA, 1mM TCEP). 1.5 ml of FAT solution was placed in the cell at a concentration of 50 μM. PWR peptide was dissolved into the dialysis buffer to a concentration of 500 μM and placed in the injection syringe. Titration were performed

at 18°C with an initial injection of 2 µl, followed by 23 injections of 10 µl. As a control, the peptide was titrated into the buffer and the resulting heats subtracted from the protein-binding curve. To titrate FAT onto Talin, proteins were dialyzed in ITC buffer (20mM Phosphate buffer pH=7, 100mM NaCl, 2mM EDTA, 1mM TCEP). 1.5 ml of Talin was placed in the cell at a concentration of 25 µM. FAT at 400 µM concentration was placed in the injection syringe. For FAT:MBD2 titrations, proteins were dialyzed in 20 mM HEPES pH 7.5, 150 mM NaCl and 0.5 mM TCEP. 1.5 ml of FAT constructs were placed in the cell at a concentration of 20/10/5 µM. MBD2 fragments at 200/100 µM concentration were placed in 250 µl injection syringe

Titration were performed at 15°C with an initial injection of 2 µl, followed by 23 or 30 injections of 8 µl. ITC was performed on a Nano ITC from TA Instruments, and data were fitted using NanoAnalyze Software.

7.5 Microscale Thermophoresis

For FAT dimerization and FAT:FERM interactions, the recombinant fragment of 8xHis-$FAK_{(892\text{-}1052)}$, and 6xHis-$FAK^{+}_{(892\text{-}1055)}$ were labelled with the His tagged labelling kit Red-tris-NTA 2nd Generation provided by the manufacturer at 50 nM and kept in 1xPBS-T. The unlabeled proteins (50 µM) were serially diluted in the same buffer accordingly. For FAT:LD motifs interactions, the labelled peptides were diluted in 20 mM HEPES, 150 mM NaCl, 1 mM TCEP, 2 mM EDTA 0.05% Tween-20 at pH 7.5. Labelled peptides were added to a final concentration of 50 nM and mixed at 1:1 ratio with serially diluted FAT isoform (330 µM as highest concentration). The measurements were performed at 60% LED power and 40% MST power in MST Premium Capillaries on a Monolith NT.115 device at 25 °C (NanoTemper Technologies). Thermophoresis analysis was done using MO. Affinity Analysis software provided by NanoTemper.

7.6 Crosslinking

Crosslinking experiments were designed similar to the hanging drop crystallization experiment. Protein samples with varied concentrations (0.5 to 2 mg/mg) were incubated with metal ion solutions (Zn^{2+}, Ca^{2+}, Mg^{2+} and Mn^{2+}) or 2 mM EDTA (for control samples) for 2h at room temperature. 10 µl of 6-8% (v/v) glutaraldehyde and 10 µl of the protein solution were placed onto a siliconized glass circle coverslip so that the protein and the crosslinker form two hanging drops inside the wells of VDX plate with sealant. The coverslip was sealed by the grease applied to the rim of the well to ensure an isolation of the system from the environment. Plates were left at room temperature for different time intervals (10, 20, 30, 40 and 60 min). Crosslinked protein samples were then run on native gels for 2h in the cold room or on SDS–PAGE gels.

7.7 Gel-shift assay

Protein samples of 0.1 to 6mg/ml were incubated with 0.1, 0.5 or 1mM of Zn^{2+} for 2h at room temperature and then run on native gels for 2h in the cold room.

7.8 Pull-down assay

Simple Pull-down assay was carried out by incubating Nickel beads with either Talin and FAT or with FAT alone. Beads were directly washed 4 times with washing buffer (50mM HEPES pH=7.4, 150mM NaCl, 10% Glycerol and 1% triton-x) and bound protein was eluted with 400mM imidazole.

7.9 Immunoprecipitation and western blot

Beads were washed with the corresponding buffer and incubated with proteins overnight. GST-tagged FAT was used to fish out His-tagged Talin in the presence of GST beads and His-tagged Talin was used to fish out GST-tagged FAT in the presence of Nickel beads. Proteins were run on gels and stained with SYBRORUBY or Invision His-tag or analyzed by western blot using anti-His antibody or anti-GST antibody. Buffers,

staining solutions and anti-GST antibody were offered by Prof. Jasmeen Merzaban and experiments were carried out in her lab.

7.10 Single angle X-ray scattering

All our SAXS experiments were carried out at the SWING beamline at SOLEIL synchrotron, France. Data were analyzed by using ATSAS- primus and and plotted using sasplot.

7.11 X-ray crystallography

Screening for FAT-plus crystals was carried by Alois Bräuer in the Technical University of Munich (TUM). Diffraction data were recorded at the SOLEIL beamlines PROXIMA I and IIA.

7.12 Nuclear Magnetic Resonance

Cells were grown with ^{15}N-NH_4Cl and $^{13}C_6H_{12}O_6$ dissolved in M9 minimal media solution, induced at OD=0.8 with 300uM IPTG and harvested after incubation overnight at 20°C (293.12 K). Protein samples were purified and NMR samples were prepared by dissolving the ^{15}N-labeled protein in a 10% D_2O/90% H_2O solution in the conditions described in the table below.

Study	transmitter frequency	experiment	Protein conc.	Solution conditions
FAT assignment	950 MHz	^{1}H-^{15}N HSQC, HNCA, HNCO, HNCABA, HN(CO)CA, HN(CA)CO	100 μM	20mM HEPES pH=7.5 and pH=6.5, 150mM NaCl
FAT^{+} assignment	950 MHz	^{1}H-^{15}N HSQC, HNCA, HNCO, HNCABA, HN(CO)CA, HN(CA)CO	80 μM	20mM HEPES pH=7.5 and pH=6.5, 150mM NaCl
Assignment confirmation	950 MHz	3D ^{1}H-^{15}N NOESY	550 μM	20mM HEPES pH=6.5, 100mM NaCl

Zn^{2+} titrations	700 MHz	^{1}H-^{15}N HSQC	100 μM	20mM HEPES pH=7.5 and pH=6.5, 150mM NaCl
MBD2 and Talin titrations	700 MHz	^{1}H-^{15}N HSQC	100 μM	0mM HEPES pH=7.5, 150mM NaCl, 1mM TCEP
LD motif titrations	700 MHz	^{1}H-^{15}N HSQC	100 μM	20mM HEPES pH=7.5, 150mM NaCl, 2mM EDTA and 2mM DTT

The samples were stable over the course of the NMR experiments. The 2D ^{1}H-^{15}N HSQC titrations (FERM, Zn^{2+}, MBD2 and Talin), 3D ^{15}N-resolved NOESY and triple resonance experiments of FAT and FAT^{+} were performed at a temperature of 25 ^{o}C using a Bruker Avance III 950 MHz NMR spectrometer equipped with a triple resonance inverse TCI CryoProbe. Spectra were acquired with 2048 (^{1}H) × 200-256 (^{15}N) complex points, a spectral width of 16 ppm for ^{1}H, 40 ppm for ^{15}N and 30 ppm for ^{13}C, and averaged for 36-88 scans depending on sample concentration (80 to 100 μM). ^{1}H-^{15}N HSQC spectra analysis was done using NMRFAM-SPARKY v1.4 software (Lee, Tonelli et al. 2015) while backbone assignments were done using CARA v1.8.4 software (Keller 2005). Changes in chemical shifts for ^{1}H and ^{15}N were measured in ppm (δH and δN) where we multiplied the ^{15}N shift changes by a scaling factor α=0.2, and then calculated the total change in chemical shift perturbation $(CSPi) = \Delta HN = \sqrt{\frac{1}{2}[\delta_H^2 + (\alpha.\delta_N^2)]}$ (Williamson 2013).

7.13 Data-driven molecular docking

The data-driven HADDOCK 2.1 protocol (van Zundert, Rodrigues et al. 2016) was used to generate the models of complexes for FAT:CCDC158 and FAT:LPP. Crystal structures of FAT (1ow8 and 1ow7) were used for the modelling. Initial models for CCDC158 and LPP were modelled in helical form based on the LD4 peptide. The NMR chemical shift perturbation (CSP) data was used to define the residues, which could be potentially involved in the binding known as active residues. The residues 915, 926, 929, 933, 934,

936, 938, 940, 956, 1031, 1032, 1033, 1035, 1036 and 1038 were marked on FAT helix 1/4 as active residues for FAT:CCDC158. The residues 914, 916, 934, 936, 938, 1022, 1027, 1031, 1032 and 1033 were marked on FAT helix 1/4 and 948, 955, 956, 957, 959, 962, 963, 964, 991 and 1007 were marked on FAT helix 2/3 as active residues for FAT:LPP. The CSP data was only used to define the binding site and not the binding poses. Structures that were listed in the output clusters with best scores were further analysed using PyMol (pymol.org).

BIBLIOGRAPHY

Alam, T., M. Alazmi, R. Naser, F. Huser, A. A. Momin, V. Astro, S. Hong, K. W. Walkiewicz, C. G. Canlas, R. Huser, A. J. Ali, J. Merzaban, A. Adamo, M. Jaremko, L. Jaremko, V. B. Bajic, X. Gao and S. T. Arold (2019). "Proteome-level assessment of origin, prevalence and function of Leucine-Aspartic Acid (LD) motifs." Bioinformatics.

Andreev, J., J. P. Simon, D. D. Sabatini, J. Kam, G. Plowman, P. A. Randazzo and J. Schlessinger (1999). "Identification of a new Pyk2 target protein with Arf-GAP activity." Molecular and Cellular Biology **19**(3): 2338-2350.

Anson, K. J. and A. Palmer (2018). "Exploring the intersection of cellular zinc and kinase activity with single cell imaging." Faseb Journal **32**(1).

Armendariz, B. G., M. Masdeu Mdel, E. Soriano, J. M. Urena and F. Burgaya (2014). "The diverse roles and multiple forms of focal adhesion kinase in brain." Eur J Neurosci **40**(11): 3573-3590.

Arold, S. T. (2011). "How focal adhesion kinase achieves regulation by linking ligand binding, localization and action." Curr Opin Struct Biol **21**(6): 808-813.

Arold, S. T., M. K. Hoellerer and M. E. Noble (2002). "The structural basis of localization and signaling by the focal adhesion targeting domain." Structure **10**(3): 319-327.

Aulakh, G. K., B. Petri, K. M. Wojcik, P. Colarusso, J. J. Lee and K. D. Patel (2018). "Inhibiting focal adhesion kinase (FAK) blocks IL-4 induced VCAM-1 expression and eosinophil recruitment in vitro and in vivo." Journal of Leukocyte Biology **104**(1): 147-158.

Bird, A. P. and A. P. Wolffe (1999). "Methylation-induced repression--belts, braces, and chromatin." Cell **99**(5): 451-454.

Borowsky, M. L. and R. O. Hynes (1998). "Layilin, a novel talin-binding transmembrane protein homologous with C-type lectins, is localized in membrane ruffles." J Cell Biol **143**(2): 429-442.

Brami-Cherrier, K., N. Gervasi, D. Arsenieva, K. Walkiewicz, M. C. Boutterin, A. Ortega, P. G. Leonard, B. Seantier, L. Gasmi, T. Bouceba, G. Kadare, J. A. Girault and S. T. Arold (2014). "FAK dimerization controls its kinase-dependent functions at focal adhesions." EMBO J **33**(4): 356-370.

Brown, M. C., M. S. Curtis and C. E. Turner (1998). "Paxillin LD motifs may define a new family of protein recognition domains." Nat Struct Biol **5**(8): 677-678.

Burgaya, F. and J. A. Girault (1996). "Cloning of focal adhesion kinase, pp125FAK, from rat brain reveals multiple transcripts with different patterns of expression." Brain Res Mol Brain Res **37**(1-2): 63-73.

Burgaya, F., A. Menegon, M. Menegoz, F. Valtorta and J. A. Girault (1995). "Focal adhesion kinase in rat central nervous system." Eur J Neurosci **7**(8): 1810-1821.

Burgaya, F., M. Toutant, J. M. Studler, A. Costa, M. Le Bert, M. Gelman and J. A. Girault (1997). "Alternatively spliced focal adhesion kinase in rat brain with increased autophosphorylation activity." J Biol Chem **272**(45): 28720-28725.

Calalb, M. B., T. R. Polte and S. K. Hanks (1995). "Tyrosine phosphorylation of focal adhesion kinase at sites in the catalytic domain regulates kinase activity: a role for Src family kinases." Mol Cell Biol **15**(2): 954-963.

Ceccarelli, D. F., H. K. Song, F. Poy, M. D. Schaller and M. J. Eck (2006). "Crystal structure of the FERM domain of focal adhesion kinase." J Biol Chem **281**(1): 252-259.

Chen, H. C., P. A. Appeddu, J. T. Parsons, J. D. Hildebrand, M. D. Schaller and J. L. Guan (1995). "Interaction of focal adhesion kinase with cytoskeletal protein talin." J Biol Chem **270**(28): 16995-16999.

Contestabile, A., D. Bonanomi, F. Burgaya, J. A. Girault and F. Valtorta (2003). "Localization of focal adhesion kinase isoforms in cells of the central nervous system." Int J Dev Neurosci **21**(2): 83-93.

Cooley, M. A., J. M. Broome, C. Ohngemach, L. H. Romer and M. D. Schaller (2000). "Paxillin binding is not the sole determinant of focal adhesion localization or dominant-negative activity of focal adhesion kinase/focal adhesion kinase-related nonkinase." Mol Biol Cell **11**(9): 3247-3263.

Corsi, J. M., C. Houbron, P. Billuart, I. Brunet, K. Bouvree, A. Eichmann, J. A. Girault and H. Enslen (2009). "Autophosphorylation-independent and -dependent functions of focal adhesion kinase during development." J Biol Chem **284**(50): 34769-34776.

Cox, B. D., M. Natarajan, M. R. Stettner and C. L. Gladson (2006). "New concepts regarding focal adhesion kinase promotion of cell migration and proliferation." J Cell Biochem **99**(1): 35-52.

de Pereda, J. M., K. L. Wegener, E. Santelli, N. Bate, M. H. Ginsberg, D. R. Critchley, I. D. Campbell and R. C. Liddington (2005). "Structural basis for phosphatidylinositol phosphate kinase type Igamma binding to talin at focal adhesions." J Biol Chem **280**(9): 8381-8386.

Derkinderen, P., J. Siciliano, M. Toutant and J. A. Girault (1998). "Differential regulation of FAK+ and PYK2/Cakbeta, two related tyrosine kinases, in rat hippocampal slices: effects of LPA, carbachol, depolarization and hyperosmolarity." Eur J Neurosci **10**(5): 1667-1675.

Derkinderen, P., M. Toutant, F. Burgaya, M. Le Bert, J. C. Siciliano, V. de Franciscis, M. Gelman and J. A. Girault (1996). "Regulation of a neuronal form of focal adhesion kinase by anandamide." Science **273**(5282): 1719-1722.

Desai, M. A., H. D. Webb, L. M. Sinanan, J. N. Scarsdale, N. M. Walavalkar, G. D. Ginder and D. C. Williams, Jr. (2015). "An intrinsically disordered region of methyl-CpG binding domain protein 2 (MBD2) recruits the histone deacetylase core of the NuRD complex." Nucleic Acids Res **43**(6): 3100-3113.

Dixon, R. D., Y. Chen, F. Ding, S. D. Khare, K. C. Prutzman, M. D. Schaller, S. L. Campbell and N. V. Dokholyan (2004). "New insights into FAK signaling and localization based on detection of a FAT domain folding intermediate." Structure **12**(12): 2161-2171.

Eom, J. W., J. M. Lee, J. Y. Koh and Y. H. Kim (2016). "AMP-activated protein kinase contributes to zinc-induced neuronal death via activation by LKB1 and induction of Bim in mouse cortical cultures." Mol Brain **9**: 14.

Ezratty, E. J., M. A. Partridge and G. G. Gundersen (2005). "Microtubule-induced focal adhesion disassembly is mediated by dynamin and focal adhesion kinase." Nature Cell Biology **7**(6): 581-U515.

Fan, H., X. Zhao, S. Sun, M. Luo and J. L. Guan (2013). "Function of focal adhesion kinase scaffolding to mediate endophilin A2 phosphorylation promotes epithelial-mesenchymal transition and mammary cancer stem cell activities in vivo." J Biol Chem **288**(5): 3322-3333.

Fan, Y., G. Abrahamsen, R. Mills, C. C. Calderon, J. Y. Tee, L. Leyton, W. Murrell, J. Cooper-White, J. J. McGrath and A. Mackay-Sim (2013). "Focal adhesion dynamics are altered in schizophrenia." Biol Psychiatry **74**(6): 418-426.

Felsenfeld, D. P., P. L. Schwartzberg, A. Venegas, R. Tse and M. P. Sheetz (1999). "Selective regulation of integrin--cytoskeleton interactions by the tyrosine kinase Src." Nat Cell Biol **1**(4): 200-206.

Fenwick, R. B., D. Oyen, H. J. Dyson and P. E. Wright (2018). "Slow Dynamics of Tryptophan-Water Networks in Proteins." Journal of the American Chemical Society **140**(2): 675-682.

Fung, H. Y., S. C. Fu, C. A. Brautigam and Y. M. Chook (2015). "Structural determinants of nuclear export signal orientation in binding to exportin CRM1." Elife **4**.

Garcia-Alvarez, B., J. M. de Pereda, D. A. Calderwood, T. S. Ulmer, D. Critchley, I. D. Campbell, M. H. Ginsberg and R. C. Liddington (2003). "Structural determinants of integrin recognition by talin." Mol Cell **11**(1): 49-58.

Garron, M. L., D. Arsenieva, J. Zhong, A. B. Bloom, A. Lerner, G. M. O'Neill and S. T. Arold (2009). "Structural insights into the association between BCAR3 and Cas family members, an atypical complex implicated in anti-oestrogen resistance." J Mol Biol **386**(1): 190-203.

Girault, J. A., G. Labesse, J. P. Mornon and I. Callebaut (1999). "The N-termini of FAK and JAKs contain divergent band 4.1 domains." Trends Biochem Sci **24**(2): 54-57.

Golubovskaya, V. M., K. Conway-Dorsey, S. N. Edmiston, C. K. Tse, A. A. Lark, C. A. Livasy, D. Moore, R. C. Millikan and W. G. Cance (2009). "FAK overexpression and p53 mutations are highly correlated in human breast cancer." Int J Cancer **125**(7): 1735-1738.

Golubovskaya, V. M., R. Finch and W. G. Cance (2005). "Direct interaction of the N-terminal domain of focal adhesion kinase with the N-terminal transactivation domain of p53." J Biol Chem **280**(26): 25008-25021.

Goni, G. M., C. Epifano, J. Boskovic, M. Camacho-Artacho, J. Zhou, A. Bronowska, M. T. Martin, M. J. Eck, L. Kremer, F. Grater, F. L. Gervasio, M. Perez-Moreno and D. Lietha (2014). "Phosphatidylinositol 4,5-bisphosphate triggers activation of focal adhesion kinase by inducing clustering and conformational changes." Proc Natl Acad Sci U S A **111**(31): E3177-3186.

Grant, S. G., K. A. Karl, M. A. Kiebler and E. R. Kandel (1995). "Focal adhesion kinase in the brain: novel subcellular localization and specific regulation by Fyn tyrosine kinase in mutant mice." Genes Dev **9**(15): 1909-1921.

Gupta, A. and C. S. Dey (2012). "PTEN, a widely known negative regulator of insulin/PI3K signaling, positively regulates neuronal insulin resistance." Mol Biol Cell **23**(19): 3882-3898.

Hall, J. E., W. Fu and M. D. Schaller (2011). "Focal adhesion kinase: exploring Fak structure to gain insight into function." Int Rev Cell Mol Biol **288**: 185-225.

Hashido, M., K. Hayashi, K. Hirose and M. Iino (2006). "Ca2+ lightning conveys cell-cell contact information inside the cells." Embo Reports **7**(11): 1117-1123.

Haskell, H., M. Natarajan, T. P. Hecker, Q. Ding, J. Stewart, Jr., J. R. Grammer and C. L. Gladson (2003). "Focal adhesion kinase is expressed in the angiogenic blood vessels of malignant astrocytic tumors in vivo and promotes capillary tube formation of brain microvascular endothelial cells." Clin Cancer Res **9**(6): 2157-2165.

Hayashi, I., K. Vuori and R. C. Liddington (2002). "The focal adhesion targeting (FAT) region of focal adhesion kinase is a four-helix bundle that binds paxillin." Nat Struct Biol **9**(2): 101-106.

Hens, M. D. and D. W. DeSimone (1995). "Molecular analysis and developmental expression of the focal adhesion kinase pp125FAK in Xenopus laevis." Dev Biol **170**(2): 274-288.

Hoellerer, M. K., M. E. Noble, G. Labesse, I. D. Campbell, J. M. Werner and S. T. Arold (2003). "Molecular recognition of paxillin LD motifs by the focal adhesion targeting domain." Structure **11**(10): 1207-1217.

Kadare, G., N. Gervasi, K. Brami-Cherrier, H. Blockus, S. El Messari, S. T. Arold and J. A. Girault (2015). "Conformational dynamics of the focal adhesion targeting domain control specific functions of focal adhesion kinase in cells." J Biol Chem **290**(1): 478-491.

Klein, E. A., L. Yin, D. Kothapalli, P. Castagnino, F. J. Byfield, T. Xu, I. Levental, E. Hawthorne, P. A. Janmey and R. K. Assoian (2009). "Cell-cycle control by physiological matrix elasticity and in vivo tissue stiffening." Curr Biol **19**(18): 1511-1518.

Ladbury, J. E. and S. T. Arold (2011). "Energetics of Src homology domain interactions in receptor tyrosine kinase-mediated signaling." Methods Enzymol **488**: 147-183.

Lawson, C., S. T. Lim, S. Uryu, X. L. Chen, D. A. Calderwood and D. D. Schlaepfer (2012). "FAK promotes recruitment of talin to nascent adhesions to control cell motility." J Cell Biol **196**(2): 223-232.

Lee, J., A. K. Borboa, H. B. Chun, A. Baird and B. P. Eliceiri (2010). "Conditional deletion of the focal adhesion kinase FAK alters remodeling of the blood-brain barrier in glioma." Cancer Res **70**(24): 10131-10140.

Leonhardt, H. and M. C. Cardoso (2000). "DNA methylation, nuclear structure, gene expression and cancer." J Cell Biochem Suppl **Suppl 35**: 78-83.

Lev, S., H. Moreno, R. Martinez, P. Canoll, E. Peles, J. M. Musacchio, G. D. Plowman, B. Rudy and J. Schlessinger (1995). "Protein-Tyrosine Kinase Pyk2 Involved in Ca2+-Induced Regulation of Ion-Channel and Map Kinase Functions." Nature **376**(6543): 737-745.

Lietha, D., X. Cai, D. F. Ceccarelli, Y. Li, M. D. Schaller and M. J. Eck (2007). "Structural basis for the autoinhibition of focal adhesion kinase." Cell **129**(6): 1177-1187.

Lim, S. T. (2013). "Nuclear FAK: a new mode of gene regulation from cellular adhesions." Mol Cells **36**(1): 1-6.
Lim, S. T., X. L. Chen, Y. Lim, D. A. Hanson, T. T. Vo, K. Howerton, N. Larocque, S. J. Fisher, D. D. Schlaepfer and D. Ilic (2008). "Nuclear FAK promotes cell proliferation and survival through FERM-enhanced p53 degradation." Mol Cell **29**(1): 9-22.
Lim, S. T., N. L. Miller, X. L. Chen, I. Tancioni, C. T. Walsh, C. Lawson, S. Uryu, S. M. Weis, D. A. Cheresh and D. D. Schlaepfer (2012). "Nuclear-localized focal adhesion kinase regulates inflammatory VCAM-1 expression." J Cell Biol **197**(7): 907-919.
Lorenz, S., I. Vakonakis, E. D. Lowe, I. D. Campbell, M. E. Noble and M. K. Hoellerer (2008). "Structural analysis of the interactions between paxillin LD motifs and alpha-parvin." Structure **16**(10): 1521-1531.
Lu, Y., N. Yeung, N. Sieracki and N. M. Marshall (2009). "Design of functional metalloproteins." Nature **460**(7257): 855-862.
Luo, S. W., C. Zhang, B. Zhang, C. H. Kim, Y. Z. Qiu, Q. S. Du, L. Mei and W. C. Xiong (2009). "Regulation of heterochromatin remodelling and myogenin expression during muscle differentiation by FAK interaction with MBD2." EMBO J **28**(17): 2568-2582.
Mace, P. D., Y. Wallez, M. K. Dobaczewska, J. J. Lee, H. Robinson, E. B. Pasquale and S. J. Riedl (2011). "NSP-Cas protein structures reveal a promiscuous interaction module in cell signaling." Nat Struct Mol Biol **18**(12): 1381-1387.
Manzerra, P., M. M. Behrens, L. M. Canzoniero, X. Q. Wang, V. Heidinger, T. Ichinose, S. P. Yu and D. W. Choi (2001). "Zinc induces a Src family kinase-mediated up-regulation of NMDA receptor activity and excitotoxicity." Proc Natl Acad Sci U S A **98**(20): 11055-11061.
Maret, W. (2015). "Analyzing free zinc(II) ion concentrations in cell biology with fluorescent chelating molecules." Metallomics **7**(2): 202-211.
Marlowe, T., A. Dementiev, S. Figel, A. Rivera, M. Flavin and W. Cance (2019). "High resolution crystal structure of the FAK FERM domain reveals new insights on the Druggability of tyrosine 397 and the Src SH3 binding site." BMC Mol Cell Biol **20**(1): 10.
Menegon, A., F. Burgaya, P. Baudot, D. D. Dunlap, J. A. Girault and F. Valtorta (1999). "FAK+ and PYK2/CAKbeta, two related tyrosine kinases highly expressed in the central nervous system: similarities and differences in the expression pattern." Eur J Neurosci **11**(11): 3777-3788.
Mierke, C. T. (2013). "The role of focal adhesion kinase in the regulation of cellular mechanical properties." Phys Biol **10**(6): 065005.
Mitra, S. K., D. A. Hanson and D. D. Schlaepfer (2005). "Focal adhesion kinase: in command and control of cell motility." Nat Rev Mol Cell Biol **6**(1): 56-68.
Mohanty, P. and S. Bhatnagar (2017). "Structural basis of focal adhesion targeting domain-mediated signaling in cardiac hypertrophy." J Recept Signal Transduct Res **37**(1): 38-50.
Naser, R., A. Aldehaiman, E. Diaz-Galicia and S. T. Arold (2018). "Endogenous Control Mechanisms of FAK and PYK2 and Their Relevance to Cancer Development." Cancers (Basel) **10**(6).

Navarro, A. I. and B. Rico (2014). "Focal adhesion kinase function in neuronal development." Curr Opin Neurobiol **27**: 89-95.
Palazzo, A. F., C. H. Eng, D. D. Schlaepfer, E. E. Marcantonio and G. G. Gundersen (2004). "Localized stabilization of microtubules by integrin- and FAK-facilitated Rho signaling." Science **303**(5659): 836-839.
Panera, N., A. Crudele, I. Romito, D. Gnani and A. Alisi (2017). "Focal Adhesion Kinase: Insight into Molecular Roles and Functions in Hepatocellular Carcinoma." Int J Mol Sci **18**(1).
Petit, M. M., J. Fradelizi, R. M. Golsteyn, T. A. Ayoubi, B. Menichi, D. Louvard, W. J. Van de Ven and E. Friederich (2000). "LPP, an actin cytoskeleton protein related to zyxin, harbors a nuclear export signal and transcriptional activation capacity." Mol Biol Cell **11**(1): 117-129.
Petit, M. M., S. M. Meulemans and W. J. Van de Ven (2003). "The focal adhesion and nuclear targeting capacity of the LIM-containing lipoma-preferred partner (LPP) protein." J Biol Chem **278**(4): 2157-2168.
Provenzano, P. P., D. R. Inman, K. W. Eliceiri and P. J. Keely (2009). "Matrix density-induced mechanoregulation of breast cell phenotype, signaling and gene expression through a FAK-ERK linkage." Oncogene **28**(49): 4326-4343.
Rees, D. J., S. E. Ades, S. J. Singer and R. O. Hynes (1990). "Sequence and domain structure of talin." Nature **347**(6294): 685-689.
Ritt, M., J. L. Guan and S. Sivaramakrishnan (2013). "Visualizing and manipulating focal adhesion kinase regulation in live cells." J Biol Chem **288**(13): 8875-8886.
Schaller, M. D. (2010). "Cellular functions of FAK kinases: insight into molecular mechanisms and novel functions." J Cell Sci **123**(Pt 7): 1007-1013.
Schaller, M. D., J. D. Hildebrand and J. T. Parsons (1999). "Complex formation with focal adhesion kinase: A mechanism to regulate activity and subcellular localization of Src kinases." Mol Biol Cell **10**(10): 3489-3505.
Schaller, M. D., J. D. Hildebrand, J. D. Shannon, J. W. Fox, R. R. Vines and J. T. Parsons (1994). "Autophosphorylation of the focal adhesion kinase, pp125FAK, directs SH2-dependent binding of pp60src." Mol Cell Biol **14**(3): 1680-1688.
Schlaepfer, D. D., S. K. Hanks, T. Hunter and P. van der Geer (1994). "Integrin-mediated signal transduction linked to Ras pathway by GRB2 binding to focal adhesion kinase." Nature **372**(6508): 786-791.
Shan, Y., L. Yu, Y. Li, Y. Pan, Q. Zhang, F. Wang, J. Chen and X. Zhu (2009). "Nudel and FAK as antagonizing strength modulators of nascent adhesions through paxillin." PLoS Biol **7**(5): e1000116.
Sousa, S. F., A. B. Lopes, P. A. Fernandes and M. J. Ramos (2009). "The Zinc proteome: a tale of stability and functionality." Dalton Trans(38): 7946-7956.
Sulzmaier, F. J., C. Jean and D. D. Schlaepfer (2014). "FAK in cancer: mechanistic findings and clinical applications." Nat Rev Cancer **14**(9): 598-610.

Suter, D. M. and P. Forscher (1998). "An emerging link between cytoskeletal dynamics and cell adhesion molecules in growth cone guidance." Curr Opin Neurobiol **8**(1): 106-116.

Tai, Y. L., L. C. Chen and T. L. Shen (2015). "Emerging roles of focal adhesion kinase in cancer." Biomed Res Int **2015**: 690690.

Thomas, J. W., B. Ellis, R. J. Boerner, W. B. Knight, G. C. White, 2nd and M. D. Schaller (1998). "SH2- and SH3-mediated interactions between focal adhesion kinase and Src." J Biol Chem **273**(1): 577-583.

Tomar, A. and D. D. Schlaepfer (2009). "Focal adhesion kinase: switching between GAPs and GEFs in the regulation of cell motility." Curr Opin Cell Biol **21**(5): 676-683.

Tompa, P. (2012). "Intrinsically disordered proteins: a 10-year recap." Trends Biochem Sci **37**(12): 509-516.

Toutant, M., A. Costa, J. M. Studler, G. Kadare, M. Carnaud and J. A. Girault (2002). "Alternative splicing controls the mechanisms of FAK autophosphorylation." Mol Cell Biol **22**(22): 7731-7743.

Toutant, M., J. M. Studler, F. Burgaya, A. Costa, P. Ezan, M. Gelman and J. A. Girault (2000). "Autophosphorylation of Tyr397 and its phosphorylation by Src-family kinases are altered in focal-adhesion-kinase neuronal isoforms." Biochem J **348 Pt 1**: 119-128.

Walkiewicz, K. W., J. A. Girault and S. T. Arold (2015). "How to awaken your nanomachines: Site-specific activation of focal adhesion kinases through ligand interactions." Prog Biophys Mol Biol **119**(1): 60-71.

Wang, P., C. Ballestrem and C. H. Streuli (2011). "The C terminus of talin links integrins to cell cycle progression." J Cell Biol **195**(3): 499-513.

Wei, H., M. Malik, A. M. Sheikh, G. Merz, W. Ted Brown and X. Li (2011). "Abnormal cell properties and down-regulated FAK-Src complex signaling in B lymphoblasts of autistic subjects." Am J Pathol **179**(1): 66-74.

Williamson, M. P. (2013). "Using chemical shift perturbation to characterise ligand binding." Progress in Nuclear Magnetic Resonance Spectroscopy **73**(Supplement C): 1-16.

Xie, J., K. H. Allen, A. Marguet, K. A. Berghorn, S. P. Bliss, A. M. Navratil, J. L. Guan and M. S. Roberson (2008). "Analysis of the calcium-dependent regulation of proline-rich tyrosine kinase 2 by gonadotropin-releasing hormone." Mol Endocrinol **22**(10): 2322-2335.

Xu, S., Y. Liu, X. Li, Y. Liu, R. Meijers, Y. Zhang and J. H. Wang (2018). "The binding of DCC-P3 motif and FAK-FAT domain mediates the initial step of netrin-1/DCC signaling for axon attraction." Cell Discov **4**: 8.

Zaidel-Bar, R. and B. Geiger (2010). "The switchable integrin adhesome." J Cell Sci **123**(Pt 9): 1385-1388.

Zheng, C., Z. Xing, Z. C. Bian, C. Guo, A. Akbay, L. Warner and J. L. Guan (1998). "Differential regulation of Pyk2 and focal adhesion kinase (FAK). The C-terminal domain of FAK confers response to cell adhesion." J Biol Chem **273**(4): 2384-2389.

Zheng, Y., Y. Xia, D. Hawke, M. Halle, M. L. Tremblay, X. Gao, X. Z. Zhou, K. Aldape, M. H. Cobb, K. Xie, J. He and Z. Lu (2009). "FAK phosphorylation by ERK primes ras-induced tyrosine dephosphorylation of FAK mediated by PIN1 and PTP-PEST." Mol Cell **35**(1): 11-25.

Zheng, Y., W. Yang, Y. Xia, D. Hawke, D. X. Liu and Z. Lu (2011). "Ras-induced and extracellular signal-regulated kinase 1 and 2 phosphorylation-dependent isomerization of protein tyrosine phosphatase (PTP)-PEST by PIN1 promotes FAK dephosphorylation by PTP-PEST." Mol Cell Biol **31**(21): 4258-4269.

Zhou, J., Q. Yi and L. Tang (2019). "The roles of nuclear focal adhesion kinase (FAK) on Cancer: a focused review." J Exp Clin Cancer Res **38**(1): 250.

APPENDICES

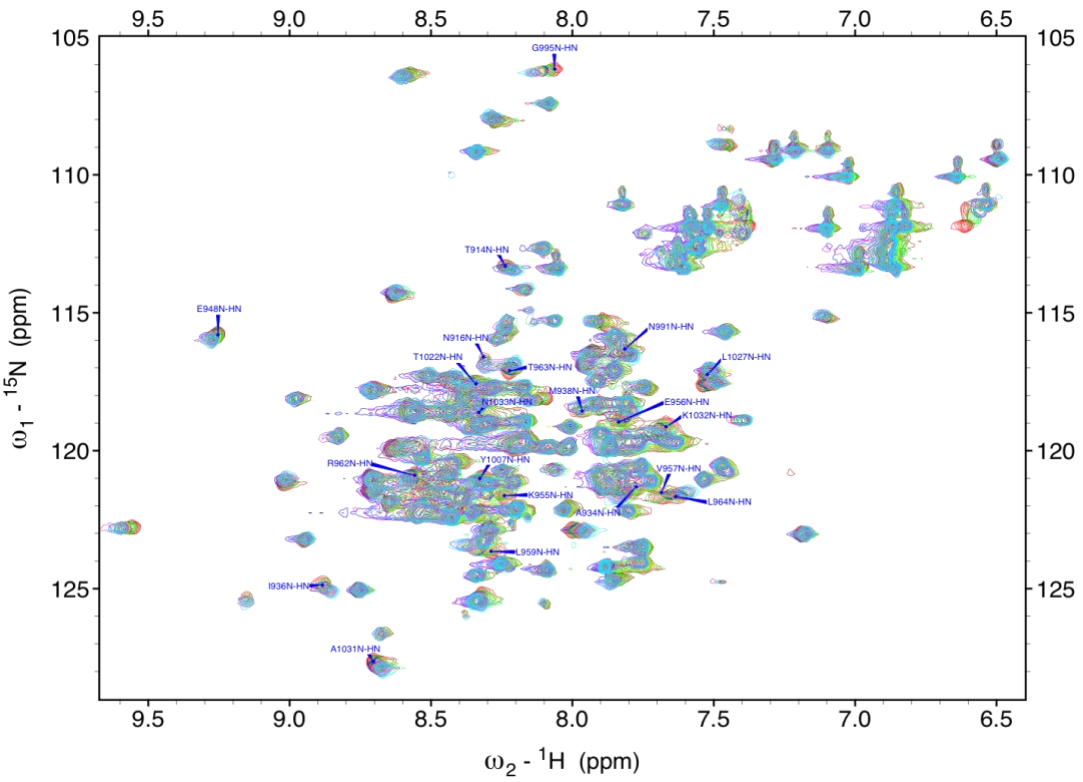

Appendix Figure 1: ^{1}H-^{15}N HSQC of FAT titrated with LPP

Overlay of ^{1}H-^{15}N-HSQC spectra of 100 µM ^{15}N-FAT in the absence (red) and presence of 1 (green), 2 (blue), 3 (yellow), 4 (magenta) and 5 (cyan) times molar excess of LPP peptide. Resonances that disappeared upon LPP addition are labelled in red. Resonances that significantly shifted >2σ= 0.06 are labelled in blue. All spectra were recorded at 25°C at a proton frequency of 950 MHz.

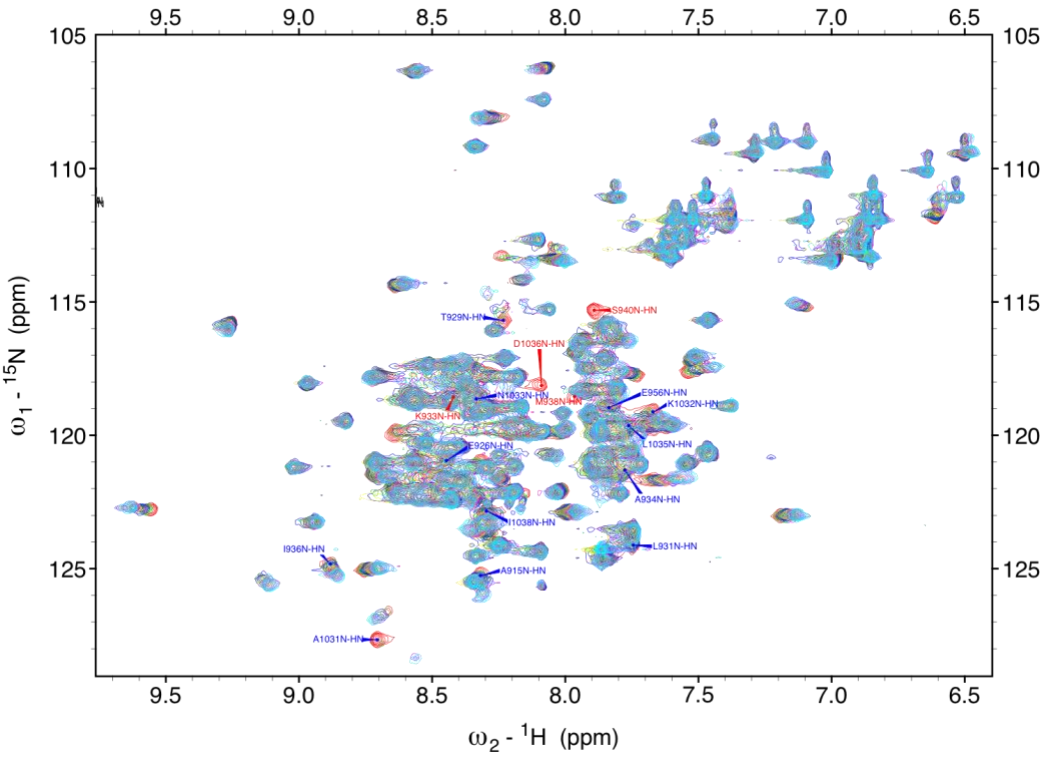

Appendix Figure 2: ^{1}H-^{15}N HSQC of FAT titrated with CCDC158

Overlay of ^{1}H-^{15}N HSQC spectra of 100 µM 15N-FAT in the absence (red) and presence of 0.5 (green), 1 (blue), 2 (yellow), 3 (magenta) and 4 (cyan) times molar excess of CCDC158 peptide. Resonances that disappeared upon CCDC158 addition are labelled in red. Resonances that significantly shifted >2σ= 0.114 are labelled in blue. All spectra were recorded at 25°C at a proton frequency of 950 MHz.

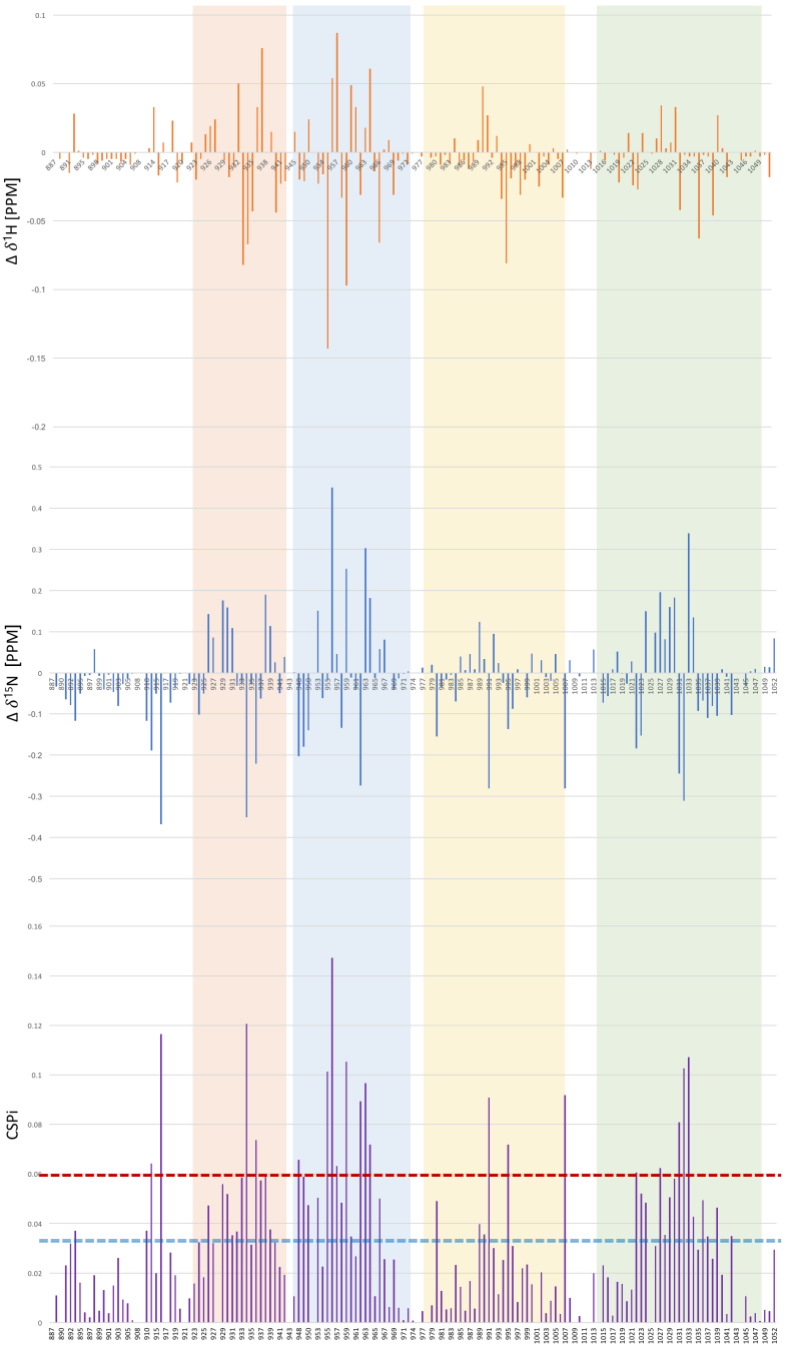

Appendix Figure 3: Chemical shift changes in FAT induced by LPP peptide

Chemical shift differences in ppm where calculated for ^{1}H (top panel), ^{15}N (middle panel) and the weighted combined ^{1}H,^{15}N (lower panel) chemical shift perturbation of FAT in the presence of a five times molar excess of LPP peptide. Red dashed line indicates the upper threshold of 2σ= 0.06 and the blue double-dashed line indicates the lower threshold of σ= 0.03. The shaded areas represent the helices (red for helix 1, blue for helix 2, orange for helix 3, green for helix 4).

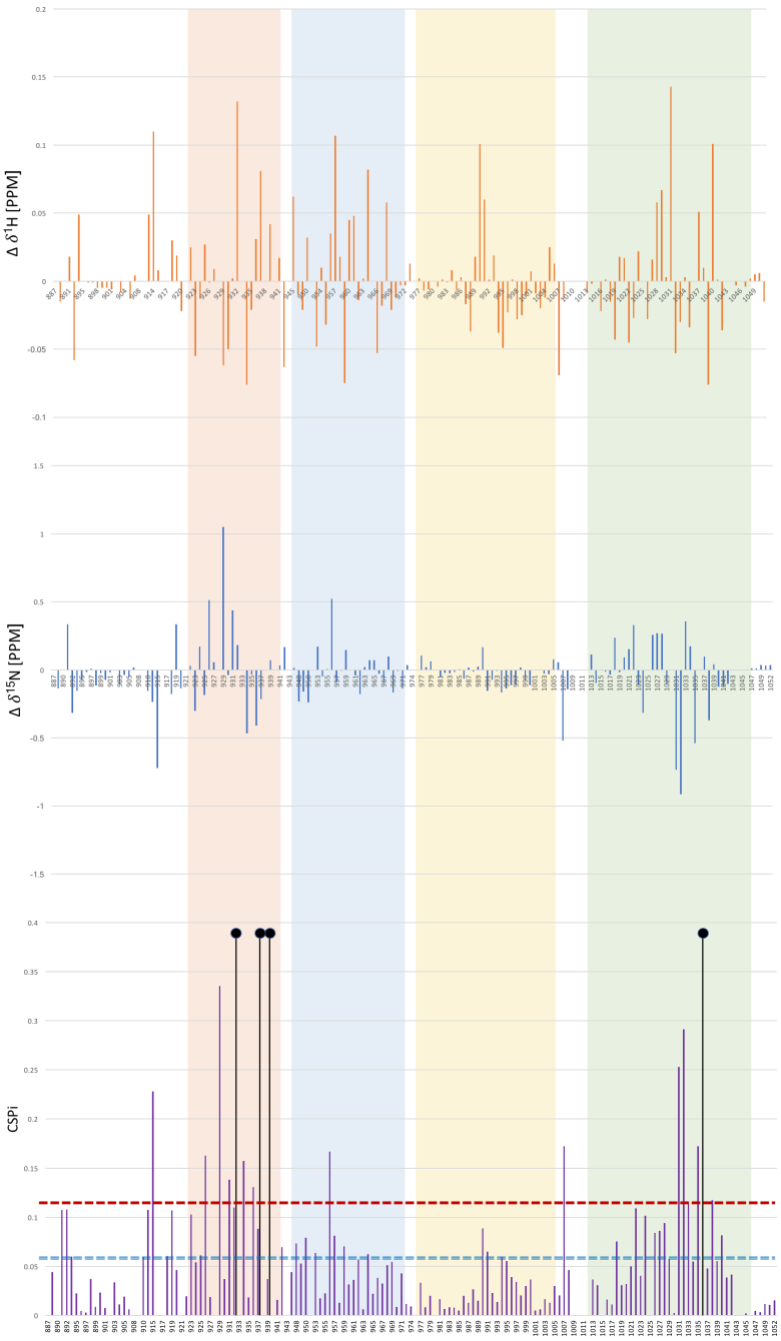

Appendix Figure 4: Chemical shift changes in FAT induced by CCDC158 peptide
Chemical shift differences in ppm where calculated for ^{1}H (top panel), ^{15}N (middle panel) and the weighted combined ^{1}H,^{15}N (lower panel) chemical shift perturbation of FAT in the presence of a four times molar excess of CCDC158 peptide. Red dashed line indicates the upper threshold of 2σ= 0.114 and the blue double-dashed line indicates the lower threshold of σ= 0.057. Others that disappeared upon CCDC158 addition are marked by full black circles. The shaded areas represent the helices (red for helix 1, blue for helix 2, orange for helix 3, green for helix 4).

Appendix Table 1: Updated Chemical shift values of H, N, CA and CB of Human FAK FAT

Newly assigned residues are labeled in green and uncertain assignments are labeled in blue. Residues whose assignments did not match on our spectrum are labeled in orange whereas completely unassigned ones are shown in red. Prolines are shown in gray.

	Residue	Number	H	N	CA	CB
Vector	G	887	8.356	109.069	45.445	
	P	888			63.242	32.537
	L	889	8.558	122.337	55.563	42.203
	G	890	8.436	109.878	45.343	
	S	891	8.221	115.505	58.258	64.014
N-terminal loop	S	892	8.438	117.711	58.364	64.164
	S	893	8.403	118.849	56.478	63.5
	P	894			63.639	32.041
	A	895	8.327	123.228	52.978	19.2
	D	896	8.169	118.877	54.589	41.393
	S	897	8.071	115.243	58.693	63.675
	Y	898	8.197	122.023	58.35	38.552
	N	899	8.266	120.707	53.26	39.113
	E	900	8.31	121.179	57.041	30.018
	G	901	8.369	109.392	45.415	
	V	902	7.879	119.622	62.538	32.607
	K	903	8.35	125.319	56.072	32.81
	L	904	8.265	124.027	54.86	42.27
	Q	905	8.385	122.409	53.546	28.905
	P	906			63.511	31.9
	Q	907	8.541	120.128	55.909	29.401
	E	908	8.531	121.059	55.645	29.644
	I	909	8.536	121.183	63.319	32.194

	S	910	8.12	113.049	61.973	69.91
	P	911				
	P	912				
	P	913			63.048	32
	T	914	8.227	113.185	62.469	69.4
	A	915	8.331	125.238	52.727	19.089
	N	916	8.326	116.791	53.22	38.511
	L	917	7.713	121.771	54.631	42.4
	D	918	8.459	121.567	54.309	41.011
	R	919	8.85	124.41	54.079	29.962
	S	920	8.564	118.651	61.67	62.682
	N	921	8.562	119.617	52.916	38.8
	D	922	7.422	118.825		40.9
Helix 1	K	923	8.677	126.614	58.249	32.768
	V	924	7.926	119.353	67.15	30.831
	Y	925	8.079	120.559	62.199	38.2
	E	926	8.458	120.934	59.92	29.9
	N	927	8.442	117.407	55.697	38.74
	V	928			58.431	31.6
	T	929	8.248	115.478	67.202	68.275
	G	930	8.289	108.031	47.285	
	L	931	7.765	124.034	58.12	41.6
	V	932	8.666	119.859	67.793	31.6
	K	933	8.426	118.534	60.39	32
	A	934	7.793	121.149	55.153	17.6
	V	935	8.43	120.203	67.38	31.4

	I	936	8.913	124.974	65.501	
	E	937	8.554	121.52	59.819	
	M	938	8.023	118.486	59.222	32.5
	S	939	8.639	114.203	62.436	63.5
	S	940	7.908	115.455	60.58	63.5
	K	941	7.629	119.577	57.02	34.595
	I	942	7.718	117.608	64.641	38.6
Loop1	**Q**	**943**				
	P	944			64.015	31.6
	A	945	7.212	122.957	51.401	19.06
	P	946				
Helix 2	P	947			64.632	
	E	948	9.282	115.755	59.59	28.4
	E	949	7.952	116.387	57.02	30.925
	Y	950	7.977	116.764	58.996	37.913
	V	**951**				
	P	952			65.95	30.6
	M	953	7.115	115.105	59.562	33.1
	V	**954**			**66.5**	**31.4**
	K	955	8.265	121.552	59.874	31.7
	E	956	7.85	118.875		29
	V	957	7.698	121.506	67.1	31.3
	G	958	8.605	106.302	47.871	
	L	959	8.313	123.471	58.087	41.3
	A	960	8.017	122.849	55.081	17.3
	L	961	8.753	121.429	58.14	40.7

	R	962	8.583	120.816	60.476	29.7
	T	963	8.237	117.043	66.7	68.7
	L	964				
	L	965	8.994	118.093	58.922	40
	A	966	7.839	121.19	55.288	17.643
	T	967	8.178	117.681	66.058	68.33
	V	968	8.772	124.935	68.079	31
	D	969	8.504	122.091	58.296	39.9
	E	970	7.47	115.624	57.861	30
	T	971	7.862	116.899	65.283	69.2
Loop 2	I	972	7.814	122.052	67.809	38.6
	P	973			65.267	31.4
	L	974	7.853	115.698	55.084	41.784
	L	975	8.431	122.321	53.7	42.27
	P	976				
Helix 3	A	977				
	S	978			60.558	62.1
	T	979	8.089	112.455	62.909	70.9
	H	980	7.521	120.008	59.023	30.9
	R	981	8.846	119.476	59.63	29.2
	E	982	8.379	118.96	59.609	29.6
	I	983	7.706	120.87	66.039	37.7
	E	984	8.73	120.854	59.384	29.4
	M	985	8.414	118.059	58.614	32.2
	A	986	7.756	123.428	55.106	18.4
	Q	987	8.594	118.46	60.26	30.7

	K	988	8.158	119.47	59.95	32.1
	L	989	7.914	121.161	57.82	41.3
	L	990	7.536	117.549	58.102	41.2
	N	991	7.833	116.295	56.852	38.825
	S	992	8.446	118.566	61.94	63.41
	D	993	8.951	123.148	56.08	38.5
	L	994	8.337	122.089	58.12	40.4
	G	995	8.095	106.101	47.521	
	E	996	8.034	122.058	59.022	29.5
	L	997	7.927	120.793	59.018	41.4
	I	998	8.592	118.541	65.506	37.8
	N	999	8.307	118.88	56.653	38.359
	K	1000	8.526	117.205	57.578	30.896
	M	1001	8.569	122.134	59.561	33.618
	K	1002	8.373	118.799	59.805	32
	L	1003	7.555	120.934	58.313	40.612
	A	**1004**			**56.523**	**18**
	Q	1005	8.182	114.072	58.82	28.2
	Q	**1006**	**8.065**	**119.634**	**55.047**	**30.063**
Loop 3	**Y**	**1007**	**8.312**	**121.098**	**56.597**	**38.561**
	V	**1008**	**8.206**	**121.977**	**60.931**	**30.182**
	M	**1009**	**8.345**	**120.975**	**56.268**	**32**
	T	**1010**	**8.14**	**115.304**	**58.606**	**70.734**
	S	**1011**	**8.134**	**117.176**	**55.705**	**64.087**
	L	**1012**	**8.238**	**122.539**	**53.832**	**42.1**
Heli x 4	**Q**	**1013**			60.75	28.2

	Q	1014	8.285	115.93	58.83	28
	E	1015	7.458	120.728	58.631	28.63
	Y	1016	7.932	117.429	62.42	37.058
	K	1017	8.413	121.566	60.83	33
	K	1018	7.819	119.591	60.235	31.5
	Q	1019	7.934	118.293	59.409	27.9
	M	1020	8.562	122.039	60.35	33.3
	L	1021	8.069	119.836	58.54	40.9
	T	1022	8.378	117.944	66.836	68.6
	A	1023	7.884	124.758	54.912	18
	A	1024	8.714	121.616	55.195	18.3
	H	1025	8.384	117.046	59.751	29.5
	A	1026	7.861	121.044	55.377	17.8
	L	1027	7.547	117.093	58.446	42.4
	A	1028	7.67	119.484	55.726	18.6
	V	1029	8.188	119.778	66.72	31.7
	D	1030	9.065	121.139	56.931	37.893
	A	1031	8.712	127.558	55.68	18.3
	K	1032	7.642	119.039	59.625	31.344
	N	1033	8.335	118.37	56.699	38
	L	1034	7.756	120.455	58.409	40.7
	L	1035	7.761	119.605	58.26	41.3
	D	1036	8.146	118.078	58.1	40.3
	V	1037	8.205	119.668	66.592	31.7
	I	1038	8.314	122.809	65.471	36.8
	D	1039	9.563	122.64	58.08	39.6

	Q	1040	8.325	117.695	58.97	28
	A	1041	8.097	124.232	55.52	19.7
	R	1042	8.72	117.742	59.797	30.4
	L	1043	8.171	119.597	57.829	41.9
	K	1044	7.891	119.913	58.631	32.258
	M	1045	7.824	118.202	57.686	33.272
C-trminal tail	L	1046	7.891	119.854	56.26	41.9
	G	1047	8.098	107.292	45.921	
	Q	1048	8.027	118.996	55.9	29.636
	T	1049	8.152	114.634	62.156	69.951
	R	1050	8.332	124.392	54.041	30.195
	P	1051			63.48	32
	H	1052	8.024	123.532	57.241	30.32

Appendix Table 2: Comparison of CSP changes for FAT/LD2 NMR titration with the literature

Residues with significant change in CSPs matching the literature are highlighted in red. Residues that previously showed slight changes in CSPs but detected in our titration experiments are highlighted in magenta. Residues that were previously noted to be at the contact surface of interaction between FAT and LD2 by experiments other than ^{1}H-^{15}N HSQC titrations and matched our data are highlighted in yellow. (X) indicates residues for which we failed to assign their corresponding peaks in our spectra.

Region	Residue	Number	Chemical shift perturbation changes	
			Previously reported	Our data
Helix 1	V	928	smaller change	significant change
	G	930	not reported	significant change
	V	932	smaller change	peak disappeared
	K	933	peak disappeared	X
	A	934	smaller change	significant change
	I	936	smaller change	significant change
	E	937	increased amide exchange protection	peak disappeared
	M	938	peak disappeared	peak disappeared
	S	939	smaller change	significant change
	S	940	not reported	peak disappeared
	K	941	smaller change	peak disappeared
	I	942	peak disappeared	significant change
Helix 2	E	948	smaller change	significant change
	M	953	not reported	significant change
	K	955	peak disappeared	peak disappeared
	E	956	peak disappeared	peak disappeared
	V	957	peak disappeared	X
	G	958	peak disappeared	significant change
	L	959	peak disappeared	peak disappeared
	A	960	smaller change	significant change
	L	961	smaller change	significant change
	T	963	peak disappeared	peak disappeared
	L	964	peak disappeared	peak disappeared
	A	966	peak disappeared	peak disappeared
Helix 3	L	990	smaller change	peak disappeared
	N	991	peak disappeared	peak disappeared
	D	993	increased amide exchange protection	significant change
	L	994	increased amide exchange protection, contacting residue in the crystal structure	peak disappeared
	G	995	peak disappeared	peak disappeared
	E	996	increased amide exchange protection	significant change
Helix 4	A	1024	smaller change	significant change
	A	1028	smaller change	significant change
	A	1031	smaller change	significant change
	K	1032	smaller change	peak disappeared
	L	1035	peak disappeared	peak disappeared
	D	1036	not reported	peak disappeared
	D	1039	smaller change	significant change

Appendix Table 3: Updated Chemical shift values of H, N, CA and CB of Human FAK FAT^{+}
The PWR inserted residues are highlighted in beige. Residues whose assignments did not match on our spectrum are labeled in orange whereas completely unassigned ones are shown in red. Prolines are shown in gray.

	Residue	Number	H	N	CA	CB
Vector	G	884	8.32	108.817	45.063	
	P	885			62.944	32.1
	L	886	8.544	122.36	55.284	41.9
	G	887	8.425	109.927	45.136	
	S	888	8.217	115.575	58.037	63.79
N-terminal loop	S	889	8.431	117.766	58.162	63.5
	S	890	8.399	118.886	56.239	63.352
	P	891			63.444	31.841
	A	892	8.314	123.229	52.67	18.696
	D	893	8.161	118.894	54.382	40.744
	S	894	8.056	115.272	58.321	63.523
	Y	895	8.182	121.985	58.149	38.242
	N	896	8.248	120.607	53.128	38.9
	E	897	8.281	121.04	56.89	29.757
	G	898	8.337	109.136	45.086	
	V	899	7.882	119.231	62.061	32.203
	K	900	8.314	126.179	53.651	32.203
	P	**901**			63.278	31.587
	W	**902**	7.976	120.354	57.188	28.93
	R	**903**	**8.251**	**123.996**	**54.86**	**42.27**
	L	904				
	Q	905	8.159	120.24	55.4	29.21
	P	906			63.352	31.746

	Q	907	8.518	119.865	55.715	29.052
	E	908	7.835	122.06	57.237	30.765
	I	909				
	S	910				
	P	911				
	P	912				
	P	913			62.76	31.684
	T	914	8.258	113.27	62.444	69.242
	A	915	8.344	125.005	52.617	18.601
	N	916	8.338	116.494	53.144	38.2
	L	917	7.615	121.452	54.172	42.628
	D	918	8.463	121.413	53.961	40.571
	R	919	8.857	124.68	53.736	32.045
	S	920	8.565	118.633	61.499	62.43
	N	921	8.582	119.792	52.591	38.673
	D	922	7.414	118.906	52.657	40.9
Helix 1	K	923	8.671	126.51	57.965	
	V	924	7.912	119.347	66.895	
	Y	925	8.076	120.671	61.969	38.643
	E	926	8.451	120.894	59.756	29.563
	N	927	8.442	117.319	55.477	39.226
	V	928			58.08	
	T	929	8.245	115.631	67.076	67.776
	G	930	8.286	108.047	46.967	
	L	931	7.75	124.033	57.912	41.6
	V	932	8.651	119.881	67.554	31.286

	K	933	8.451	118.584	60.112	32.045
	A	934	7.782	121.317	54.962	17.099
	V	935	8.392	120.313	67.251	31.176
	I	936	8.904	124.908	65.37	
	E	937	8.542	121.505	59.519	28.93
	M	938	7.995	118.461	58.992	32.5
	S	939	8.633	114.352	62.206	
	S	940	7.911	115.349	60.342	63.348
	K	941	7.607	119.605	56.687	34.529
	I	942	7.724	117.706	64.313	37.929
Loop1	**Q**	**943**				
	P	944			63.839	27.254
	A	945	7.194	123.01	51.2	19.289
	P	946				
Helix 2	P	947			64.366	
	E	948	9.263	115.654	59.348	28.123
	E	949	7.941	116.355	56.727	30.717
	Y	950	7.985	116.766	58.768	37.613
	V	**951**	8.21	121.3	60.8	32.73
	P	952			65.696	
	M	953	7.093	115.253	59.269	
	V	954				
	K	955	8.251	121.592	59.69	
	E	956	7.859	118.979	59.466	29
	V	957	7.699	121.644	66.856	32.629
	G	958	8.589	106.358	47.636	

	L	959	8.305	123.627	57.939	41.204
	A	960	8.008	122.785	54.804	16.941
	L	961	8.742	121.405	57.899	40.7
	R	962	8.574	120.911	60.164	29.451
	T	963	8.233	117.092	66.5	68.7
	L	964			57.807	
	L	965	8.994	118.061	58.663	40
	A	966	7.829	121.277	54.988	17.494
	T	967	8.179	117.7	65.894	67.032
	V	968	8.774	125.038		
	D	969	8.505	122.122	58.044	39.9
	E	970	7.465	115.689	57.623	29.816
	T	971	7.86	117.01	65.059	68.993
Loop 2	I	972	7.806	122.06	67.58	38.6
	P	973			65.038	31.033
	L	974	7.857	115.828	54.751	41.44
	L	975	8.299	122.007	53.381	42.27
	P	976				
Helix 3	A	977				
	S	978			60.268	61.625
	T	979	8.088	112.523	62.587	70.742
	H	980	7.501	120.234	58.716	30.512
	R	981	8.835	119.501	59.374	28.85
	E	982	8.358	118.992	59.427	29.6
	I	983	7.705	120.978	65.815	37.819
	E	984	8.721	120.928	59.203	29.008

	M	985	8.402	118.136	58.43	32.2
	A	986	7.753	123.508	54.83	18.27
	Q	987	8.589	118.542	60.033	30.101
	K	988	8.151	119.553	59.677	31.935
	L	989	7.907	121.295	57.622	41.3
	L	990	7.561	117.621	57.886	41.2
	N	991	7.83	116.296	56.477	38.4
	S	992	8.432	118.69	61.69	63.205
	D	993	8.948	123.22	55.871	36.744
	L	994	8.33	122.164	57.857	
	G	995	8.083	106.152	47.258	
	E	996	8.024	122.097	58.772	29.057
	L	997	7.917	120.889	58.758	41.4
	I	998	8.586	118.632	65.209	37.535
	N	999	8.3	118.928	56.39	37.9
	K	1000	8.521	117.252	57.391	30.633
	M	1001	8.552	122.315	59.322	
	K	1002	8.37	118.701	59.559	31.602
	L	1003	7.54	121.042	57.873	40.603
	A	1004	8.409	121.862	56.424	
	Q	**1005**	**8.173**	**114.145**	**58.596**	**28.2**
	Q	1006	8.072	119.72	54.791	28.2
Loop 3	**Y**	**1007**			56.49	38.547
	V	1008	8.146	121.518	60.8	30.132
	M	1009	8.262	120.399	55.914	
	T	**1010**	**8.13**	**115.433**	**58.377**	

	S	1011	8.124	117.231	55.449	63.822
	L	1012	8.19	121.996	53.7	42.1
Helix 4	Q	1013			60.441	28.2
	Q	1014	8.271	115.92	58.597	28
	E	1015	7.437	120.628		
	Y	1016	7.921	117.429	62.167	36.789
	K	1017	8.402	121.648	60.573	32.684
	K	1018	7.81	119.756	60.164	
	Q	1019	7.907	118.308	59.032	27.9
	M	1020	8.55	122.068	60.02	33.3
	L	1021	8.053	119.884	58.36	40.9
	T	1022	8.364	117.791	66.645	68.234
	A	1023	7.854	124.692	54.527	17.304
	A	1024	8.695	121.718	55.09	18.3
	H	1025	8.433	117.534	59.48	29.057
	A	1026	7.853	121.122	55.107	17.304
	L	1027	7.555	117.2	58.07	42.4
	A	1028	7.7	119.583	55.515	18.08
	V	1029	8.208	119.816	66.5	31.651
	D	1030	9.058	121.148	56.753	37.6
	A	1031	8.715	127.583	55.331	17.778
	K	1032	7.669	119.169	59.545	30.986
	N	1033	8.348	118.576	56.411	37.866
	L	1034	7.754	120.614	58.097	40.476
	L	1035	7.773	119.67	58.031	41.49
	D	1036	8.127	118.157	57.82	39.89

	V	1037	8.2	119.736	66.381	31.7
	I	1038	8.309	122.851	65.209	
	D	1039	9.566	122.784	57.86	39.732
	Q	1040	8.314	117.706	58.755	28
	A	1041	8.097	124.266	55.335	19.234
	R	1042	8.714	117.762	59.664	30.21
	L	1043	8.168	119.736	57.583	41.963
	K	1044	7.89	119.918	58.4	32.062
	M	1045	7.819	118.261	57.438	33.074
C-terminal tail	L	1046	7.88	119.889	56.068	42.027
	G	1047	8.089	107.429	45.651	
	Q	1048	8.021	119.148	55.689	29.3
	T	1049	8.149	114.796	61.903	69.6
	R	1050	8.326	124.447	53.763	30.116
	P	1051			63.286	31.761
	H	1052	7.998	123.741	57.017	30.116

Appendix Table 4: ΔHN and ΔCA changes calculated between FAT^0 and FAT$^+$.
Changes are shown for all helices and loops of the FAT domain. ΔHN changes that are greater than 2σ (σ ΔHN = 0.025) are shown in bold red, changes greater than 1.5σ are shown in magenta, and those greater than 1σ are shown in black. ΔCA changes that are greater than 2σ (σ ΔCA = 0.19) are shown in bold red, changes greater than 1.5σ are shown in magenta.

	ΔHN	ΔCA
N-terminal loop	**887**, 900, **901**, **902**, **903**, **907**, 914, 915, **916**, **917**, 918, **919**, 921	**887**, 895, 897, 901, **902**, **903**, **917**, 918, 919, 921, 922
Helix 1	929, 934, 935	930, 937, 941, 942
Loop 1		
Helix 2	948, 953, 957, 959, **964**	949, 953, 962, 966
Loop 2	974, **975**	974, 975
Helix 3	980, 989, 992, 1001	979, 980, 991, 998, **1003**
Loop 3	**1008**, **1009**, 1010	1009
Helix 4	1015, 1018, 1022, 1023, 1024, **1025**, 1028, 1033, 1034, 1039, 1043, 1047, 1048, 1049, 1052	1019, 1020, **1023**, 1027, 1031, 1033, 1034